RSC Advances

REVIEW

View Article Online
View Journal | View Issue

Cite this: *RSC Adv.*, 2026, **16**, 2816

Unveiling the chemistry of polynuclear copper complexes: current synthetic strategies, properties and emerging applications

Mohsin Ali,[a] Habib Ullah,[*b] Rajwali Khan,[*c] Noor Ul Islam,[*a] Ezzat Khan,[*d] Maaz Ahmad,[a] Asad Ullah,[a] Ambreen Begum,[a] Ghafar Ali[e] and Yi Xie[*b]

Polynuclear copper complexes (PNCCs), featuring an intricate interplay of multiple copper (Cu) ions, represent a highly diverse and complex field of coordination chemistry. In this review, we cover the synthesis, characteristics, factors affecting structural diversity, and applications of PNCCs. The synthesis methods, including direct synthesis, template synthesis, self-assembly, coordination-driven self-assembly, supramolecular approach and solvothermal methods, are described in detail. Various strategies to make stable Cu(I) and Cu(II) polynuclear networks and to control the nuclearity of PNCCs are documented in detail. The role of density functional theory (DFT) in the optimization of geometry and the prediction of the structure and reactivity of PNCCs is also explained. Physicochemical properties, including electronic, optical, geometrical, structural, and magnetic aspects, are discussed to highlight their fascinating chemistry. For the optimization of PNCC functionality, parameters such as the nature of the ligands and the coordination number of the Cu ions are explored. The potential biomedical applications of PNCCs, particularly due to their binding ability to DNA (opening new windows for cancer treatment) and magnetic properties (opening new avenues for applications in molecular electronics), are also discussed. Additionally, the roles of PNCCs in catalysis, the large-scale separation of C_2 hydrocarbons (C_2H_2) at the industrial level, and the development of new materials (such as vapochromic compounds for organic light-emitting diodes) are highlighted. Besides, their roles in electrochemical CO_2 reduction and H_2 production and as photosensitizers for photocatalytic systems of CO_2 reduction and H_2 production are explored. All these fields require further exploration for their optimized and practical applications, as discussed in this review.

Received 2nd September 2025
Accepted 18th December 2025

DOI: 10.1039/d5ra06568b

rsc.li/rsc-advances

1. Introduction

Polynuclear copper complexes (PNCCs) have drawn increasing attention in coordination chemistry due to their structural flexibility and diversity, magnetic properties, and widespread functional range.[1] PNCCs consist of multiple copper (Cu) centers connected by bridging ligands, creating diverse coordination frameworks and cooperative interactions among the Cu centers. Such Cu–Cu and Cu–ligand communication generates distinctive electronic, magnetic, and catalytic features, making PNCCs an active topic of both fundamental and applied research. PNCCs exhibit remarkable structural diversity, and geometries at the Cu centers can be significantly influenced by the ligand nature, ligand-to-Cu ratios, nature of the solvent and pH of the solution.[2] In addition, the oxidation state of Cu affects the coordination geometry. For instance, complexes containing Cu(II) often display pronounced Jahn–Teller distortions due to the d^9 configuration, which can produce a variety of geometries, such as square-planar, square-pyramidal, tetrahedral, or octahedral structures. On the other hand, Cu(I)-based PNCCs with a d^{10} configuration typically favor tetrahedral arrangements controlled by steric factors rather than ligand-field effects. However, tetracoordinate Cu(I)-based complexes also occur, especially in systems with very bulky ligands or a low coordination number.[2,3]

Because of this tunable coordination behavior and redox activity, PNCCs have been explored in catalysis, materials chemistry, and biomedical research. In the biological context, they exhibit notable antioxidant, antimicrobial,[4–6] anti-inflammatory, and anticancer properties.[7,8] These biomedical activities are associated with the ability of redox-active Cu

[a]*Department of Chemistry, Government Degree College Lalqilla Dir Lower, Lalqilla 18350, Khyber Pakhtunkhwa, Pakistan. E-mail: nooruomchem@gmail.com*

[b]*State Key Laboratory of Silicate Materials for Architectures, Wuhan University of Technology, Wuhan 430070, P.R. China. E-mail: habib@whut.edu.cn; xiey@whut.edu.cn*

[c]*National Water and Energy Center, United Arab Emirates University, Al Ain, 15551, United Arab Emirates. E-mail: rajwali@uaeu.ac.ae*

[d]*Department of Chemistry, College of Science, University of Bahrain, Sakhir 32038, Bahrain. E-mail: ekhan@uom.edu.pk*

[e]*Nanomaterials Research Group (NRG), Physics Division, PINSTECH, Nilore, Islamabad, Pakistan*

centers to facilitate electron transfer and modulate reactive oxygen species. These findings indicate that PNCCs could serve as promising frameworks for the design of new drugs with high therapeutic efficiency. PNCCs have gained immense interest for their potential to catalyze various reactions.[8–10] Catalytically, the synergistic interaction among the multiple Cu centers in PNCCs enhances both activity and selectivity compared with their mononuclear analogues. Consequently, PNCCs have been applied in selective oxidation, hydrogen evolution, and CO_2 reduction reactions, serving as sustainable alternatives to precious-metal catalysts.[11,12] PNCCs have also been investigated for the energy-efficient separation of C_2 hydrocarbons, which is a challenging industrial process due to the similar boiling points of ethane, ethylene, and acetylene. Their π–π interactions, tunable pore architecture, and π-complexation with Cu centers enable the selective adsorption and separation of these gases.[13] In recent years, Cu(I) PNCCs have also gained attention as promising materials for use in organic light-emitting diodes (OLEDs), owing to their strong photoluminescence, low cost, and structural tunability. Their efficient inter-ligand charge transfers and potential for thermally activated delayed fluorescence make them excellent light emitters, especially when enhanced by π-conjugated ligands. Furthermore, the earth abundance of Cu, as well as its stability and structural tunability, enables its use in diverse device architectures.[14]

Compared with other transition metals widely used in coordination chemistry, such as Fe, Co, Ni, Mn, Cr, Zn, Pt, Ag, Au and Ru, Cu stands out for its remarkable structural flexibility and chemical adaptability. Unlike Fe, Ni and Co, whose strong ligand-field effects and spin-state preferences frequently limit geometric adaptation, Cu(II) freely undergoes Jahn–Teller distortion and adopts different coordination numbers, typically ranging from four to six, with diverse architectures: mononuclear, binuclear, and polynuclear.[15–18] This flexibility allows Cu to form a broad range of nuclearity and bridging patterns, which is challenging to accomplish with more inflexible systems like Ni(II).[16] In addition, the accessible Cu(I/II/III) redox states permit smooth electron transfer and mixed-valence behavior, properties not commonly observed in many 3d metals, such as Ni, Co, Fe, and Mn.[16–19] Complexes of Mn and Cr, though magnetically interesting, are habitually constrained by high-spin configurations,[19,20] while Zn(II) acts mostly as a structural analogue because of its redox inactivity.[21] Noble-metal complexes, such as Pt(II), Ag(I), Au(I/III) and Ru(II), have also been extensively reviewed for their excellent photochemical and catalytic performances.[22–24] However, their high cost, lower abundance, and less adaptable coordination chemistry reduce their suitability for use in constructing extended polynuclear frameworks. Overall, these comparisons emphasize the special role of Cu-based multi-nuclear complexes. They bring together the structural flexibility, rich redox chemistry, and biological relevance found in both 3d and noble metals. These characteristics make them valuable materials for catalysis, magnetism, and biomedical functions.

Though a lot of research has been conducted on PNCCs and many features have been explored, researchers are still searching to find the best synthetic routes, exploring fascinating properties and practical applications in numerous fields. Therefore, keeping in view the unique properties and enormous applications of PNCCs, this review aims to provide consolidated knowledge about PNCCs to help scholars identify research gaps and explore them further. In this regard, various aspects such as synthesis routes, structural diversity, and factors influencing their synthesis and properties are explored. Additionally, their potential applications in many fields are discussed. Furthermore, this review highlights the role of computational studies, particularly density functional theory (DFT), in studying various aspects of PNCCs, such as electronic structure, magnetic interactions, and other fundamental

Table 1 Standardized ligand nomenclature: full names and abbreviations used in this review

Ligand name	Abbreviation	Ligand name	Abbreviation
Dibenzo-1,12-[*N*,*N*′′-bis{(3-formyl-2-hydroxy-5-methyl}benzyl)-diaza]-5,8-dioxacyclotetradecane	L^1	1,3,5-Tris(1,2,4-triazol-1-ylmethyl)-2,4,6-trimethylbenzene	L^{28}
Dibenzo-1,12-[*N*,*N*′′-bis{(3-formyl-2-hydroxy-5-methyl}benzyl)diaza]-5,8-dioxacyclopentadecane	L^2	2,6-di(1,8-naphthyridine-2-yl)pyridine	L^{29}
4-Bromo-2-{(2-morpholinoethylamino)methyl}-phenol	L^3	Pyridine-2,6-dicarbohydrazide based imine	L^{30}
4-Chloro-2-{(2-(dimethylamino) ethylamino) methyl}-phenol	L^4	(*E*)-2-[(2-(1*H*-imidazole-4-yl)-3-carboxypropyl)imino)methyl]phenol	L^{31}
6,6-Dihydroxy-2,2′-[(1,2-ethylene-dioxy-bis(nitrilomethylidyne))phenol	L^5	Naphthaline-2,6-dicarboxylate	L^{32}
2-[2-(2,4-dioxypentan-3-ylidene)hydrazinyl] terephthalate	L^6	4-(Trifluoromethyl)phenyl-substituted-2,9-di(diphenylphosphinobutyl)-1,10-phenanthroline	L^{33}
2-[2-(4,4-dimethyl-2,6-dioxocyclohexylidene)hyrazinyl] terephthalate	L^7	1,3-Bis(phenylthiol)propane	L^{34}
1,3-Diisobutyl thiourea	L^8	(*N*,*N*′-Bis(2-hydroxybenzylidene) pentane-1,3-diamine = H_2L)	L^{35}
N,*N*′-bis[2-carboxybenzo-methyl]-*N*,*N*′-bis[2-pyridylmethyl]-1,3-diaminopropan-2-ol	L^9	2,2′–((1*E*,1′*E*)–(1,4-phenylenebis(azanylylidene)) bis(methaneylylidene))bis(4-*tert*-butyl-6-methylphenol)	L^{36}
4-(Pyridine-3-yl)methyleneamino-1,2,4-triazole	L^{10}	2,3-Pyrazine dicarboxylic acid	$H_2Pyaz^{2,3\text{-dc}}$

Table 2 Standardized ligand nomenclature: full names and abbreviations used in this review

Ligand name	Abbreviation	Ligand name	Abbreviation
2-[2-(Pyridylamino)phenylazo]-pyridine	L^{11}	2,5-Pyridinedicarboxylic acid	$H_2Py^{2,5\text{-dc}}$
1((2-Methylamino)ethylamino)-naphthalene-2-ol	L^{12}	3,5-Pyrazoldicarboxylic acid	$H_3Pz^{3,5\text{-dc}}$
N,*N*,-Bis(2-hydroxybenzylidene)-malonohydrazide	L^{13}	Tris(2-pyridylmethyl)amine	TPA
6,6′–(((Pyridin-2-ylmethyl)azanediyl)bis(methylene))bis(4-chloro-2-methylphenol)	L^{14}	Tris(isopropyl-2-ethyl)amine	Iptren
(*E*)-*N*-(2-(2-Hydroxy benzylidene amino)phenyl)acetamide	L^{15}	Diethylenetriamine	Dien
(*E*)-*N*-(2-(5-Chloro-2-hydroxybenzylideneamino)phenyl) acetamide	L^{16}	*N*,*N*,*N*′,*N*″,*N*″-Pentamethyl-dieethylenetriamine	Pmdien
(*E*)-*N*-(2-(5-Bromo-2-hydroxybenzylideneamino)phenyl) acetamide	L^{17}	Tris(3-aminopropyl)amine	trpn
2-((Bis(pyridin-2-ylmethyl)amino)methyl)-6-methoxy-4-methylphenol	L^{18}	Bis(3,5-dimethylpyrazolyl-1H-ethyl)amine	Bedmpza
2-((Bis(pyridin-2-ylmethyl)amino)methyl)-4-chloro-6-methoxyphenol	L^{19}	Terephthalic acid	H_2tp
6,6′–(((Pyridin-2-ylmethyl)azanediyl)bis(methylene))bis(4-chloro-2-methylphenol)	L^{20}	Phthalic acid	H_2phth
6,6′–(((Pyridin-2-ylmethyl)azanediyl)bis(methylene))bis(2-*tert*-butyl-4-methylphenol)	L^{21}	Isophthalic acid	$H_2isophth$
6,6′–(((*N*,*N*-Diisopropylethylenediamine)azanediyl) bis(methylene))bis(2,4-dimethylphenol)	L^{22}	2-Pyridine-methanol	Piconol
6,6′–(((*N*,*N*-Diisopropylethylenediamine)azanediyl) bis(methylene))bis(2-chloro-4-methylphenol)	L^{23}	Dicyanamide	dca
2,4-Dimethyl-6-(((3-(dimethylamino)propyl)azanediyl) methyl)phenol	L^{24}	1*H*-[1,10]phenanthrolin-2-one	Ophen
2,2′–((1*E*,1′*E*)–((2-Hydroxy-1,2-naphthalene-1,2-diyl) bis(methanylylidene))bis(oxy))bis(*N*′-(2-hydroxy-3-(hydroxyimino)propylidene)benzohydrazide)	L^{25}	2,9-Dimethyl-1,10-phenanthroline	dmp
N,*N*′-Bis(quinolin-2-ylmethylene)cyclohexane-1,4-diamine	L^{26}	4,7-Diphenyl-2,9-di(diphenylphosphinotetramethylene)-1,10-phenanthroline	P2bph
N,*N*′-Bis(4-carboxybenzylidene) terephthalohydrazide	L^{27}	5-(2-Pyridyl) tetrazole	2-ptz
Ethyl-4′-benzoate-3,5-dimethylpyrazolate	EBPz	Methyl-4′-benzoate-3,5-dimethylpyrazolate	MBPz

properties. To enhance clarity, ensure smooth readability throughout the manuscript, and avoid repetition of lengthy chemical names, Tables 1 and 2 summarize the full names and corresponding abbreviations of all ligands used in this review.

2. Synthetic methods for PNCCs

PNCCs have been synthesized by employing various techniques, as listed in Table 3. These techniques include the following: direct synthesis, where Cu salts are made to react with the ligand under reflux conditions;[25,26] template synthetic method, which uses pre-synthesized ligand scaffold to regulate Cu ions' arrangement and geometry;[5] coordination-driven self-assembly, which uses the spontaneous organization of Cu ions and designed ligands to form well-defined structures;[27] and supramolecular method, which depends on non-covalent interactions, like hydrogen bonding and π–π stacking, to make dynamic and functional assemblies of Cu ions and ligands.[28] Besides, the solvothermal method, which involves the heating of ligands and Cu salts under solvothermal conditions, has also been employed for the synthesis of PNCCs.[29] Together, these techniques offer malleable pathways for designing and synthesizing PNCCs with controlled structures and desired properties. Further details of the synthetic strategies, including the reaction parameters, are discussed in the upcoming Sections 2.1 to 2.5.

2.1. Direct synthesis or spontaneous self-assembly

The direct synthetic approach involves the reaction of Cu salts, mostly Cu(II), directly with organic ligands under controlled conditions to produce polynuclear complexes by *in situ* deprotonation, ligand bridging, and simple aggregation, without a pre-organized scaffold. Typically, the reaction proceeds in solution *via* room-temperature mixing, reflux, and slow diffusion or crystallization, resulting in ligand coordination and metal–metal interactions and, finally, the self-assembly of discrete multinuclear species or extended frameworks.[25,26] While Cu(II) salts are commonly used in this method owing to their stability, solubility, and commercial availability, Cu(I) and Cu(0) precursors are also viable starting materials. Cu(I) complexes can be prepared by various approaches: (i) comproportionation reaction between Cu(II) salts and metallic Cu in the presence of stabilizing ligands; (ii) direct reaction of Cu(I) halides to form a stable species, such as (NHC)CuX; or synthesis of soluble Cu(I) salts like $[Cu(CH_3CN)_4]PF_6$ through Cu_2O reduction.[30] These methods often use an inert environment or specialized techniques to prevent oxidation or

Table 3 Polynuclear copper complexes synthesized through various strategies

Complexes	Reaction conditions	Synthetic methods	Ref.
$[Cu_2L^1](ClO_4)_2$	Ligand (L^1) was dissolved in hot $CHCl_3$, then methanolic $Cu(ClO_4)_2\cdot 6H_2O$ was added to it, followed by 1,2-diaminoethane and trimethylamine; lastly, more $Cu(ClO_4)_2$ was added after 1 h, followed by reflux for 24 h, filtering of hot mixture, cooling to 25 °C, evaporating slowly, washing, drying, and recrystallizing from CH_3CN to yield dark-green crystals	Template synthesis	8
$[Cu_2L^2](ClO_4)_2$	Prepared using the same procedure used for $[Cu_2L^1](ClO_4)_2$ but replacing 1,2-diaminoethane with 1,3-diaminopropane and L^1 with L^2, giving dark-green crystals after work-up and recrystallization	Template synthesis	8
$[Cu_3(L^3)Cl_4]$	L^3 was reacted with $CuCl_2\cdot 2H_2O$ under stirring for 30 min and refluxing for 1 h, and the filtrate left at ambient temperature yielded black single crystals after a few days	Direct synthesis	15
$[Cu(L^4)N_3]_n$	L^4 was reacted with $Cu(ClO_4)_2\cdot 6H_2O$ under stirring for 30 min, followed by dropwise addition of sodium azide and refluxing for 1 h. Upon cooling, the filtrate was left at ambient temperature for several days, yielding green single crystals	Direct synthesis	15
$[Cu(bpca)Cl]_n$	$[Cu(tptz)Cl_2]$ in water was stirred and filtered, and the filtrate was left to evaporate at room temperature for Cu-mediated hydrolysis, yielding single crystals of $[Cu(bpca)Cl]_n$ within one week	Template synthesis	77
$[Cu_7(\mu\text{-adeninato})_6(\mu_3\text{-}OH_2)_6]$–(fumarate)$\cdot 22H_2O$	Adenine and $Cu(NO_3)_2\cdot 3H_2O$ in methanol–water (1 : 1) at 60 °C, pH were adjusted to 9.2 with NaOH or HNO_3; next, fumaric acid was added, and the solution was left at room temperature to yield blue cubic crystals in 3 to 4 days, assembled through π–π stacking and hydrogen bonding to form porous supramolecular box-like architectures with adjustable internal cavity sizes	Supramolecular assembly	78
$[Cu_7(\mu\text{-adeninato})_6(\mu_3\text{-}OH_2)_6](L^{32})\cdot 32H_2O$	Prepared using the same procedure for $[Cu_7(\mu\text{-adeninato})_6(\mu_3\text{-}OH_2)_6]$–(fumarate)$\cdot 22H_2O$, but with naphthalene-2,6-dicarboxylic acid, giving blue square crystals in 6 to 7 days at room temperature	Supramolecular assembly	78
$[Cu_2(HL^{25})(NO_3)(H_2O)]$	A pre-organized bicompartmental L^{25} ligand with ethyl acetate with $Cu(NO_3)_2\cdot 3H_2O$ in ethanol at 35 to 40 °C, followed by filtration and slow solvent evaporation at room temperature for about three weeks to yield a single crystal	Coordination-driven self-assembly	79
$[Cu_4(L^{26})_4]^{+4}$ (53)	L^{26} was dissolved in acetonitrile, followed by the addition of an equimolar amount of $Cu(MeCN)_4PF_6$ and stirring for 24 h, followed by solvent evaporation and ether precipitation	Coordination-driven self-assembly	80
Centa-poly[Cu-μ-L^{27}]	A mixture of the corresponding ligand and $Cu(CH_3COO)_2\cdot H_2O$ was heated in ethanol at 80 °C under solvothermal conditions for 60 min, followed by ethanol removal, filtration, and washing with cold ethanol	Solvothermal method	45
$H_2(Cu_4Br_6)$ $[(Cu_4Br_3)(L^{28})_2(H_2O)]_n$	Sealing equimolar amounts of CuSCN and the respective N-donor ligand in acetonitrile within a 15 mL Teflon-lined stainless-steel reactor, heating at 140 to 170 °C for 72 h, and cooling to room temperature at a rate of 10 °C h^{-1} to yield the crystalline product	Solvothermal method	47

disproportionation of Cu(I) species. Metallic copper, *i.e.*, Cu(0), can also serve as a precursor, either through a direct reaction with ligands under oxidative conditions or through electrochemical processes that generate Cu(I) or Cu(II) intermediates *in situ*.[31,32] The advantages of the direct synthesis method include a reduced need for multi-step ligand synthesis and the potential for high yields. However, this method exerts limited control over nuclearity and geometry, and it may result in the possible formation of side products. Researchers are now trying to tune the solvent polarity, temperature, and ligand steric or electronic effects to achieve specific nuclearity and geometry targets, as well as employ additives to suppress undesired byproducts.[33,34] Besides these, DFT predictions and *in situ* monitoring either by spectroscopic or diffraction methods have been adopted to screen the reaction and understand the reaction pathway to avoid byproducts and optimize topology.[35]

2.2. Template synthesis method

Template preparation method uses pre-synthesized scaffold ligands (macrocycles, calixarenes, cryptands, or ligands formed *in situ* under templation), having specific coordination sites or templating metal ions that direct the assembly of Cu ions in a predefined geometry. The scaffold ligands direct the preparation of PNCCs with a particular geometry and connectivity of Cu–ligands. This method has various advantages, including controlling the assembly process and obtaining PNCCs with well-defined geometrical structures and preferred properties.[8,36–43] However, this approach often needs pre-synthesized complex scaffold ligands, which add complexity to the synthesis procedure and may limit ligand diversity. Although this method faces some challenges, recent studies are focusing on developing dynamic and switchable templates that respond to external stimuli, enabling on-demand structural

reconfiguration and functional tuning. For instance, metal-assisted *in situ* ligand formation (templation) is being tuned to half-condensed or selectively condensed Schiff bases by adjusting the pH, stoichiometry, and solvent, enabling new ligand variants without full pre-synthesis.[44]

2.3. Solvothermal synthesis approach

Solvothermal approach is one of the powerful methods for the synthesis of PNCCs and coordination polymers, as the high-temperature and high-pressure environment in sealed vessels endorses slow and controlled assembly of multinuclear nodes (*e.g.*, Cu_2, Cu_3, Cu_4) with excellent crystallinity and phase purity. Under self-generated pressure, ligand solubility and coordination modes shift, allowing the preparation of mixed-valence motifs and complex bridging architectures, which are difficult to obtain under ambient conditions.[29] Recent studies report a rapid, about 60 min, formation of mesoporous Cu(II) coordination polymers and evolution from trinuclear clusters to extended frameworks.[45,46] In Cu(I) systems, solvothermal control over solvent, temperature, and ligands has been shown to tune dimensionality and nuclearity.[46,47] This method offers various advantages, such as high-quality single-crystal growth, kinetic control over nuclearity, tolerance to volatile ligands, and high thermal stability of the complexes. However, this method also has some limitations, such as the requirement of specialized equipment, batch variability, trouble in precise stoichiometric control, imperfect *in situ* monitoring, solvent inclusion, and scale-up challenges for pressure-dependent phases. Recent advances in solvothermal synthesis have focused on fine-tuning reaction parameters, introducing modulators, and using *in situ* monitoring, which have allowed precise control over nuclearity, dimensionality, and functional properties.[48]

2.4. Coordination-driven self-assembly

Coordination-driven self-assembly (CDSA) has arisen as a powerful strategy among other promising techniques for the synthesis of PNCCs with predictable nuclearity and geometry by exploiting the directional preferences of metal–ligand coordination bonds and pre-organized polydentate ligands.[49,50] In this method, rigid or conformationally biased donor scaffolds are matched to chosen geometries of Cu-centers, enabling the planned formation of discrete cages, helicates, grids, or cluster-based secondary building units with high structural reliability.[51,52] These differ abruptly from spontaneous or direct self-assembly, in which simple mixing of Cu salts and ligands, often flexible, under ambient or reflux conditions allows thermodynamics to dictate product identity, commonly leading to condition-dependent mixtures.[53] While CDSA requires deliberate ligand design and tighter control of stoichiometry, it offers superior reproducibility and functional tunability for targeted applications, whereas the direct method remains valuable for rapid exploratory synthesis and unexpected discovery.[54] This approach also faces some challenges of kinetic traps and competing assemblies. However, current research is focusing on multi-component systems, solvent mixtures, and ligand flexibility to improve selectivity and functional integration in the assemblies.[52,55–66]

2.5. Supramolecular chemistry approaches

Supramolecular approaches utilize non-covalent interactions, such as hydrogen bonding, π–π stacking, and van der Waals forces, in combination with metal–ligand coordination to organize Cu-centers into polynuclear clusters. These non-covalent interactions allow for the construction of dynamic and adaptive structures with programmable properties. Supramolecular approaches offer opportunities to design functional materials and molecular devices based on PNCCs.[27,53,67–74] However, this technique has some disadvantages, such as lower stability in harsh environments and potential structural heterogeneity. Current studies focus on incorporating stimuli-responsive motifs, hybridizing with covalent frameworks, and using soft-matter supports to enhance stability while retaining dynamic features.[75,76]

2.6. Strategies for nuclearity control and stability

The aforementioned synthetic routes have proven effective for synthesizing PNCCs. However, a challenge that cuts across all these methods is the inherent lability of Cu ions and their thermodynamic tendency to redistribute into mixtures of clusters of different sizes. This uncertainty presents stability complications for both Cu(I) and Cu(II) systems, each requiring tailored strategies to achieve control over nuclearity and stability.[81,82]

In the case of Cu(I), its d^{10} configuration and tendency for low coordination numbers lead to a highly dynamic coordination sphere and strong cuprophilic interactions.[83] These features are vital to the fascinating photophysical and catalytic properties of Cu(I) clusters; however, they also make these arrangements susceptible to cluster interconversion and disproportionation. Consequently, isolating a specific nuclearity becomes challenging. The solution to this challenge lies not in rigid pre-organization alone, but also in kinetic stabilization, producing a protective coordination sphere that imposes a high kinetic barrier to metal-ion exchange.[81,84]

For the formation of stable Cu(I) PNCCs, the most effective and significant approaches involve steric shielding with *N*-heterocyclic carbene or bulky phosphine,[85,86] encapsulation within macrocycles or cage ligands,[81,84] and the utilization of strong π-acceptor ligands (like CNR and CO).[87] These strategies improve Cu(I)–ligand bond strength and prevent their dissociation. The goal of these approaches is to slow down ligand substitution rates and physically hinder pathways for cluster aggregation and fragmentation. An influential example of this approach has been demonstrated by Wang *et al.*,[84] who employed a flexible multi-nucleating macrocycle as a molecular mold. By using a transmetalation strategy from Ag(I) templates, they were able to accomplish a complete series of mono-, di-, tri-, and tetra-nuclear Cu(I) clusters. Remarkably, this method produced well-defined clusters, including a rare $[Cu_3(\mu_3\text{-}Cl)]^{2+}$ core similar to enzymatic active sites. Even more excitingly, the system revealed reversible interconversion between

nuclearities, indicating that these clusters were kinetically trapped rather than thermodynamically fixed. Their detailed NMR investigations showed that the dynamic behavior was modulated by ligand dissociation, highlighting how the macrocycle and ancillary ligands collaborate to uphold cluster integrity. This methodology provides a fascinating strategy for using flexible, encapsulating ligands to control Cu(I) nuclearity, offering a modular pathway to otherwise inaccessible Cu(I) clusters for fundamental studies and applications.

In contrast, Cu(II) complexes face a different issue, namely the Jahn–Teller distortion associated with the d^9 configuration. This frequently results in distorted geometries, various structural polymorphs, and unpredictable coordination modes.[88] The significant strategy here is thermodynamic control through ligand design to control the coordination sphere and direct the geometry. This is efficiently achieved by employing polydentate, often rigid ligands, such as Schiff bases, pyrazolates, or polycarboxylates.[88,89] These ligands chelate the Cu(II) ions firmly, minimizing the tendency for distortion and interlinking the Cu(II) into a specific geometry. For instance, the use of compartmental ligands or tripodal N or O donors can preorganize coordination pockets for specific nuclearites, such as di-, tri-, or tetranuclear core, thermodynamically stabilizing symmetric and well-defined Cu(II) complexes. The solvothermal method has also emerged as a powerful method for synthesizing stable Cu(II) PNCCs. The high temperatures enable the system to reach its global thermodynamic minimum, forming exceptionally stable, crystalline clusters like precise nuclearities, such as paddle-wheel Cu_2 units or square-planar Cu_4 cores, which are otherwise challenging to obtain under mild conditions.[90,91] Moreover, to produce stable Cu(II) PNCCs with specific geometries and nuclearities, the use of bridging ligands with fixed angles, such as oxo, hydroxo or pyrazolate, enforces a precise nuclearity, while counterion templation directs the assembly process.[92–95]

3. Physicochemical properties of PNCCs

Polynuclear copper complexes are a fascinating class in chemistry as they exhibit unique structures, geometry, applications, *etc.* The distinctive properties of polynuclear complexes show great relevance to their physicochemical characteristics. Therefore, for the exploration of PNCCs, some of their characteristics are described below. Furthermore, these characteristics, along with the techniques used to characterize them, are summarized in Table 8.

3.1. Vibrational characteristics

Fourier Transform Infrared (FTIR) spectroscopy is a widely used technique for confirming the formation and coordination environment of PNCCs through functional-group analysis. Rather than only identifying vibrational modes, FTIR studies on PNCCs also offer analytical evidence for ligand binding modes and Cu···Cu connectivity. When ligands coordinate to Cu centers, a distinct shift in the frequencies of IR absorption bands occurs, exhibiting changes in electron density and metal–ligand bonding. When such spectral distinctions are studied in conjunction with crystallographic or UV-vis data, they offer valuable insights into the bridging modes and nuclearity of PNCCs. An in-depth understanding of these shifts not only helps to predict the coordination mode of ligands but also aids in understanding the involvement of multiple Cu centers in a complex, as shown in Table 4. For example, the carboxylate group ($-COO^-$) in its uncoordinated form shows two characteristic vibrational modes: one typically appears between 1550 and 1610 cm^{-1} due to asymmetric stretching (υ_{as}), while another, which is due to symmetric stretching (υ_s), lies between 1300 and 1420 cm^{-1}. Upon bonding to Cu ions, the frequencies of these two bands shift depending on the mode of coordination of $-COO^-$ with Cu ions. In the case of monodentate coordination, the difference in the stretching frequency ($\Delta\upsilon \geq \upsilon_{as} - \upsilon_s$) increases to more than 200 cm^{-1}, while in the case of bidentate (chelating) coordination, it decreases to less than 100 cm^{-1}. Furthermore, $\Delta\nu$ in the range of 140–200 cm^{-1} indicates the bridging coordination mode of $-COO^-$.[96] However, in the case of the participation of $-COO^-$ in hydrogen bonding with either aqua or lattice H_2O, the splitting of these bands does not allow researchers to predict their coordination mode.[97] For example, the complexes $[(TPA)Cu\text{-}(\mu_2\text{-}Py^{2,4\text{-}dc})_2\text{-}Cu(H_2O)_2\text{–}Cu(TPA)](ClO_4)_2$ and $[Cu_2(iptren)_2(Pyaz^{2,5\text{-}dc})](ClO_4)_2\cdot H_2O$ prepared by Massoud *et al.*, as well as $[Cu_3(dien)_2(\mu_2\text{-}Pz^{3,5\text{-}dc})_2(H_2O)_2]\cdot 4H_2O$ and $centa\text{-}[Cu_2(bedmpza)(\mu_2\text{-}Py^{2,4\text{-}dc})](ClO_4)_2\cdot H_2O$ synthesized by Louka *et al.*, involve the participation of $-COO^-$ with aqua or lattice H_2O molecules, and no information on the $-COO^-$ coordination modes in these complexes is provided.[98,99] In such cases, it is difficult to differentiate between bridging and chelating modes based

Table 4 Important FTIR vibrational shifting modes of various functional groups in PNCCs

Functional groups	Free ligands bands (cm^{-1})	Coordinated shift (cm^{-1})	Coordination indication
Carboxylate ($-COO^-$)	υ_{as} = 1550–1610 υ_{as} = 1300–1420	$\Delta\upsilon > 200$ → monodentate $\Delta\upsilon < 100$ → bidentate $\Delta\upsilon \geq 140$ to 200 → bridging	Types of binding
Imine (C=N)	1600–1650	↓ 10–30	N-donor coordination
Phenolic hydroxyl –OH	3200–3600	Disappear	O-donor coordination
C–O	1200–1300	↑ 10–50	O-donor coordination
Amine ($-NH_2$)	3300–3500	↓20–50	N-donor coordination
Cu–O and Cu–N	Absent	400–600	Cu–ligand bond confirmation

Table 5 Important Raman vibrational shifting modes of various functional groups in PNCCs

Functional groups	Frequencies of free ligands (cm^{-1})	Shifting of frequencies upon coordination (cm^{-1})	Remarks
C=O	~1700	1620–1650	Shows O → Cu coordination
C=N	1610–1640	1580–1620	Shows N → Cu coordination
$-COO^-$ asymmetric	1550–1600	1540–1590	Change in $\Delta\upsilon$ exhibits a binding mode
$-COO^-$ symmetric	1400–1440	1370–1430	Paired with asymmetric to evaluate the binding mode
Cu–Cl/Cu–N/Cu–O	Absent	200–600	Shows Cu metal coordination

solely on $\Delta\upsilon$.[99] Therefore, critical correlation of FTIR data with complementary structural and electronic techniques, such as UV-vis spectroscopy or X-ray diffraction, is essential for accurately identifying the connectivity and coordination topology in PNCCs.

The stretching band of imine (C=N) groups in their free form typically lies between 1600 and 1650 cm^{-1}. This absorption band of C=N groups, upon coordination to Cu, shifts to lower frequency by nearly 10–30 cm^{-1}. This shifting occurs as a result of a decrease in bond order due to electron donation from the nitrogen lone pair to Cu ions. Such types of shifts have been observed in Schiff base PNCCs.[100] For example, Ray *et al.*[101] reported that the sharp band around 1631 cm^{-1} in the IR spectrum of Schiff base ligand (*N*, *N*′-bis(2-hydroxybenzylidene) pentane-1,3-diamine = L^{35}) can be ascribed to C=N stretching. In the $[Cu_3(l\text{-}L^{35})_2(ClO_4)_2]$ $[Cu_3(l\text{-}L^{35})_2(H_2O)(ClO_4)_2]$ complex, this band shifts to a lower frequency of 1618 cm^{-1} upon complexation with the Cu metal, which can be attributed to the coordination of the imine *via* N-atom to the Cu center.

In a free state, stretching vibrations of the N–H are observed between 3300 and 3500 cm^{-1}. In coordinated form in PNCCs, these stretching bands shift to lower frequencies by 20–50 cm^{-1}, indicating the coordination of amino acid ligands with Cu ions through the nitrogen atom.[102] For example, the medium ν(N–H) stretching frequencies were observed over the 3210–3340 cm^{-1} region for complexes reported by Louka *et al.* Furthermore, Louka *et al.*[98] and Massoud *et al.*[88] reported that the absorption band over a region of 3595–3440 cm^{-1} is characteristic of the ν(O–H) stretching of aqua or lattice H_2O molecules involved in hydrogen bonding.

The vibrational mode of phenolic hydroxyl (–OH) groups appears as a wide band between 3200 and 3500 cm^{-1} in the uncoordinated form. However, upon coordination, the stretching band of the ν(O–H) phenolic compound typically disappears from the IR spectrum due to loss of the hydroxyl proton, which occurs during coordination. Similarly, the stretching of phenolic ν(C–O) stretching appears around 1200–300 cm^{-1}. However, upon coordination, its stretching band shifts by 10–50 cm^{-1} to a higher frequency, owing to increased electron density around the oxygen atom.[103]

Besides these changes in vibrational modes of functional groups, the appearance of new vibrational modes between 400 and 600 cm^{-1} in the IR spectrum is strong evidence of complex formation. These stretching bands can be attributed to the Cu–O and Cu–N stretching modes.[100] For example, Zhang *et al.*[79] reported that the stretching band appearing at 3400 cm^{-1}, corresponding to phenolic ν(O–H) in the uncoordinated ligand, disappears upon coordination to Cu metal to form $[Cu_2(HL^{36})(NO_3)(H_2O)]$. Additionally, two new absorption bands at 449 and 547 cm^{-1} correspond to ν(Cu–O) and ν(Cu–N), respectively.

Raman spectroscopy is another valuable technique often used as an alternative to FTIR for the analysis of vibrational modes of various bonds in PNCCs, as Raman studies have two advantages over FTIR: firstly, it is unaffected by the H_2O molecule, and secondly, it is able to detect small vibrational bands at low wavelengths, attributed to Cu–ligands symmetric stretching. These bands are absent in some cases or overlapped in other cases in the FTIR spectrum. Like FTIR spectroscopy, Raman spectroscopy uses the same principles of shifting vibrational frequencies in free ligands upon coordination and appearance of new bands to predict the formation of Cu complexes, as shown in Table 5.

For example, the stretching band of free carbonyl (C=O) shifts from 1700 cm^{-1} to lower frequencies (1620–1650 cm^{-1}) upon coordination, reflecting the weakening of the C=O bond due to binding with Cu ions. Similarly, the shift in the stretching frequencies of imine (C=N), C–S and C–O to lower frequencies occurs upon coordination. Besides these changes, new bands appear at low-wavelength regions, attributed to Cu–ligand vibrations, further confirming the formation of Cu complexes.[104,105] Additionally, the change in band position and separation ($\Delta\upsilon$) for symmetric and asymmetric stretching of $-COO^-$ helps to determine its bonding mode (monodentate, bidentate and bridging modes).[104,105]

3.2. Electronic and optical properties

UV-visible spectroscopy is widely used for studying the electronic and optical properties of PNCCs, as it provides direct insights into the electronic transitions and Cu–ligand interactions. This technique helps identify the formation of complexes through characteristic transition bands, such as ligand-to-metal charge transfer (LMCT), metal-to-ligand charge transfer (MLCT), and d–d transitions, which are often absent in free ligands, as shown in Table 6. In contrast to free ligands, where π–π or n–π transitions dominate, the appearance of new LMCT or d–d bands in the 200–800 nm region provides substantial evidence of Cu–ligand coordination and complex formation. Moreover, indirectly, this technique also helps in the prediction of the coordination geometry of Cu ions in a given complex by examining some spectral features.[5,102] In the case of mononuclear Cu(II) complexes (a d^9 system), they typically give a low

Table 6 UV-visible spectral data of the electronic transition of PNCCs and their interpretations

Features	Region (nm)	Observation	Interpretation
d–d transition	600–900	Broad, weak bands	Changes reflect ligand field effects
LMCT	200–400	Strong bands	Coordination through O, N or S donor atoms
MLCT	359–600	Strong bands	Multinuclear Cu(I) with conjugated ligands
ILCT (n–π* or π–π*)	200–350	Slight shift in position and increase in molar absorptivity	Confirming the coordination of ligands with the Cu ion
Shift in λ_{max}	Any	Blue or red shift	Stronger or weaker ligand field
New bands arising/splitting of existing bands	Varies	Multiple Cu centers	Different coordinating environments around Cu or Cu–Cu interactions

intensity band due to a d–d transition that appears around 550–750 nm, owing to the Jahn–Teller distortion in square planar or octahedral geometries.[5,102] In contrast, broader and more intense bands appear in this range for PNCCs, highlighting the multiple coordination environments or Cu–Cu interactions.[5,74] Some bands are usually observed around the 200–400 nm region, which are stronger in intensity than d–d bands and are due to LMCT. These types of transitional bands originate from the donation of electrons from halogens (such as chlorine, bromine and iodine) and oxygen or nitrogen atoms to Cu centers. In the case of PNCCs, the LMCT bands become broader, more intense or shift owing to differences in ligand field splitting.[8,15,77,106–108]

For example, the UV-vis spectra of Cu(II) complexes [(TPA)Cu-(μ_2-Py$^{2,4\text{-dc}}$)$_2$-Cu(H$_2$O)$_2$–Cu(TPA)](ClO$_4$)$_2$, [Cu(TPA)Cu(μ_2-Py$^{2,4\text{-dc}}$)$_2$Cu(TPA)](ClO$_4$), [(TPA)Cu-(μ_2-Pyaz$^{2,3\text{-dc}}$)$_2$Cu(ClO$_4$)$_2$-Cu(TPA)], [Cu(TPA)–(H$_2$O)]$_2$(ClO$_4$)$_4$·H$_2$O, and [Cu$_2$(iptren)$_2$(-Pyaz$^{2,5\text{-dc}}$)](ClO$_4$)$_2$·H$_2$O reported by Massoud *et al.*[88] exhibit two distinct d–d transition bands that are characteristic of five-coordinate Cu(II) centers. Complexes [(TPA)Cu(μ_2-Py$^{2,4\text{-dc}}$)$_2$-Cu(H$_2$O)$_2$Cu(TPA)](ClO$_4$)$_2$, [Cu(TPA)Cu(μ_2-Py$^{2,4\text{-dc}}$)$_2$-Cu(TPA)](ClO$_4$), and [Cu$_2$(iptren)$_2$(Pyaz$^{2,5\text{-dc}}$)](ClO$_4$)$_2$·H$_2$O show broad absorptions around 650–670 nm and at λ_{max} beyond 830 nm, whereas complexes [(TPA)Cu(μ_2-Pyaz$^{2,3\text{-dc}}$)$_2$Cu(ClO$_4$)$_2$-Cu(TPA)] and [Cu(TPA)(H$_2$O)]$_2$(ClO$_4$)$_4$·H$_2$O lack the higher-energy band. The more intense low-energy transitions and additional shoulders at 830–840 nm observed in complexes [(TPA)Cu(μ_2-Pyaz$^{2,3\text{-dc}}$)$_2$Cu(ClO$_4$)$_2$Cu(TPA)] and [Cu$_2$(iptren)$_2$(-Pyaz$^{2,5\text{-dc}}$)](ClO$_4$)$_2$·H$_2$O are evidence of distorted trigonal bipyramidal (TBP) geometries. The presence of two absorption bands (*e.g.*, 840 and 967 nm in complex [(TPA)Cu(μ_2-Pyaz$^{2,3\text{-dc}}$)$_2$Cu(ClO$_4$)$_2$Cu(TPA)] and 834 and 962 nm in complex [Cu$_2$(iptren)$_2$(Pyaz$^{2,5\text{-dc}}$)](ClO$_4$)$_2$·H$_2$O) suggests noticeable distortion within the TBP geometry. Interestingly, the observed spectral features in solution align well with the geometries observed in the solid state. Similarly, Louka *et al.*[98] reported that complexes [Cu$_3$(dien)$_2$(μ_2-Pz$^{3,5\text{-dc}}$)$_2$(H$_2$O)$_2$]·4H$_2$O, [Cu$_3$(trpn)$_2$(μ-Py$^{2,5\text{-dc}}$)$_2$(ClO$_4$)$_2$]centa-[Cu$_2$(bedmpza)(μ_2-Py$^{2,4\text{-dc}}$)](ClO$_4$)$_2$·H$_2$O and [Cu$_4$(L^5)$_2$(MeOH)$_2$]·2MeOH show a shoulder around 500–570 nm and a wide band around 640–680 nm. Such spectral characteristics are typical for d–d transitions and five-coordinated Cu(II) complexes with distorted square pyramidal (SP) geometry. Moreover, in certain cases, an additional low-energy band beyond 800 nm with higher intensity indicates a distorted TBP geometry, as observed in tripodal tetraamine Cu(II) complexes ([Cu$_3$(trpn)$_2$(μ-Py$^{2,5\text{-dc}}$)$_2$(ClO$_4$)$_2$] and centa-[Cu$_2$(bedmpza)(μ_2-Py$^{2,4\text{-dc}}$)](ClO$_4$)$_2$·H$_2$O), resulting from ligands such as TPA, ip$_3$tren, and trpn. Notably, it is interesting to remark that the geometries around the Cu(II) ion, observed in all the complexes, are retained according to XRD analysis. However, the geometry around the Cu(II) ion in [Cu$_4$(L^5)$_2$(-MeOH)$_2$]·2MeOH is clearly SP according to the solution spectrum, while its XRD study revealed the existence of TBP and SP geometries for two Cu(II) ions.

3.3. Molecular mass, composition, and nuclearity

Mass spectrometry (MS), particularly Electrospray Ionization Mass Spectrometry (ESI-MS), has arisen as one of the most reliable and analytical tools for elucidating the molecular mass, composition, and nuclearity of PNCCs. MS, particularly ESI-MS, is used to analyze the mass-to-charge ratio of PNCCs, offering valuable information about their molecular weight, composition, and nuclearity of Cu-complexes by identifying *m*/*z* values and isotopic patterns characteristic of Cu isotopes: ^{63}Cu and ^{65}Cu. Unlike traditional elemental analysis, which delivers information only about empirical stoichiometry, ESI-MS allows the direct detection of intact molecular ions and their fragmentation profiles, thus offering molecular-level evidence of oligomeric species and metal–ligand connectivity. Typically, the MS spectrum of PNCCs displays multiple peaks between 500 and 800 *m*/*z*, reflecting different isotopes and charge states of complex ions.[9] MS is especially useful for identifying the presence of mono-, di- and multi Cu species in solution.

More critically, tandem MS (MS/MS) gives a fragmentation pattern that allows deep insights into the connectivity of the Cu center and the coordination mode of ligands. This discloses the stepwise dissociation of bridging ligands or Cu–Cu units, thereby assisting in distinguishing between μ-oxo, μ-hydroxo, and μ-carboxylato bridging modes. It also helps in confirming the presence of solvent molecules, counter-anions and adducts.[9,15,109] Therefore, the interpretation of the ESI-MS spectra of PNCCs necessitates careful consideration of solvent and ionization effects, as soft ionization conditions can sometimes result in partial complex dissociation or adduct formation, obscuring nuclearity assignment. Furthermore, the MS

spectrometric data combined with other analytical tools, including FTIR and UV-visible spectroscopic techniques, contribute to a deeper understanding of the structural and functional properties of Cu complexes, enabling the rational design and optimization of novel Cu complexes.[9,15,109] Consequently, ESI-MS should be critically linked with complementary techniques, such as FTIR (for ligand coordination shifts) and UV-vis spectroscopy (for d–d and charge-transfer transitions), to achieve a coherent structural picture.

ESI-MS was employed by Hari *et al.*[110] to analyze a series of prepared Cu(II)-M(II)–Cu(II) complexes (where M = Ni, Co, Fe, Zn). The spectrum for the Cu analogue (M = Cu) displayed a dominant peak at m/z = 864.0 (matching well with the calculated m/z = 864.1) for the $[Cu_3(L)_2(\mu_3\text{-}OH)(NO_3)_2(H_2O)]^+$ complex ion, consistent with the presence of a Cu_3 core. Interestingly, the substitution of the central metal (M = Ni, Co, Fe, or Zn) produced characteristic shifts in the m/z values (859–868), signifying the sensitivity of MS to the Cu identity while conserving the trinuclear framework. Moreover, the isotopic pattern well matched with the ^{63}Cu and ^{65}Cu distribution, clearly distinguishing the complex from mono- or dinuclear species. Critically, the ESI-MS observation was correlated with X-ray and FTIR data, confirming that the solution-phase Cu_3 unit detected by MS corresponds to the solid-state μ_3-hydroxo-bridged structure, positioning ESI-MS as a powerful tool for confirming both composition and nuclearity in PNCCs.

3.4. Structure and geometry

Single-crystal X-ray diffraction (SC-XRD) is not simply a structural confirmation tool but a decisive analytical technique for resolving the nuclearity, dimensionality, and coordination architecture of PNCCs at the atomic level. By examining the diffraction pattern of the scattering, precise information about the arrangement of ions in the lattice, crystal structure and other structural details can be obtained. Unlike spectroscopic methods, SC-XRD directly reveals the Cu–Cu connectivity, the nature of bridging ligands, and the resulting network topology of the Cu–ligand framework.[111,112] Furthermore, this characterization tool aids in differentiating between mono-, di- and polynuclear 3D frameworks among Cu complexes.[113] However, SC-XRD requires high-quality crystals, which are sometimes difficult to obtain. In such cases, powder XRD is employed for the characterization of PNCCs.

For instance, Massoud *et al.*[99] systematically studied a series of five Cu(II) complexes made from tripodal amines (TPA, iptren) and polycarboxylate ligands, such as pyridinedicarboxylates and terephthalate. SC-XRD analysis revealed that complexes $[(TPA)Cu(\mu_2\text{-}Py^{2,4\text{-}dc})_2Cu(H_2O)_2Cu(TPA)](ClO_4)_2$, $[Cu(TPA)Cu(\mu_2\text{-}Py^{2,4\text{-}dc})_2Cu(TPA)](ClO_4)$, and $[(TPA)Cu(\mu_2\text{-}Pyaz^{2,3\text{-}dc})_2Cu(ClO_4)_2Cu(TPA)]$ display centrosymmetric trinuclear subunits of the type $[(TPA)Cu(\mu_2\text{-}L)_2Cu(\mu_2\text{-}L)_2Cu(TPA)]^{2+}$, where the central Cu(II) is located on an inversion center and is bridged by two heteroaromatic dicarboxylate ligands (L = $Py^{2,4\text{-}dc}$, $Py^{2,5\text{-}dc}$, or $Pyaz^{2,3\text{-}dc}$). The bridging mode was confirmed as N,O,O′-type, involving one nitrogen and two oxygen donors from the carboxylate ligand. Moreover, SC-XRD established Cu–O and Cu–N distances of 1.92–2.18 Å and Cu⋯Cu separations between 7.6 and 8.7 Å, signifying weak magnetic coupling potential owing to long super exchange pathways. Significantly, the coordination geometry differed across the series: $[(TPA)Cu(\mu_2\text{-}Py^{2,4\text{-}dc})_2Cu(H_2O)_2Cu(TPA)](ClO_4)_2$ contained an axially elongated CuO_4N_2 octahedron, $[Cu(TPA)Cu(\mu_2\text{-}Py^{2,4\text{-}dc})_2Cu(TPA)](ClO_4)$ displayed a square-planar CuN_2O_2 center, while $[(TPA)Cu(\mu_2\text{-}Pyaz^{2,3\text{-}dc})_2Cu(ClO_4)_2Cu(TPA)]$ exhibited a CuO_4N_2 environment elongated by weak Cu–O (ClO_4^-) interactions. On the other hand, complexes $[Cu_2(iptren)_2(tp)](ClO_4)_2$ and $[Cu_2(iptren)_2(\text{-}Pyaz^{2,5\text{-}dc})](ClO_4)_2\cdot H_2O$ featured dinuclear cations: $[Cu_2(\text{-}iptren)_2(\mu_2\text{-}tp)]^{2+}$ and $[Cu_2(iptren)_2(\mu_2\text{-}Pyaz^{2,5\text{-}dc})]^{2+}$, respectively. SC-XRD analysis conclusively showed that the carboxylate groups bridge the two Cu(II) centers in a bis-monodentate mode, leading to Cu⋯Cu distances of 10.9–11.0 Å, which are more elongated than in the trinuclear analogues. Each Cu center adopted a distorted TBP CuN_4O geometry (τ = 0.67–0.86), confirming a weaker Cu–Cu interaction and reduced structural compactness. From spectroscopic data alone, the observed difference in bridging mode and nuclearity between the TPA- and iptren-based systems could not be deduced. Fortunately, only SC-XRD provided a complete atomic picture, revealing that both the steric bulk and donor topology of the tripod ligand dictate whether dinuclear or trinuclear species form. In addition, a detailed description of the topologies of these complexes and other structurally diverse PNCCs is comprehensively discussed in Section 6 (Structural Diversity), where the decisive role of SC-XRD in determining the nuclearity, bridging modes of various ligands, and coordination geometries of Cu centers is further explained.

3.5. Bulk-crystallinity and phase

Powder X-ray Diffraction (PXRD) is used to determine the phase purity and crystallinity of bulk PNCCs. Unlike SC-XRD, PXRD analyzes a powdered sample composed of various microcrystals in random orientation. Monochromatic X-rays are allowed to fall on the sample to obtain the diffraction pattern. This diffraction pattern is recorded as a function of 2θ and shows the average of all possible crystal orientations, allowing the analysis of bulk materials.[102] PXRD is generally used for phase analysis, crystallinity assessment and the confirmation of PNCCs by comparing the observed pattern with the simulated form of SC-XRD data.[103] However, advanced PXRD analysis *via* Rietveld refinements allows the extraction of semi-quantitative structural information,[114] but it is not as precise as SC-XRD.

3.6. Magnetic properties

The magnetic properties of Cu-complexes arise due to the presence of unpaired electrons and also from the intera ction among Cu centers within polynuclear species. Electron spin resonance (ESR) or electron paramagnetic resonance (EPR) is a promising technique that is currently widely utilized for the investigation of magnetic properties of PNCCs, as it is capable of detecting unpaired electrons.[115,116] It also gives information about the oxidation state of Cu and the nature of the donor

Table 7 Magnetic properties of selected polynuclear copper complexes

Complexes	Magnetic properties	Equation used to fit the data	J (cm^{-1})	G	Ref.
$[Cu_2L^1](ClO_4)_2$	Antiferrom-agnetic	$\chi = 2Ng^2\beta^2/kT\left[3+\exp\left(-J/kT\right)\right]$	−1.04	2.04	8
$[Cu_2L^2](ClO_4)_2$	Antiferrom-agnetic	$\chi = 2Ng^2\beta^2/k(T-\Theta)\left[3+\exp\left(-J/kT\right)\right]$	9.88 and $\Theta = -0.24$ k	2.01	8
$[Cu_2(L^{12})_2(\mu_{1,1}\text{-}N_3)_2]\cdot H_2O$	Antiferrom-agnetic	$\hat{H} = -2JS_1 \times S_2 + \mu BgSH$	−2.313	2.103	122
$[Cu_2(L^{12})_2(\mu_{1,1}\text{-}NCO)_2]$	Ferromagn-etic	$\hat{H} = -2JS_1 \times S_2 + \mu BgSH$	0.513	2.141	122
$[Cu(L^{12})(\mu_{1,5}\text{-dca})]$	Antiferrom-agnetic	$\hat{H} = -2JS_1 \times S_2 + \mu BgSH$	−0.344	2.192	122
$[Cu_2(H_2L^{13})(NO_3)(H_2O)]_n(NO_3)_n$	Antiferrom-agnetic	$H = -2J_1(SCu_1SCu_2 + SCu_3SCu_4 + SCu_5SCu_6 + SCu_7SCu_8 + SCu_9SCu_{10} + SCu_{11}SCu_{12} + SCu_{13}SCu_{14}) - 2J_2(SCu_1SCu_2 + SCu_3SCu_4 + SCu_5SCu_6 + SCu_7SCu_8 + SCu_9SCu_{10} + SCu_{11}SCu_{12} + SCu_{13}SCu_{14}$	$J_1 = -1.84$ $J_2 = -4.35$	2.10	123

atoms surrounding the Cu centers; further, it helps in revealing the geometry of Cu-sites in PNCCs with the help of parameters such as g-value and hyperfine coupling constants.[117] This technique is especially useful for the detection of magnetic exchange interactions between Cu-centers, which can be observed *via* changes in signal intensity, line shape, and the appearance of half-field signals.[118] The temperature-dependent measurement of susceptibility helps in understanding whether the interaction between various Cu ions is ferromagnetic or antiferromagnetic.[119] In addition, advanced approaches, such as high-frequency ESR/EPR and pulsed techniques, are capable of high-resolution identification of atoms in bridging ligands and measurement of the distance between Cu ions within PNCCs.[120] Besides these advantages, this method has some disadvantages too, such as the inability to detect Cu(I) ions or strong antiferromagnetic coupling of Cu(II) pairs and the frequent requirement of low-temperature measurements.[121]

The variable-temperature magnetic susceptibility $\chi_M{}^T$ values of selected complexes are listed in Table 7. The $\chi_M{}^T$ value of $[Cu_2L^1](ClO_4)_2$ at room temperature (300 K) is 0.76 cm^3 K mol^{-1}, which is consistent with the spin-only value, $\chi_M{}^T = 0.75$ cm^3 K mol^{-1}, for uncoordinated two Cu(II) ions ($S = \frac{1}{2}$), with $g = 2.00$. The $\chi_M{}^T$ value is almost constant up to 100 K, but on further cooling, the $\chi_M{}^T$ increases rapidly and reaches a maximum of 0.95 cm^3 K mol^{-1}. After that, it decreases to 0.90 cm^3 K mol^{-1} at 2 K. The temperature dependence of $\chi_M{}^T$ reveals a dominant ferromagnetic coupling with weak antiferromagnetic interaction of Cu ions in $[Cu_2L^1](ClO_4)_2$. Similarly, the $\chi_M{}^T$ value at room temperature for $[Cu_2L^2](ClO_4)_2$ is 0.76 cm^3 K mol^{-1}, which is also consistent with the spin-only value, $\chi_M{}^T = 0.75$ cm^3 K mol^{-1}, for uncoordinated two Cu(II) ions ($S = \frac{1}{2}$) with $g = 2.00$. It decreases gradually up to 20 K and then deceases rapidly, indicating the weak antiferromagnetic interaction between copper ions. The variable temperature magnetic susceptibility $\chi_M{}^T$ value of $[Cu_2Cl_2(L^{11})_2]\cdot H_2O$ at room temperature is 0.91 cm^3 K mol^{-1}, which, on lowering the temperature, decreases gradually. At 300 K, $\chi_M{}^T =$ 0.91 cm^3 K mol^{-1}, which is greater than that of uncoordinated two Cu(II) ions ($S = \frac{1}{2}$) with $g = 2.00$. This indicates that two Cu(II) ions are weakly coupled antiferromagnetically through the

Table 8 Comparative analysis of selected characterization methods for PNCCs

Technique	Information provided	Advantages	Limitations
FTIR spectroscopy	Confirmation of complex formation by analyzing the shift in the frequencies of bands of functional groups and the emerging vibrational bands	Simple, fast and widely available	Limited by complex mixtures and ambiguous or overlapping peak assignment at low wavenumbers
Raman spectroscopy	Complementary to FTIR, Cu–ligand bond confirmation at low-wavelength radiation, and symmetric vibration	Nondestructive and useful for Cu-metal stretches	Weak signal for some ligands and fluorescence interface
UV-visible spectroscopy	d–d transition, charge- transfer bands, ligand-field strength	Useful for the electronic structure and oxidation state of Cu ions in PNCCs	Overlapping bands, low-resolution structural information
Mass spectrometry (ESI-MS)	Molecular weight, fragmentation, nuclearity and counter anions in PNCCs	High sensitivity and detection of solution species	May not detect non-ionizable species, and exhibits less structural detail
SC-XRD	Precise 3D atomic structure, bond length, and coordination geometry of Cu in PNCCs	Gold standard for structural determination	Requires high-quality and single crystals in the solid state only
PXRD	Phase identification and crystallinity	Useful for bulk analysis, phase purity	Cannot provide a full structure like SC-XRD

bridging ligand in $[Cu_2Cl_2\ (L^{11})_2]\cdot H_2O$. The magnetic data were fitted using the expression shown in Table 7, with the magnetic properties derived by Bleany and Bowers. The $\chi_M{}^T$ value of $[Cu_2(L^{12})_2(\mu_{1,1}\text{-}N_3)_2]\cdot H_2O$ at room temperature is 0.802 cm^3 K mol^{-1}, and the value is 1.777 cm^3 K mol^{-1} for $[Cu_2(L^{12})_2(\mu_{1,1}\text{-}NCO)_2]$. Until 50 K, the $\chi_M{}^T$ value is constant for both complexes. As the temperature decreases further, the $\chi_M{}^T$ value starts to decrease, indicating the antiferromagnetic exchange coupling between the Cu(II) centers in $[Cu_2(L^{12})_2(\mu_{1,1}\text{-}N_3)_2]\cdot H_2O$ and $[Cu_2(L^{12})_2(\mu_{1,1}\text{-}NCO)_2]$. The $[Cu(L^{12})(\mu_{1,5}\text{-dca})]$ complex shows a temperature-independent $\chi_M{}^T$ value between 25 and 300 K. However, below 25 K, it increases, which indicates the ferromagnetic exchange coupling between the copper(II) centers. For $\chi_M{}^T$ *versus* T simulation plots, the standard Heisenberg-Dirac-van Vleck Hamiltonian ($\hat{H} = -2JS_1 \times S_2 + \mu_B gSH$) was used, which gives $J = -2.313$ cm^{-1} for $[Cu_2(L^{12})_2(\mu_{1,1}\text{-}N_3)_2]\cdot H_2O$ and $J = -0.344$ cm^{-1} for $[Cu(L^{12})(\mu_{1,5}\text{-dca})]$. The negative J-value indicates the antiferromagnetic interaction between the copper(II) centers. While for $[Cu_2(L^{12})_2(\mu_{1,1}\text{-}NCO)_2]$, it gives a positive J value ($J = 0.513$ cm^{-1}), which indicates ferromagnetic exchange coupling between Cu(II) centers.

The room temperature $\chi_M{}^T$ value of $[Cu_2(H_2L^{13})(NO_3)(H_2O)]_n(NO_3)_n$ is 0.775 cm^3 K mol^{-1}, which is slightly greater than the calculated value for two uncoordinated copper(II) ions (0.750 cm^3 K mol^{-1}). In the range of 300–25 K, the χ^T value decreases gradually. At 50–300 K, the magnetic data follow the Curie–Weiss law, with $C = 0.785$ cm^3 K mol^{-1} and $\Theta = -3.20$ K, which indicates that the interaction is antiferromagnetic. MagPack software, using an example of a Cu_{14} cluster loop, was used to fit the data. The Hamiltonian of the Cu_{14} cluster loop with alternative J_1 and J_2 magnetic coupling constants was determined as follows:

$$H = -2J_1(SCu_1SCu_2 + SCu_3SCu_4 + SCu_5SCu_6 + SCu_7SCu_8 + SCu_9SCu_{10} + SCu_{11}SCu_{12} + SCu_{13}SCu_{14});\ -2\ J_2(SCu_1SCu_2 + SCu_3SCu_4 + SCu_5SCu_6 + SCu_7SCu_8 + SCu_9SCu_{10} + SCu_{11}SCu_{12} + SCu_{13}SCu_{14})$$

where $J_1 = -1.84$ cm^{-1}, $J_2 = -4.35$ cm^{-1} and $g = 2.10$. Both the J_1 and J_2 values are negative, showing antiferromagnetic interactions. The more negative J_2 value compared to J_1 indicates that the antiferromagnetic interaction through the ligand bridge is weaker than that through the O-nitrate bridge.

4. Computational studies: the role of DFT

Experimental methods such as SC-XRD, magnetic susceptibility, and spectroscopy provide structural and bulk magnetic information, but often fail in identifying microscopic spin distribution, orbital overlap, and redox-induced geometric variations that regulate the behavior of PNCCs. Fortunately, DFT bridges these gaps by providing quantum-level insights into Cu–Cu coupling, the effect of bridging ligands, and electronic rearrangements, thereby confirming experimental results and predicting properties that are otherwise inaccessible through experimental techniques.[124]

4.1. Electronic structure and magnetism

DFT permits precise modeling of the spin states, oxidation states, and magnetic coupling pathways in PNCCs, particularly in Cu(II)-based complexes where the unpaired electron interacts through bridging ligands. For instance, broken-symmetry DFT methods are mostly used to evaluate the exchange coupling constant (J values) in polynuclear species. This calculation can predict antiferromagnetic and ferromagnetic behavior and help in interpreting magnetic susceptibility data.[125] For example, an end-to-end azido-bridged Cu(II) dimer exhibiting a long Cu···Cu separation of about 5.105 Å may still display ferromagnetic coupling ($J = +16$ cm^{-1}). The experimental magnetic and crystallographic data alone could not justify the coexistence of weak interactions and ferromagnetism in the Cu ions. Interestingly, DFT and correlated *ab initio* methods reproduced the experimental J value. Collectively, they confirmed that spin polarization over the azido bridges, rather than direct Cu–Cu exchange, accounts for the magnetic behavior, showing how delocalized spin density compensates for large metal separation.[126] This clearly demonstrates how theoretical calculations resolve discrepancies between structure and magnetism that cannot be determined by experimental methods alone. Similarly, two heterobridged $Cu_2(\mu\text{–}OH)(\mu\text{–}X)$ complexes, where X = azaindole or pyrazolate, with nearly matching geometries exhibit opposite magnetic behaviors, such as weak ferromagnetism and strong antiferromagnetism. Broken symmetry-DFT demonstrated that this difference comes from orbital complementarity *versus* counter-complementarity in the bridging orbitals, a factor that cannot be presumed from the Cu–O–Cu angles or magnetic susceptibility alone. This study highlights how DFT can crumble exchange pathways into individual orbital contributions, relating electronic structure with macroscopic magnetism.[127]

4.2. Geometry optimization and structural predictions

Computational studies also help in geometry optimization of PNCCs and enable the prediction of the most stable configurations and coordination environments. DFT assists in validating experimental X-ray crystallography data or even predicting structures when crystallographic data are inaccessible. Additionally, it sheds light on the role of the nature of ligands, denticity, and coordination angles on the overall nuclearity and geometry of PNCCs.[128] For example, in the study by Liu *et al.*, time-dependent DFT (TD-DFT) provided decisive structural insights into the $[Cu_4(\mu_4\text{-S})]$ clusters that could not be fully resolved by diffraction or spectroscopic methods. DFT revealed a significant redox-driven distortion from a seesaw to a square-planar Cu_4S core, clarifying changes that were electronically governed rather than purely geometric. In addition, TD-DFT identified unequal Cu–S bond contractions and a π–π super exchange pathway through μ_4-S, explaining the magnetic behavior that experimental data alone could not justify. By quantifying spin delocalization and metal–ligand covalency, TD-DFT bridged the gap between the observed spectra and the fundamental electronic structure.[129]

4.3. Reactivity and functional property prediction

DFT aids in examining reactivity, including redox behavior, catalytic mechanisms, or binding preferences of Cu centers towards ligands and other molecules. It allows the estimation of HOMO–LUMO gaps, ligand field stabilization energies, and redox pathways.[130] Therefore, guiding the design of new PNCCs with desired properties.[130] Several researchers have studied the mechanism of Cu-complex-mediated NO_2^- reduction using spectroscopic and XRD techniques. However, these studies are limited because spectroscopic methods primarily measure N–O stretching frequencies and M–N–O angles.[131–135] Such data only help to identify intermediates and oxidation states, but do not disclose the exact reaction pathway. Consequently, researchers cannot trace the transient transition states or the detailed electron flow during the catalytic process. A study by Kametani and Shiota critically demonstrated that DFT calculations bridge the limitations of conventional spectroscopic methods by mapping the reaction pathway at the atomic level. Their work demonstrated that DFT not only explains the asynchronicity between proton and electron transfer in multistep processes but also elucidates the complex electron reorganization between Cu centers and ligands. These findings clarified the mechanistic details of nitrite (NO_2^-) and nitric oxide (NO) reduction by Cu complexes: the reduction of NO_2^- to NO through concerted proton-electron transfer and the dicopper-mediated reduction of NO to N_2O, involving N–N bond formation, N_2O_2 isomerization, and N–O bond cleavage.[136] This detailed electronic insight, inaccessible through experimental techniques alone, underscores the indispensable role of DFT in uncovering the true mechanism of Cu-mediated reduction of NO_2^-.

5. Structural diversity

In most PNCCs, the Cu ion exhibits distorted coordination geometries. It is predominantly due to the d^9 electronic configuration, which favors distorted geometries according to the Jahn–Teller distortion.[137] Moreover, according to the hard and soft acid–base (HSAB) theory, the Cu(II) ion acts as a borderline acid that exhibits intermediate properties between hard and soft acids. It typically adopts a coordination number in the range of 4–6 in its complexes, forming distorted square planar, tetrahedral, square-pyramidal and octahedral geometries.[138] Apart from this, some other factors such as the Cu-to-ligand ratio, nature of ligand and co-ligand, pH of medium and solvent also influence the coordination geometries of Cu ions, leading to widespread structural diversity.[137] These factors are outlined in the upcoming Sections from 4.1 to 4.4. The crystallographic structures of selected PNCCs are obtained from the Cambridge Crystallographic Data Center (CCDC). The *N*-heterocyclic multicarboxylic acid and amine-based ligands (Schemes 1 and 2, respectively) are vital for the synthesis and coordination behavior of polynuclear copper complexes. The influence of these ligands on the structure of Cu-centers in PNCCs is discussed in detail (Section 5.2).

5.1. Effect of copper-to-ligand stoichiometric ratio

The Cu-to-ligand ratio affects the structure and configuration of PNCCs. For example, using a 1 : 1 ratio of Cu(I) to bis(phenylthio)propane leads to the formation of the 2D coordination polymer $[\{Cu(\mu_2\text{-}I)_2Cu\}\{\mu\text{-}L^{34}\}_2]_n$, as depicted in Fig. 1(a). This structure features well-defined structural motifs, such as the $Cu(\mu_2\text{-}I)_2Cu$ unit, which are connected through four 1,3-bis(phenylthio)propane bridging ligands. On the other hand, reacting CuI with dithioether in a 2 : 1 ratio results in the development of $[Cu_4I_4\{\mu\text{-}L^{34}\}_2]_n$, as revealed in Fig. 1(b), in which cubane-like $Cu_4(\mu_3\text{-}I)_4$ clusters are connected through the dithioether ligand, leading to a 1D necklace structure.[139]

5.2. Effect of the nature of ligand, counter-ion and co-ligands

Carboxylic acid derivatives have been extensively used for the preparation of various metal organic frameworks (MOFs) and

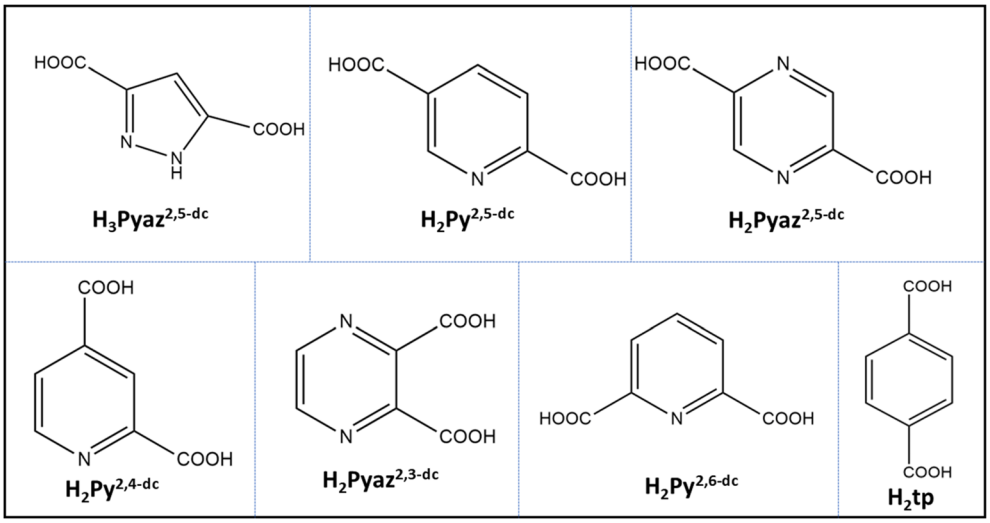

Scheme 1 Some selected *N*-heterocyclic multicorboxylic acid-based ligands discussed in this review.

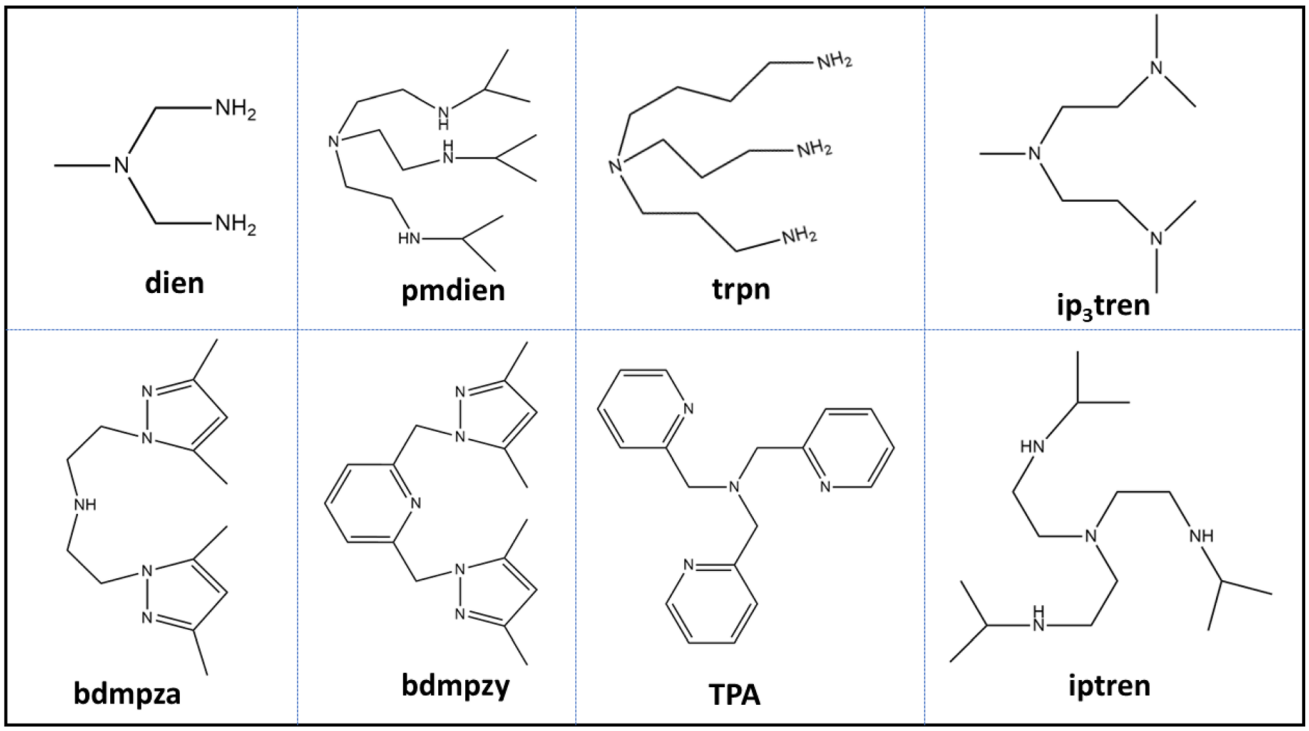

Scheme 2 Some selected amine-based ligands discussed in this review.

metal–organic coordination compounds because of their versatile physical properties, potential applications and fascinating architectural topologies.[140] It has been summarized that *via* the diverse bridging coordination modes, the interlinkage of multi-carboxylic acids with Cu ions leads to the construction of multinuclear Cu complexes and coordination polymers containing Cu in multidimensional systems.[141–143] The nature, flexibility and hydrogen-bonding ability of carboxylic acids determine their coordination modes. Furthermore, the geometry and characteristic topological coordination depend on the electronic nature of the Cu ion. Besides these, other auxiliary factors, such as the reaction conditions, solvent, pH, counter ion and nature of co-ligands, may affect the coordination between the carboxylic ligands and Cu centers.[144]

Massoud *et al.*[88] synthesized tri-nuclear Cu(II) complexes $[(TPA)Cu\text{-}(\mu_2\text{-}Py^{2,4\text{-}dc})_2\text{-}Cu(H_2O)_2\text{–}Cu(TPA)](ClO_4)_2$, $[Cu(TPA)\text{-}Cu(\mu_2\text{-}Py^{2,4\text{-}dc})_2\text{-}Cu(TPA)](ClO_4)$, and $[(TPA)Cu\text{-}(\mu_2\text{-}\ Pyaz^{2,3\text{-}dc})_2\text{-}Cu(ClO_4)_2\text{–}Cu(TPA)][Cu(TPA)(H_2O)]_2(ClO_4)_4\cdot H_2O$ and binuclear complexes $[Cu_2(iptren)_2(tp)](ClO_4)_2$ and $[Cu_2(iptren)_2(\text{-}Pyaz^{2,5\text{-}dc})](ClO_4)_2\cdot H_2O$, which are bridged by multi-carboxylic acid compounds, using the tripod co-ligands iptren and TPA and multi-carboxylic acid ligands, such as $H_2Pyaz^{2,3\text{-}dc}$, $H_2\text{-}Pyaz^{2,5\text{-}dc}$, $H_2Py^{2,4\text{-}dc}$ and $H_2Py^{2,5\text{-}dc}$ and H_2tp.[99] In $[(TPA)Cu\text{-}(\mu_2\text{-}Py^{2,4\text{-}dc})_2\text{-}Cu(H_2O)_2\text{-}Cu(TPA)](ClO_4)_2$, $[Cu(TPA)\text{-}Cu(\mu_2\text{-}Py^{2,4\text{-}dc})_2\text{-}Cu(TPA)](ClO4)$ and $[(TPA)Cu\text{-}(\mu_2\text{-}\ Pyaz^{2,3\text{-}dc})_2Cu(ClO_4)_2\text{–}Cu(TPA)][Cu(TPA)(H_2O)]_2(ClO_4)_4\cdot H_2O$ (shown in Fig. 2(a–c)), within each tri-nuclear unit, the central Cu(II) ion is positioned at an inversion center and coordinated by two hetero-atomic di-

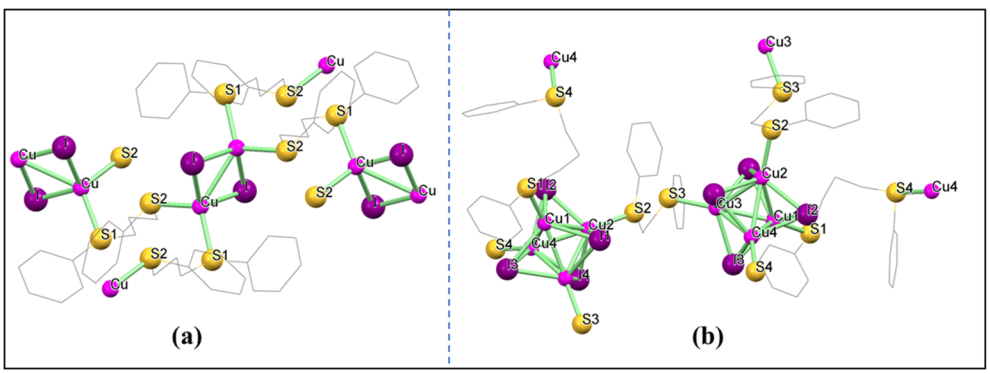

Fig. 1 Structural views of the 2D chain of polymer $[\{Cu(\mu_2\text{-}I)_2Cu\}\{\mu\text{-}L^{34}\}_2]_n$ (a) and the 1D necklace structure of $[Cu_4I_4\{\mu\text{-}L^{34}\}_2]_n$ (b). Their CCDC numbers are 906347 and 906348, respectively.

carboxylate ligands *via* their ring nitrogen atom and one carboxylate oxygen atom from a neighboring group, enabling N,O-chelate interactions. Conversely, the terminal Cu(II) centers are bridged by hetero-aromatic di-carboxylate anions through the oxygen atoms of the second carboxylate group, thus acting as N,O,O bridging ligands. In the [Cu(TPA)-Cu(μ_2-$Py^{2,4\text{-dc}}$)$_2$-Cu(TPA)](ClO$_4$) complex, the central Cu(II) atom adopts a square planar CuN_2O_2 geometry, while the central Cu(II) atoms in [(TPA)Cu-(μ_2-$Py^{2,4\text{-dc}}$)$_2$-Cu(H_2O)$_2$–Cu(TPA)](ClO$_4$)$_2$ and [(TPA)Cu-(μ_2- $Pyaz^{2,3\text{-dc}}$)$_2$Cu(ClO$_4$)$_2$–Cu(TPA)][Cu(TPA)(H_2O)]$_2$(ClO$_4$)$_4$·H_2O complexes have an extended octahedral CuO_4N_2 core with two additional trans coordinated oxygen atoms from H_2O molecules (in the case of [(TPA)Cu-(μ_2-$Py^{2,4\text{-dc}}$)$_2$-Cu(H_2O)$_2$–Cu(TPA)](ClO$_4$)$_2$) and from perchlorate (ClO$_4$) (in the case of [(TPA)Cu-(μ_2- $Pyaz^{2,3\text{-dc}}$)$_2$Cu(ClO$_4$)$_2$–Cu(TPA)][Cu(TPA)(H_2O)]$_2$(ClO$_4$)$_4$·H_2O). In [(TPA)Cu-(μ_2-$Py^{2,4\text{-dc}}$)$_2$-Cu(H_2O)$_2$–Cu(TPA)](ClO$_4$)$_2$, [Cu(TPA)-Cu(μ_2-$Py^{2,4\text{-dc}}$)$_2$-Cu(TPA)](ClO$_4$) and [(TPA)Cu-(μ_2- $Pyaz^{2,3\text{-dc}}$)$_2$Cu(ClO$_4$)$_2$–Cu(TPA)][Cu(TPA)(H_2O)]$_2$(ClO$_4$)$_4$·H_2O, each terminal Cur(II) ion is five-coordinated with one oxygen atom of a carboxylate group and four nitrogen atoms of the TPA ligand. These terminal Cu(II) centers adopt distorted trigonal bipyramidal geometries with *s*-values of 0.72, 0.63 and 0.85 for [(TPA)Cu-(μ_2-$Py^{2,4\text{-dc}}$)$_2$-Cu(H_2O)$_2$–Cu(TPA)](ClO$_4$)$_2$, [Cu(TPA)-Cu(μ_2-$Py^{2,4\text{-dc}}$)$_2$-Cu(TPA)](ClO$_4$) and [(TPA)Cu-(μ_2-$Pyaz^{2,3\text{-dc}}$)$_2$Cu(ClO$_4$)$_2$–Cu(TPA)][Cu(TPA)(H_2O)]$_2$(ClO$_4$)$_4$·H_2O, respectively.[145]

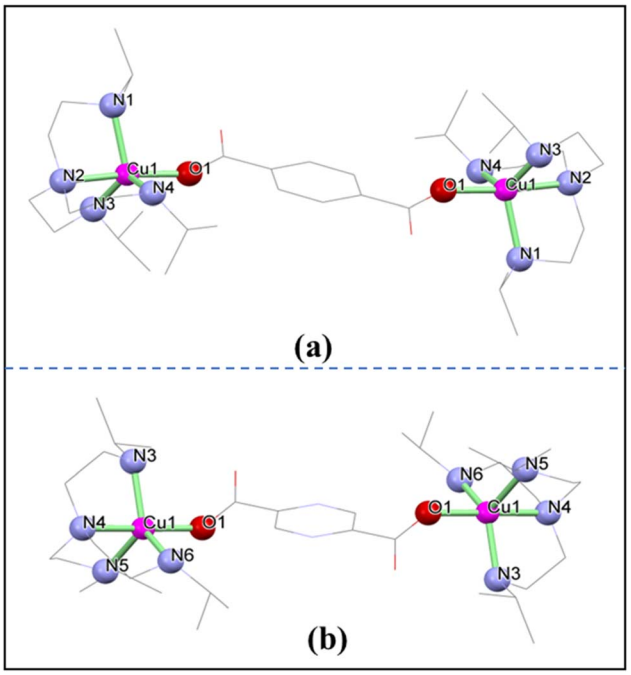

Fig. 3 Structural views of [Cu_2(iptren)$_2$(tp)](ClO$_4$)$_2$ (a) and [Cu_2(-iptren)$_2$($Pyaz^{2,5\text{-dc}}$)](ClO$_4$)$_2$·H_2O (b). Their CCDC numbers are 1441268 and 1441269, respectively.

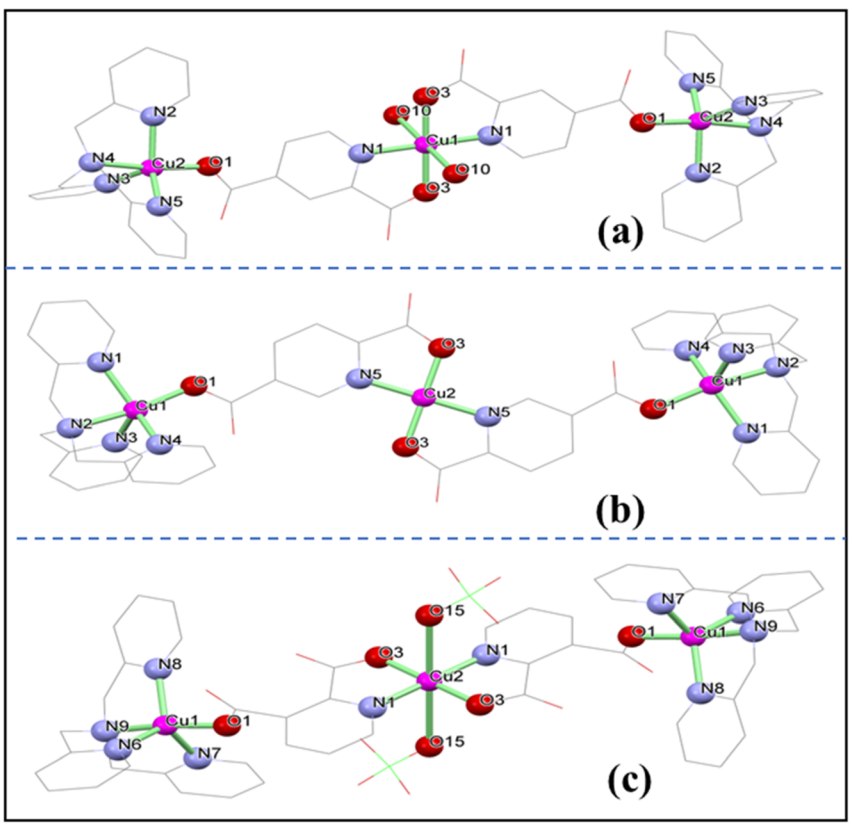

Fig. 2 Structural views of [(TPA)Cu-(μ_2-$Py^{2,4\text{-dc}}$)$_2$-Cu(H_2O)$_2$–Cu(TPA)](ClO$_4$)$_2$ (a), [Cu(TPA)-Cu(μ_2-$Py^{2,4\text{-dc}}$)$_2$-Cu(TPA)](ClO$_4$) (b) and [(TPA)Cu-(μ_2-$Pyaz^{2,3\text{-dc}}$)$_2$Cu(ClO$_4$)$_2$–Cu(TPA)][Cu(TPA)(H_2O)]$_2$(ClO$_4$)$_4$·H_2O (c). Their CCDC numbers are 1441265, 1441266 and 1441267, respectively.

In $[Cu_2(iptren)_2(tp)](ClO_4)_2$ and $[Cu_2(iptren)_2(Pyaz^{2,5\text{-dc}})](ClO_4)_2\cdot H_2O$, the di-carboxylato anions act as bis-monodentate ligands that link the two Cu-centers. The crystal structures of $[Cu_2(iptren)_2(tp)](ClO_4)_2$ and $[Cu_2(iptren)_2(Pyaz^{2,5\text{-dc}})](ClO_4)_2\cdot H_2O$, shown in Fig. 3(a and b), contain di-nuclear complex cations: $[Cu_2(iptren)_2(\mu_2\text{-tp})]^{2+}$ and $[Cu_2(iptren)_2(\mu_2\text{-Pyaz}^{2,5\text{-dc}})]^{2+}$, respectively. In both complexes, each Cu center is penta-coordinated by one oxygen of the carboxylate group and four nitrogen atoms of the iptren ligand, forming a distorted CuN_4O core with trigonal bi-pyramidal geometry. The geometries are characterized by *s* values of 0.67 and 0.86 for $[Cu_2(iptren)_2(tp)](ClO_4)_2$ and $[Cu_2(iptren)_2(Pyaz^{2,5\text{-dc}})](ClO_4)_2\cdot H_2O$, respectively.[97]

Louka *et al.*[98] prepared three trinuclear Cu(II) complexes: $[Cu_3(dien)_2(\mu_2\text{-Pz}^{3,5\text{-dc}})_2(H_2O)_2]\cdot 4H_2O$, $[Cu_3(pmdien)_2(\mu\text{-Py}^{2,5\text{-dc}})_2(ClO_4)_2(H_2O)_2]$, $[Cu_3(trpn)_2(\mu\text{-Py}^{2,5\text{-dc}})_2(ClO_4)_2]$, and one dinuclear complex centa-$[Cu_2(bedmpza)(\mu_2\text{-Py}^{2,4\text{-dc}})](ClO_4)_2\cdot H_2O$ using $H_3Pz^{3,5\text{-dc}}$, $H_2Py^{2,4\text{-dc}}$, and $H_2Py^{2,5\text{-dc}}$ as ligands, along with polyamine co-ligands, such as dien, pmdien, bedmpza, and trpn. The common feature of $[Cu_3(dien)_2(\mu_2\text{-Pz}^{3,5\text{-dc}})_2(H_2O)_2]\cdot 4H_2O$, $[Cu_3(pmdien)_2(\mu\text{-Py}^{2,5\text{-dc}})_2(ClO_4)_2(H_2O)_2]$ and $[Cu_3(trpn)_2(\mu\text{-Py}^{2,5\text{-dc}})_2(ClO_4)_2]$ (as shown in Fig. 4(a–c)) is a centrosymmetric trinuclear subunit. In each trinuclear subunit, the central Cu(II) atom is positioned at the inversion center and is coordinated to two chelating di-carboxylato anionic ligands through the nitrogen and oxygen atoms on the ring of the neighboring ligand. In $[Cu_3(dien)_2(\mu_2\text{-Pz}^{3,5\text{-dc}})_2(H_2O)_2]\cdot 4H_2O$, the di-carboxylate ligands act in a bis-N,O bridging mode, connecting the terminal Cu(II) ions through the second-ring nitrogen and oxygen atoms from another carboxylate group. Conversely, in $[Cu_3(pmdien)_2(\mu\text{-Py}^{2,5\text{-dc}})_2(ClO_4)_2(H_2O)_2]$ and $[Cu_3(trpn)_2(\mu\text{-Py}^{2,5\text{-dc}})_2(ClO_4)_2]$, the ligands adopt an N,O,O bridging mode, linking the peripheral Cu(II) ions using only the single oxygen atom of the carboxylate group. In all three complexes ($[Cu_3(dien)_2(\mu_2\text{-Pz}^{3,5\text{-dc}})_2(H_2O)_2]\cdot 4H_2O$, $[Cu_3(pmdien)_2(\mu\text{-Py}^{2,5\text{-dc}})_2(ClO_4)_2(H_2O)_2]$ and $[Cu_3(trpn)_2(\mu\text{-Py}^{2,5\text{-dc}})_2(ClO_4)_2]$), the central Cu(II) ion exhibits an axially elongated CuO_4N_2 octahedral geometry, additionally coordinated by two trans oxygen atoms, either from the H_2O molecules in $[Cu_3(dien)_2(\mu_2\text{-Pz}^{3,5\text{-dc}})_2(H_2O)_2]\cdot 4H_2O$ or the perchlorate anions in $[Cu_3(pmdien)_2(\mu\text{-Py}^{2,5\text{-dc}})_2(ClO_4)_2(H_2O)_2]$ and $[Cu_3(trpn)_2(\mu\text{-Py}^{2,5\text{-dc}})_2(ClO_4)_2]$. The peripheral Cu(II) ions in $[Cu_3(dien)_2(\mu_2\text{-Pz}^{3,5\text{-dc}})_2(H_2O)_2]\cdot 4H_2O$ and $[Cu_3(pmdien)_2(\mu\text{-Py}^{2,5\text{-dc}})_2(ClO_4)_2(H_2O)_2]$ adopt square pyramidal geometries, with τ-values of 0.22 and 0.26, respectively. The CuN_4O chromophore in $[Cu_3(dien)_2(\mu_2\text{-Pz}^{3,5\text{-dc}})_2(H_2O)_2]\cdot 4H_2O$ is composed of one nitrogen atom and one oxygen atom from the $Pz^{2,5\text{-dc}}$ ligand, as well as three nitrogen atoms from the dien ligand. Conversely, $[Cu_3(pmdien)_2(\mu\text{-Py}^{2,5\text{-dc}})_2(ClO_4)_2(H_2O)_2]$ has a CuN_3O_2 chromophore that is made by two oxygen atoms, one from carboxylato and the other from the terminal H_2O ligand, while three nitrogen atoms are from the pmdien ligand. $[Cu_3(trpn)_2(\mu\text{-Py}^{2,5\text{-dc}})_2(ClO_4)_2]$ also has CuN_4O, where one oxygen atom comes from carboxylato and four nitrogen atoms from the trpn ligand. The coordination environment around the metal center in $[Cu_3(trpn)_2(\mu\text{-Py}^{2,5\text{-dc}})_2(ClO_4)_2]$ can be described as a distorted trigonal bipyramid, with a τ-value of 0.87%.[145]

The structure of centa-$[Cu_2(bedmpza)(\mu_2\text{-Py}^{2,4\text{-dc}})](ClO_4)_2\cdot H_2O$, depicted in Fig. 5, is composed of a polymeric cationic chain consisting of $[Cu(bedmpza)(\mu_2\text{-Py}^{2,4\text{-dc}})$ units, with perchlorate anions acting as counterions. The first Cu ion (Cu_1) is penta-coordinated, bonded to the $Py^{2,4\text{-dc}}$ ligand *via* a pyridil nitrogen and carboxylate oxygen, and to the bedmpza ligand through three nitrogen atoms. The second Cu ion (Cu_2) is also penta-coordinated, being coordinated to the $Py^{2,4\text{-dc}}$ anions *via* two oxygen atoms and the bedmpza ligand *via* three nitrogen atoms. Thus, the $Py^{2,4\text{-dc}}$ ligand exhibits an N, O, O-bridging

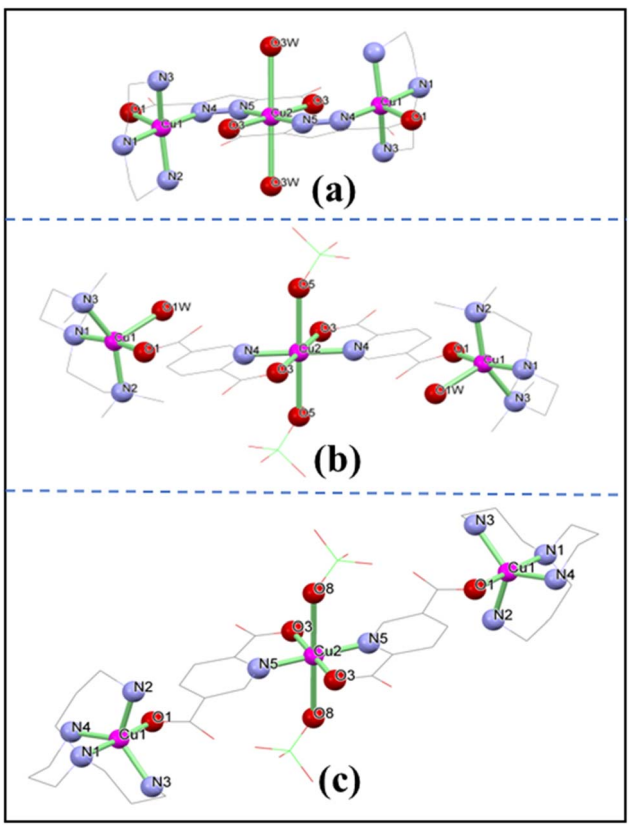

Fig. 4 Structural views of $[Cu_3(dien)_2(\mu_2\text{-Pz}^{3,5\text{-dc}})_2(H_2O)_2]\cdot 4H_2O$ (a), $[Cu_3(pmdien)_2(\mu\text{-Py}^{2,5\text{-dc}})_2(ClO_4)_2(H_2O)_2]$ (b), and $[Cu_3(trpn)_2(\mu\text{-Py}^{2,5\text{-dc}})_2(ClO_4)_2]$ (c). Their CCDC numbers are 1951426, 1951427 and 1951428, respectively.

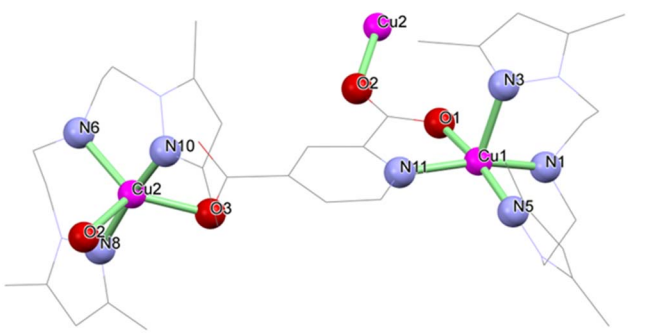

Fig. 5 Structural view of the 1D chain of centa-$[Cu_2(bedmpza)(\mu_2\text{-Py}^{2,4\text{-dc}})](ClO_4)_2\cdot H_2O$. Its CCDC number is 1951429.

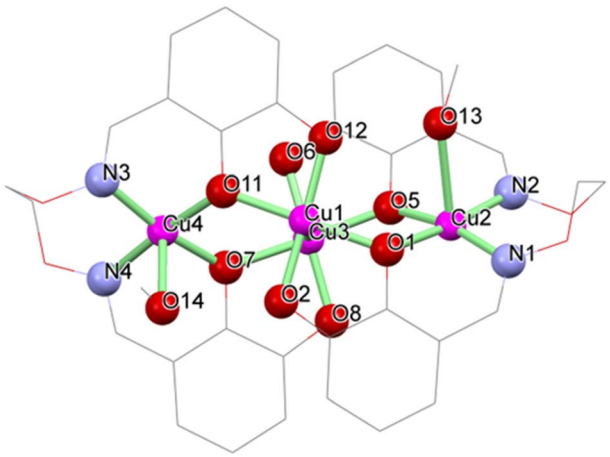

Fig. 6 Structural view of $[Cu_4(L^5)_2(MeOH)_2]\cdot 2MeOH$. Its CCDC number is 2255118.

coordination mode, connecting the Cu ions along the polymeric chain. Cu_1 adopts a distorted square pyramidal CuN_4O geometry, characterized by a τ-value of 0.19, whereas Cu_2 exhibits a distorted trigonal bi-pyramidal CuN_3O_2 geometry, with a τ-value of 0.62.

The tetra-nuclear $[Cu_4(L^5)_2(MeOH)_2]\cdot 2MeOH$ structure (depicted in Fig. 6) consists of four Cu(II) centers, where two deprotonated/anionic ligands "L^5" and two coordinated CH_3OH molecules exist. The Cu_1 atom is tetra-coordinated by four oxygen atoms of the L^{4-} ligand, adopting a slightly distorted planar quadrilateral geometry. Likewise, the central Cu_3 ion is coordinated to two L^{4-} ligands through four oxygen atoms, also adopting a slightly distorted planar quadrilateral geometry. The basal plane of Cu(II) is formed by two oxygen atoms of phenol and two nitrogen atoms of the oxime. Characteristically, the axial position of Cu_1 is occupied by one oxygen atom of the coordinated CH_3OH molecule and interacts with the terminal Cu_2 ion, resulting in a distorted tetragonal pyramid geometry with a τ-value of 0.11. The axial site of Cu_4 is coordinated by an oxygen atom of another coordinated CH_3OH, adopting a penta-coordinated, slightly twisted tetragonal pyramid geometry with a τ-value of 0.10.[146]

In the crystal structure of $[(H_2O)Cu_{0.5}\{\mu\text{-}L^6\text{-}1\kappa O{:}2\kappa^3 N,O',O''\}Cu(H_2O)_2\}_2$, as shown in Fig. 7(a), the Cu ions have different geometries because of the different modes of coordination. One of the central metal atoms possesses a distorted square pyramidal geometry with a τ_5 value of 0.24,[145] whereas another Cu atom has a square pyramidal geometry with a τ_4 value of 0.19 and is located at an inversion center.[147] The square planner geometry of one Cu center is constructed by two oxygen atoms of the $(L^6)^{3-}$ ligand and two oxygen atoms of coordinated water molecules. The geometry of the other peripheral Cu center is formed by $(L^6)^{3-}$, which occupies the three coordination basal sites, along with one coordinated water molecule. This Cu ion is positioned a little above the basal plane toward the apex, coordinating with the H_2O molecule. The Cu center participates in two fused six-membered metallocycles of $CuOC_2N_2$ and $CuNC_3O$ types because of the tridentate coordination of the $(L)^{3-}$ ligand. In the structure of $[(H_2O)Cu_{0.5}\{\mu\text{-}L^6\text{-}1\kappa O{:}2\kappa^3 N,O',O''\}Cu(H_2O)_2\}_2$, the shortest intramolecular Cu$\cdots$Cu distance is 9.6486(4) Å, whereas the intermolecular Cu(1)$\cdots$Cu(2) distance is 5.245 Å, which is considerably shorter than the intramolecular distance. The 3D framework is further stabilized

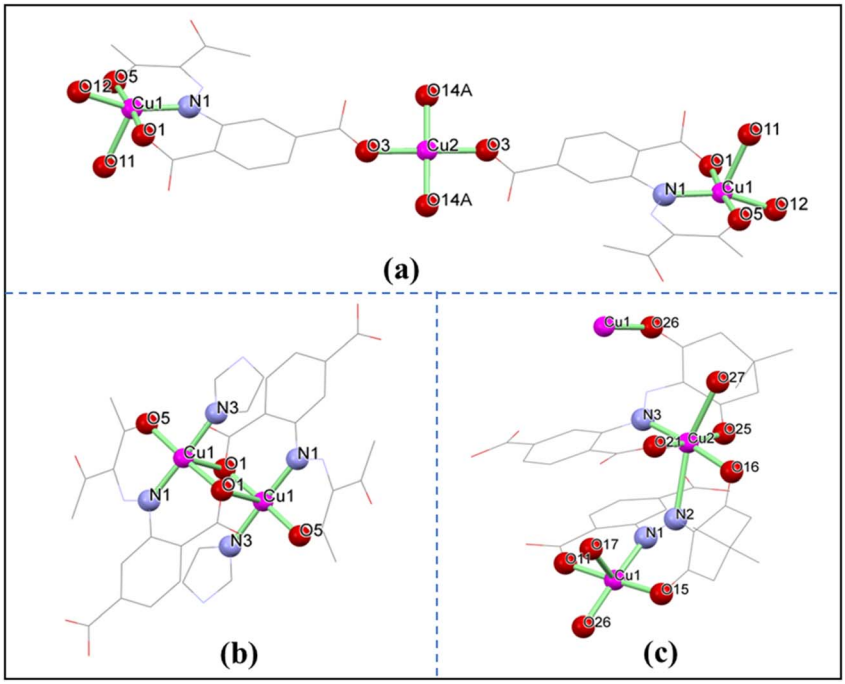

Fig. 7 Structural views of $[(H_2O)Cu_{0.5}\{\mu\text{-}L^6\text{-}1\kappa O{:}2\kappa^3 N,O',O''\}Cu(H_2O)_2\}_2$ (a), $[Cu(im)(\mu\text{-}HL^6\text{-}1\kappa O{:}2\kappa^3 N,O,O')]_2$ (b) and the 1D chain of $[Cu_2(H_2O)_2(\mu\text{-}H_2L^7\text{-}1\kappa^3 N,O,O{:}2\kappa O'')(\mu\text{-}L\text{-}1\kappa^3 N,O,O'{:}2\kappa^2 N',O'')]_n$ (c). Their CCDC numbers are 996620, 996621 and 996622, respectively.

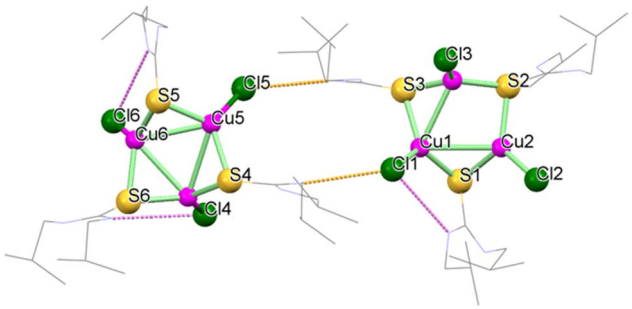

Fig. 8 Structural view of $[Cu_3(L^8)_3Cl_3]$, stabilized by the inter and intra molecular N–H···Cl interactions shown by orange and violet dotted lines, respectively. Its CCDC number is 2196016.

by hydrogen bonding, originating from the coordinated H_2O molecules (donors) and oxygen atoms of the $(L^6)^{3-}$ ligand (acceptors).

The L^6 ligand exhibits different coordination modes in $[Cu(im)(\mu\text{-}HL^6\text{-}1\kappa O{:}2\kappa^3N,O,O')]_2$, as shown in Fig. 7(b). The $[Cu(im)(\mu\text{-}HL^6\text{-}1\kappa O{:}2\kappa^3N,O,O')]_2$ complex comprises a Cu dimer containing a centrosymmetric Cu_2O_2 core. The dianionic $(HL^6)^{2-}$ species acts as a tridentate ligand through a carboxylate group and also acts as a bridging bidentate ligand between two Cu centers. The imidazole group completes the coordination sphere of each Cu center. Therefore, each Cu center adopts a perfect square-pyramidal geometry with a τ_5 value of 0.01.[145] The central Cu_2O_2 unit, along with two six-membered $CuOC_2N_2$ and $CuNC_3O$ rings, is structurally similar to that observed in $[(H_2O)Cu_{0.5}\{\mu\text{-}L^6\text{-}1\kappa O{:}2\kappa^3N,O',O''\}Cu(H_2O)_2\}_2$. The dihedral angle between the Cu_2O_2 plane and the square plane formed by the coordinated atoms is 89.07°, indicating an almost perpendicular orientation. The Cu···Cu distance within the Cu_2O_2 core is 3.4583 Å, while the intermolecular Cu···Cu separation is 3.4935 Å. The 3D framework is further stabilized by the hydrogen bonding between the nitrogen atom of the imidazole and the carboxylic acid group (as a donor) and the oxygen atom of the free keto group (as an acceptor).[145]

The crystal of the 1D coordination polymer $[Cu_2(H_2O)_2(\mu\text{-}H_2L^7\text{-}1\kappa^3N,O,O{:}2\kappa O'')(\mu\text{-}L\text{-}1\kappa^3N,O,O'{:}2\kappa^2N',O'')]_n$, shown in Fig. 7(c), is composed of two Cu(II) ions ligated by two hydrazinyl-based ligands and two H_2O molecules. These two Cu ions show different geometries because of the different coordination modes of the ligand. One of the Cu ions adopts a square-pyramidal O_4N geometry with a τ_5 value of 0.02,[145] whereas the other exhibits a distorted-octahedral O_4N_2 geometry (1.058 quadratic elongation and 82.32°).[148] The hydrogen atom of the hydrozone group prevents the octahedral elongation of the metal ion. One ligand binds to one Cu(II) ion in the κ^2-N, O mode, while the other binds in the κ^3-N′, O′, O″ mode. Conversely, the second ligand coordinates to one Cu(II) ion *via* the κ^3-N, O, O′ mode and bridges to the other through the keto oxygen atom. In both Cu centers, an axially coordinated H_2O molecule completes the coordination sphere. For Cu···Cu, the shortest intra-chain distance is 5.220(1) Å and the inter-chain Cu···Cu distance is 6.661(1) Å. The structure of the 1D chain of $[Cu_2(H_2O)_2(\mu\text{-}H_2L^7\text{-}1\kappa^3N,O,O{:}2\kappa O'')(\mu\text{-}L\text{-}1\kappa^3N,O,O'{:}2\kappa^2N',O'')]_n$ is further stabilized by hydrogen boding, originating from the interaction of the coordinated H_2O molecules (as the donor) and the carboxylate atom (as the acceptor).

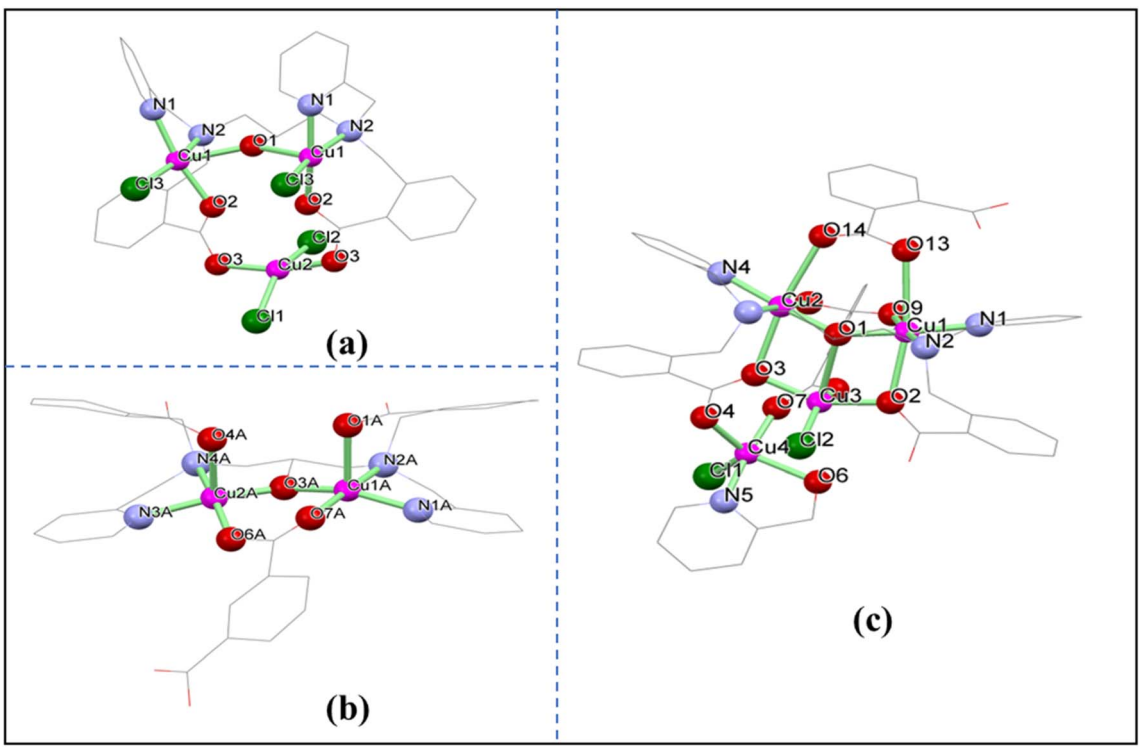

Fig. 9 Structural views of $[Cu_2(L^9)(\mu\text{-Hisophth})]_4\cdot 2H_2O$isophth$\cdot 21H_2O$ (a), $[Cu_3(L^9)(Cl)_4]$ (b), and $Cu_4(L^9)(\mu\text{-Hphth})(\mu_4\text{-phth})(piconol)(Cl)_2]\cdot 3H_2O$ (c). Their CCDC numbers are 2184098, 2184099 and 2184128, respectively.

Fig. 8 shows the crystal structure of a trimeric $[Cu_3(L^8)_3Cl_3]$. Its unit cell consists of two diastereomers.[149] In the crystal structure of complex-24, the monomeric part (L-M-Cl) is connected by the sulfur atom of the C=S group of thiourea, thus providing the Cu_3S_3 metalacyclic six-membered ring and adopting a chair conformation. At an axial position, the chlorine atom is coordinated to the Cu center. Each Cu ion displays a distorted trigonal planar geometry with varying angles in the range of 116.61°–124.36° around the Cu center. The Cu–S bond length is 2.258 Å,[150,151] and the Cu–Cl bond distance is 2.182 Å, which is shorter than that of the mononuclear complex [2.272(3) Å] with a similar ligand. In the trinuclear unit, the trigonal arrangement of Cu–Cu is stabilized by the interaction between the Cu ions at a distance of 2.850 Å.[152,153] Through a regular pattern of inter- and intra-molecular hydrogen bonding, the N–H···Cl interactions stabilize the supramolecular structure of the complex, as shown in Fig. 8.

5.3. Effect of pH and ancillary ligands

The pH values of the solution and the ancillary ligand play a significant role in the structure and composition of PNCCs. For example, Majumder *et al.*[154] described that the formation of $[Cu_2(L^9)(\mu\text{-Hisophth})]_4\cdot 2H_2$isophth$\cdot 21H_2O$, $[Cu_3(L^9)(Cl)_4]$, and $[Cu_4(L^9)(\mu\text{-Hphth})(\mu_4\text{-phth})(piconol)(Cl)_2]\cdot 3H_2O$ is strongly affected by the pH of the solution and the choice of ancillary ligands. This control over the ligand and solution pH allowed for effective tuning of the assembly process, resulting in the synthesis of PNCCs with distinct nuclearities and coordination environments around the Cu(II) ions. The structures of $[Cu_2(L^9)(\mu\text{-Hisophth})]_4\cdot 2H_2$isophth$\cdot 21H_2O$, $[Cu_3(L^9)(Cl)_4]$ and $Cu_4(L^9)(\mu\text{-Hphth})(\mu_4\text{-phth})(piconol)(Cl)_2]\cdot 3H_2O$ are depicted in Fig. 9(a–c). The $[Cu_3(L^9)(Cl)_4]$ and $Cu_4(L^9)(\mu\text{-Hphth})(\mu_4\text{-phth})(piconol)(Cl)_2]\cdot 3H_2O$ complexes are rare examples that exhibit characteristic topographies of rich coordination chemistry. For instance, the trinuclear $[Cu_3(L^9)(Cl)_4]$ complex is produced with tetra- and penta-coordinated geometries around the Cu(II) ions using a regular di-nucleating ligand, while the tetranuclear $Cu_4(L^9)(\mu\text{-Hphth})(\mu_4\text{-phth})(piconol)(Cl)_2]\cdot 3H_2O$ is produced using the same ligand with tetra-, penta-, and hexa-coordinated geometries around the Cu(II) ions. At about pH 3, $[Cu_3(L^9)(Cl)_4]$ is formed, while at pH 6.5, $[Cu_2(L^9)(\mu\text{-Hisophth})]_4\cdot 2H_2$isophth$\cdot 21H_2O$ and $Cu_4(L^9)(\mu\text{-Hphth})(\mu_4\text{-phth})(piconol)(Cl)_2]\cdot 3H_2O$ are produced. The pH controls the deprotonation of the H_3cdpd ligand.

5.4. Effect of solvent

Solvent plays a significant role in the structure and composition of coordination polymers (CPs). For example, Bazhina *et al.*[155] reported that the reaction of Cu(II) trimethylacetate with the Schiff base, 4-(pyridine-3-yl)methyleneamino-1,2,4-triazole (L^{10}), in different solvents leads to the formation of different CPs. The reaction of $[Cu_2(piv)_4(Hpiv)_2]$ in acetonitrile (MeCN, as a solvent) leads to the formation of a 1D polymeric chain of $\{[Cu_2(piv)_4(L^{10})]\cdot MeCN\}_n$, as shown in Fig. 10(a), which is

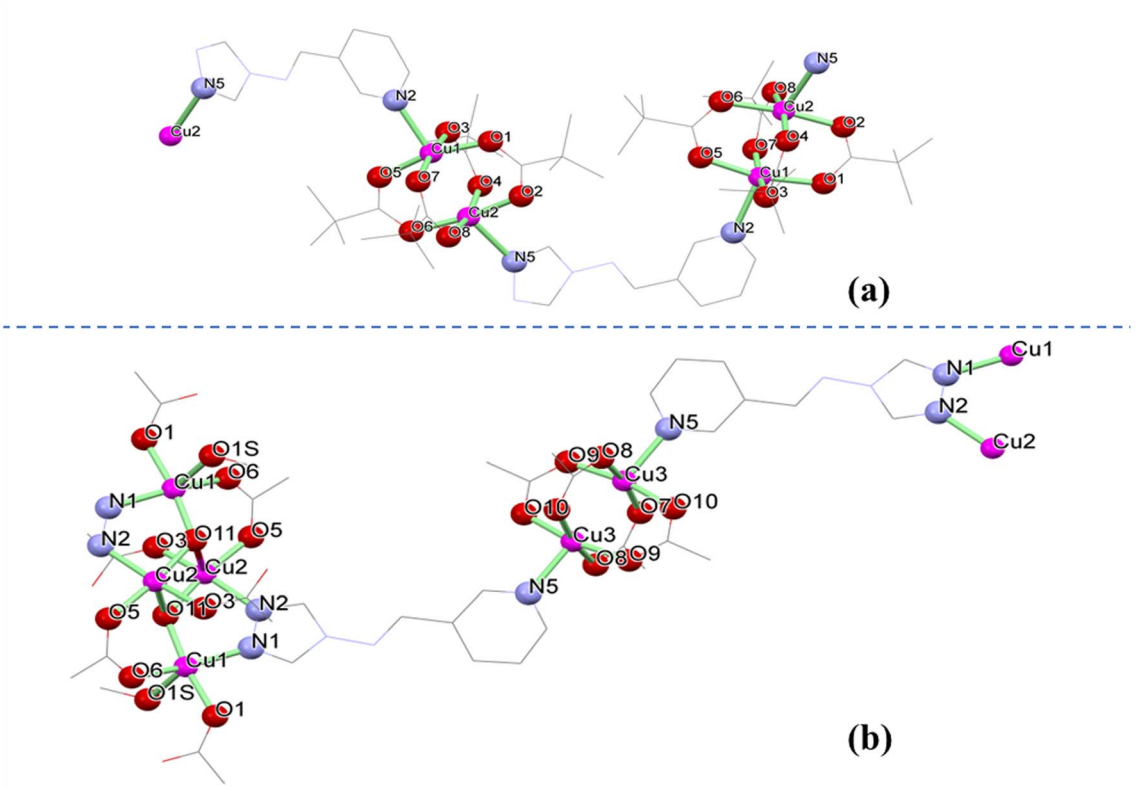

Fig. 10 Structural views of the polymeric chains of $\{[Cu_2(piv)_4(L^{10})]\cdot MeCN\}_n$ (a) and $[Cu_6(OH)_2(piv)_{10}(L^{10})_2(MeOH)_2]\cdot 4MeOH]_n$ (b). Their CCDC numbers are 2157254 and 2157255, respectively.

composed of a bi-nuclear paddle-wheel $\{Cu_2(\mu\text{-piv})_4\}$ unit connected by the bridging organic ligand. The coordination environment of these Cu ions reveals slightly distorted square pyramidal geometries. On the other hand, the same reaction in methanol or ethanol results in the formation of the 1D CPs, $[Cu_6(OH)_2(piv)_{10}(L^{10})_2(MeOH)_2\}\cdot 4MeOH]_n$ and tetranuclear $\{Cu_4(OH)_2(piv)_6(L)_2(EtOH)_2\}$. The structure of $[Cu_6(OH)_2(piv)_{10}(L^{10})_2(MeOH)_2\}\cdot 4MeOH]_n$ is composed of alternating binuclear $\{Cu_2(piv)_4\}$ units linked by an N-ligand, as shown in Fig. 10(b).

6. Applications of PNCCs

6.1. Reactivity and catalysis

PNCCs are widely used as catalysts due to their characteristic ability to mimic natural metalloenzymes. Their significant advantages over other catalysts include efficient activation of molecular oxygen, redox flexibility {Cu(I)/Cu(II) or Cu(II)/Cu(III)} and ability to stabilize reactive intermediates. These properties enable selective and mild oxidation reactions that are frequently challenging for traditional catalysts. For example, the aerial oxidation of L-ascorbic acid is catalyzed by a binuclear $[Cu_2L^1](ClO_4)_2$ complex under mild conditions.[8] This study shows that $[Cu_2L^1](ClO_4)_2$ enables the redox conversion of ascorbic acid under mild conditions by mimicking natural enzymes (oxidases). $[Cu_2L^1](ClO_4)_2$ enhances the oxidation rate through electron transfer between the Cu centers. Additionally, $[Cu_3(L^3)Cl_4]$ and $[Cu(L^4)N_3]_n$ show galactose oxidase-mimicking activity and have demonstrated the ability to oxidize benzyl alcohol into benzyl aldehyde in the presence of *tert*-butyl hydroperoxide.[15] This study indicates that the catalytic oxidation pathway of $[Cu_3(L^3)Cl_4]$ and $[Cu(L^4)N_3]_n$ supports a biomimetic approach to alcohol dehydrogenation, making them favorable candidates for green oxidation catalysts.

Besides these, other complexes, such as $[(H_2O)Cu_{0.5}\{\mu\text{-}L^6\text{-}1\kappa O{:}2\kappa^3N,O',O''\}Cu(H_2O)_2\}_2$, $[Cu(im)(\mu\text{-}HL^6\text{-}1\kappa O{:}2\kappa^3N,O,O')]_2$, and $[Cu_2(H_2O)_2(\mu\text{-}H_2L^7\text{-}1\kappa^3N,O,O{:}2\kappa O'')(\mu\text{-L-}1\kappa^3N,O,O'{:}2\kappa^2N',O'')]_n$, oxidize cyclohexane under acid-free conditions.[9] $[(H_2O)Cu_{0.5}\{\mu\text{-}L^6\text{-}1\kappa O{:}2\kappa^3N,O',O''\}Cu(H_2O)_2\}_2$ and $[Cu_2(H_2O)_2(\mu\text{-}H_2L^7\text{-}1\kappa^3N,O,O{:}2\kappa O'')(\mu\text{-L-}1\kappa^3N,O,O'{:}2\kappa^2N',O'')]_n$ selectively oxidize cyclohexane to cyclohexanone over cyclohexanol at low concentrations. The catalytic activities of $[(H_2O)Cu_{0.5}\{\mu\text{-}L^6\text{-}1\kappa O{:}2\kappa^3N,O',O''\}Cu(H_2O)_2\}_2$ and $[Cu_2(H_2O)_2(\mu\text{-}H_2L^7\text{-}1\kappa^3N,O,O{:}2\kappa O'')(\mu\text{-L-}1\kappa^3N,O,O'{:}2\kappa^2N',O'')]_n$ are due to the uncoordinated acidic –COOH groups acting in a dual role: functioning as the main catalyst and as an acid catalyst, which promotes the oxidative reaction process. For an in-depth investigation of the catalytic mechanisms of $[(H_2O)Cu_{0.5}\{\mu\text{-}L^6\text{-}1\kappa O{:}2\kappa^3N,O',O''\}Cu(H_2O)_2\}_2$ and $[Cu_2(H_2O)_2(\mu\text{-}H_2L^7\text{-}1\kappa^3N,O,O{:}2\kappa O'')(\mu\text{-L-}1\kappa^3N,O,O'{:}2\kappa^2N',O'')]_n$, a series of reactions involving oxygen-radical and carbon-radical traps revealed a significant decrease in the reaction rate. This suggests that both carbon and oxygen radicals are equally important for the catalytic activity. Moreover, the radical mechanism may be driven by the hydroxyl free radical.

Further insights into the oxygen-activation behavior of PNCCs have been comprehensively described by Singh *et al.*[156] They explored the reactivity of trinuclear and tetranuclear Cu(I)-based complexes with small molecules, like O_2 and CO. Their work demonstrated that these Cu(I) assemblies could reversibly bind CO and undergo controlled structural reorganizations upon O_2 exposure, thereby exhibiting stepwise electron transfer between Cu centers, a key characteristic of biological multicopper oxidases enzymes, such as laccase and ceruloplasmin. Although no stable Cu_3O core was isolated, the study underlined the effect of ligand coordination and nuclearity, which strongly govern the oxygen-activation pathway.[156] These findings effectively bridge the theoretical gap between synthetic PNCCs and natural oxygenase enzymes, providing a deeper understanding of how multi Cu clusters facilitate selective oxidation through cooperative redox processes. A general catalytic mechanism of PNCCs, as shown in Fig. 11, typically involves several common stages: substrate binding; activation of molecular oxygen atoms at the Cu ions, leading to the generation of ROS; and hydrogen abstraction from the substrate to form radicals. These radicals undergo further oxidation mediated by electron transfer among Cu ions, and finally, the product is released, and the Cu complex is regenerated to start the reaction again.[15]

6.2. Application as OLED emitters

PNCCs, particularly Cu(I)-based systems, are emerging as highly promising candidates for use in organic light-emitting diodes (OLEDs), owing to their low cost, strong photoluminescence, and excellent tunability.[157,158] Their efficient inter-ligand charge-transfer processes and ability to exhibit thermally activated delayed fluorescence make them exceptional light emitters, especially when enhanced through π-conjugated ligand frameworks.[159,160] Moreover, the earth-abundant and inexpensive nature of copper makes PNCCs sustainable and cost-effective. Consequently, they surpass precious-metal emitters,

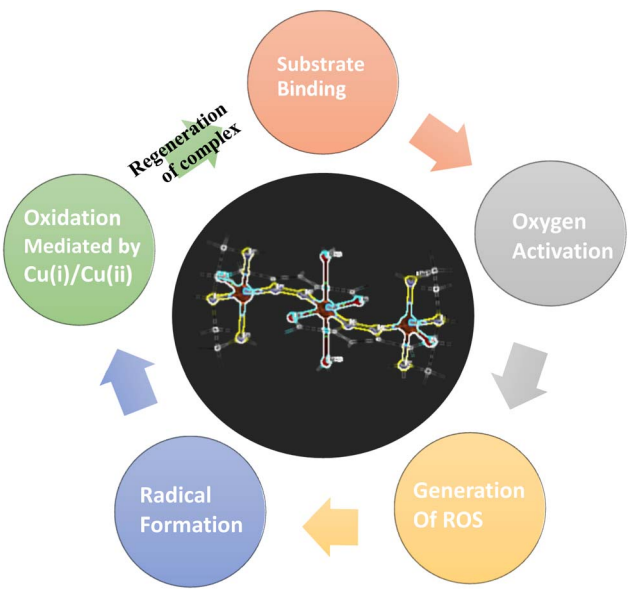

Fig. 11 General catalytic mechanism of polynuclear copper complexes.

making them ideal for scalable OLED fabrication.[161,162] Structural flexibility is another key strength: PNCCs can be readily tuned through strategic ligand modification, enabling precise control over emission colors across the visible spectrum and ensuring compatibility with diverse device architectures.[159,160] Their dual functionality, as both efficient light emitters and charge-transfer mediators, further broadens their utility in advanced OLED technologies.[162]

A notable study demonstrated that the reversible and highly selective photoluminescence observed in the crystalline solvated $[\{Cu(pyfpz)\}_2(\mu\text{-dppe})_2]$ originates from its unique "pyridyl/CH_2Cl_2/pyridyl" organic sandwich-like stacking. This was disclosed by an X-ray crystallographic analysis and was further supported by TD-DFT calculations.[163] Such molecular arrangements highlight how supramolecular organization can modulate emissive behavior in PNCCs. Further insight into structure–property relationships was provided by Xiao *et al.*[164] They described the occurrence of mechanically triggered fluorescence/phosphorescence switching in the planar trinuclear Cu(I) pyrazolate complexes, $[Cu_3(EBPz)_3]$ and $[Cu_3(MBPz)_3]$. The study revealed the occurrence of dual emission, with crystalline samples displaying bluish-violet fluorescence and ground samples exhibiting red phosphorescence. The reversible switching, accomplished *via* mechanical grinding and recrystallization, arose from a fine balance between ligand-centered singlet (S_1) and cluster-centered triplet (T_8) states, separated by only 0.18 eV. This close energy proximity allows efficient intersystem crossing and tunable emissive pathways.[164] Overall, such findings demonstrate how rational ligand design, including the incorporation of auxochromic substituents or the control of Cu···Cu metallophilic interactions, can specifically regulate emission energy, lifetime, and color. These structural strategies open new possibilities for developing stimuli-responsive, color-tunable, and high-efficiency Cu(I)-based PNCC emitters, underscoring their significant potential in next-generation OLEDs and smart optoelectronic applications.

6.3. Separation of C_2 hydrocarbons

The separation of C_2 hydrocarbons, such as ethylene (C_2H_4), from ethane and acetylene (C_2H_2) before processing them is very important for obtaining useful products. Unfortunately, these gases are purified by cryogenic distillation, which has two drawbacks. Firstly, the C_2 compounds possess very close boiling points, which are not well separated by this method, and secondly, the method is economically not viable.[165] Over the last two decades, another method called non-thermally driven separation has received widespread attention from academia and industry.[166] This method uses porous materials, such as metal complexes and metal organic framework (MOF), to separate C_2 hydrocarbons from mixtures of other gases. Among these materials, PNCCs and MOFs based on Cu clusters offer a superior alternative to traditional cryogenic distillation. Thanks to π–π interaction, precise pore architecture and tailored kinetic pathway, PNCCs can distinguish between C_2 hydrocarbons, methane, and other gases. Acetylene has a high electron density due to its triple bond, allowing it to form strong π-complexes with Cu.[167] This leads to enhanced selective adsorption of C_2H_2 over C_2H_4, as shown in Fig. 12. Further, the pore size of Cu-based MOFs is tailored to favor small molecules, such as C_2H_2 (kinetic diameter = 3.3 Å), over large molecules, such as C_2H_4 (kinetic diameter = 4.2 Å).[168] Additionally, the presence of polar functional groups inside the pores enhances the C_2H_2 affinity through dipole or hydrogen binding interactions, enhancing both the adsorption rate and capacity. Multi Cu-based MOF $(NH_4^+)\{Cu^{(II)}{}_3\cdot[Cu^{(II)}Cu^{(I)}{}_6(OH)_6(Ad)_6]_2\}\cdot(H_2O)_x$ excels in separating acetylene from ethylene (C_2H_4) efficiently and effectively, with a selectivity greater than 10 : 1,[13] due to the combined strategies mentioned earlier.

6.4. Biological and medicinal applications

PNCCs exhibit significantly higher antimicrobial, anticancer and antioxidant activities than their mono- or low-nuclear counterparts and even outperform conventional transition metal drugs, such as cisplatin.[169] In addition, PNCCs show higher biological activity than the polynuclear complexes of other transition metals, such as Co(II), Cr(III), Mn(II), Zn(II), Fe(III) and Ni(II).[170–172] This enhanced performance is due not only to their higher nuclearity but also to numerous organized structural and electronic factors. One of these factors is the presence of multiple Cu centers, which facilitate cooperative redox

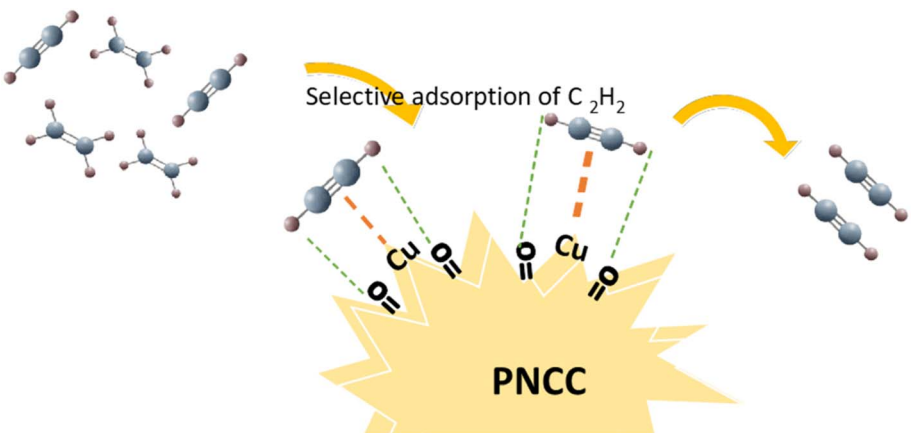

Fig. 12 Selective adsorption and separation of C_2H_2 from the C_2H_2/C_2H_4 mixture using PNCCs.

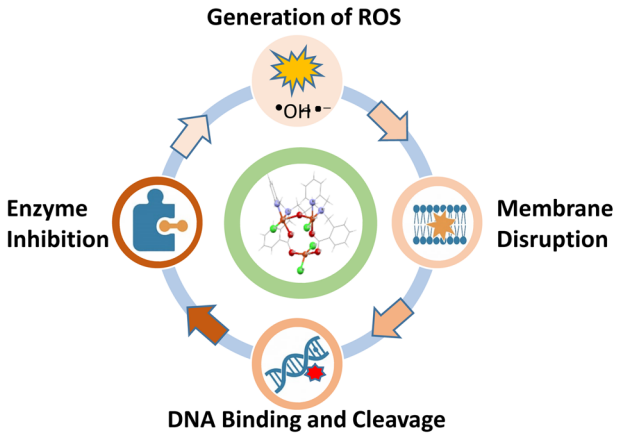

Fig. 13 Mechanism of antimicrobial activity of PNCCs.

interactions. These interactions, which enhance the electron transfer and strengthen binding with biomolecules, such as DNA and proteins, become stronger, leading to more efficient oxidative damage in cancer cells. Other notable factors include the coordination environment, oxidation state of Cu ions, and nature of the coordination of bridging ligands. Coordination modes, particularly those involving donor atoms, such as S, N, and O, play crucial roles.[173] These parameters collectively determine the redox potential, solubility, and cellular uptake efficiency of PNCCs.

PNCCs also exhibit remarkable selectivity, preferentially targeting bacterial, fungal and cancer cells, while showing minimal effects on normal body cells, as revealed by a selectivity index that is several times higher than that of cisplatin. Their reduced toxicity is due to the controlled release of active Cu species and the absence of severe side effects, such as nephrotoxicity or hepatotoxicity, which are usually associated with platinum-based drugs.[169,174] Furthermore, PNCCs exhibit enhanced solution stability during biological exposure, maintaining their structural integrity and activity over prolonged periods.[169] Altogether, the combination of multinuclear interactions, suitable coordination design, high selectivity, low toxicity, and excellent stability makes PNCCs a superior and safer class of metallodrugs compared to mononuclear and conventional transition-metal complexes.

6.4.1. Antifungal and antibacterial activity. Traditional antibiotics and antifungal drugs target a single bacterial and fungal species or even only one site of bacterial or fungal cells. This mode of action makes traditional drugs less effective over time as bacteria develop resistance through mutation or efflux mechanisms. Furthermore, these drugs struggle against multi-strain bacterial biofilms. Therefore, the design and synthesis of new materials to overcome these limitations are necessary. In this context, PNCCs offer a potential alternative to traditional antibacterial and antifungal drugs. PNCCs offer multiple modes of action, such as disrupting the cell membrane, generating reactive oxygen species (ROS), damaging bacterial or fungal DNA and interacting directly with enzymes, as shown in Fig. 13, making it harder for bacteria or fungi to resist.[175–177]

These ROS cause damage to the protein, DNA and lipid membranes of both bacterial and host cells, causing cell death.[178] In addition, the lipophilic nature of PNCCs and the presence of multiple Cu centers and tunable ligands with antibacterial and antifungal properties further enhance the antimicrobial activities of PNCCs. Due to these characteristics, PNCCs are more versatile, effective and less prone to resistance, making them a more favorable alternative to traditional antibacterial and antifungal drugs. $[Cu_2(phen)_2(OH)_2(H_2O)_2]\cdot 2PAc\cdot 6H_2O$ was tested for its antibacterial activity against *Escherichia coli* (a Gram-negative strain), *Micrococcus luteus*, and *Bacillus subtilis* (Gram-positive strains). $[Cu_2(phen)_2(OH)_2(H_2O)_2]\cdot 2PAc\cdot 6H_2O$ showed the highest antibacterial activity compared with the commercially available drug, cefixime. It also exhibited antibacterial activity against the Gram-negative strain, *Escherichia coli*, although *E. coli* typically shows

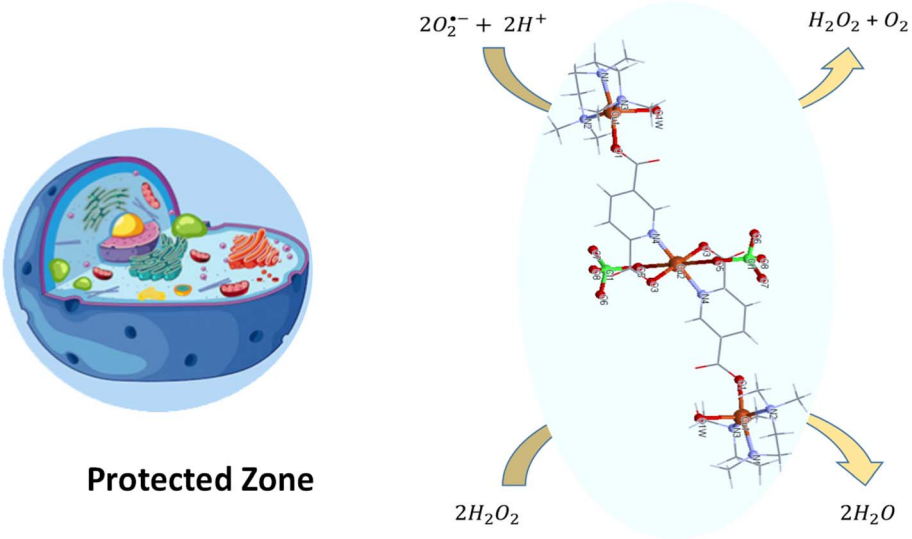

Fig. 14 Antioxidant activity of PNCC protecting cells from ROS.

resistance to antimicrobial agents.[179] $[Cu_2(phen)_2(OH)_2(H_2O)_2]\cdot 2PAc\cdot 6H_2O$ was also studied for its antifungal activity against *Mucor piriformis* and *Helminthosporium solani*. It was found that the complex showed the highest antifungal activity, 75%, compared to the 42% activity of the terbinafine drug.[179] Furthermore, three tetranuclear complexes, $[(Cu_4Ocl_6)Cl(PhIm)_3](HPIm)\cdot H_2O$, $[(Cu_4Ocl_6)(PyNO)_4]\cdot 1/5(H_2O)$, and $[(Cu_4Ocl_6)(MeIm)_4]\cdot 3(CH_3OH)$, exhibit antibacterial activity, mainly against Gram-negative bacteria. However, among these complexes, $[(Cu_4Ocl_6)Cl(PhIm)_3](HPIm)\cdot H_2O$ exhibited antibacterial activity against both Gram-negative and -positive bacteria.[7]

6.4.2. Antioxidant activity. PNCCs have gained significant attention as antioxidant agents because of their unique structural and redox properties, as shown in Fig. 14. PNCCs mimic the activity of natural antioxidant enzymes, such as superoxide dismutase (SOD), which converts superoxide radicals into hydrogen peroxide and oxygen.[180] Furthermore, they exhibit catalase and peroxidase-like activities by decomposing hydrogen peroxide into water and oxygen.[181,182] In addition, PNCCs contain multiple redox-active Cu centers (Cu(I)/Cu(II)) that cooperatively neutralize ROS, making them highly effective antioxidants.[183] A notable study by Sugich-Miranda *et al.* has demonstrated that two binuclear Cu(II) complexes: Cu_2PO and Cu_2PC, showed stronger antioxidant activity than ascorbic acid and potent SOD-like activity, with IC_{50} values of 52 nM and 0.5 μM, respectively.[96] These two complexes were also non-toxic to human cells, showing their potential in biomedical applications. This reveals the superior efficiency and safety of PNCCs over traditional antioxidants. Similarly, $[Cu_2L^1](ClO_4)_2$ exhibited the highest antioxidant activity and protected erythrocytes during H_2O_2-induced hemolysis.[8] The activity of $[Cu(L^4)N_3]_n$ against the 2,2-diphenyl-1-picrylhydrazyl free radical was examined, and it exhibited 19.5% inhibition at a concentration of 100 ppm in the reaction mixture.[10]

6.4.3. DNA binding ability. PNCC complexes bind to the DNA of the host using unique and versatile mechanisms, such as intercalation and groove binding, which tend to cause damage to the DNA of the host cell by generating reactive oxygen species, as depicted in Fig. 15. Unlike other organic DNA binders, the multiple Cu centers, as well as the planar organic ligands (such as aromatic rings), enhance the interaction of PNCCs with DNA, resulting in strong binding. Unlike conventional drugs, like cisplatin, PNCCs exhibit superior redox activity for DNA cleavage. Therefore, they have significant potential for use in biomedicine, including in antimicrobial, anticancer, and biosensing applications.[184] $[Cu_2(phen)_2(OH)_2(H_2O)_2]\cdot 2PAc\cdot 6H_2O$ was tested for its ability to bind with the DNA of salmon sperm by voltammetry and absorption spectroscopy, and it was found that it could bind successfully.[185]

6.4.4. Anticancer activity. In current research on anticancer drug development, PNCCs have emerged as effective anticancer agents compared to conventional platinum-based drugs, such as cisplatin, which, in spite of their medical success, are limited by severe side effects, limited selectivity, and drug resistance. PNCCs represent a new therapeutic dimension by integrating redox-active behavior, DNA-binding affinity, and the generation of ROS into a single molecular system.[186] Furthermore, these complexes can selectively target cancer cells, trigger mitochondrial-mediated apoptosis, and overcome multi-drug resistance, while exhibiting low toxicity to human cells.[187] Their structural tunability with versatile and flexible ligands allows researchers to fine-tune their interaction with biomolecules and living cells, cytotoxic potency and selectivity. Moreover, PNCCs not only attack cancer cells *via* multiple cellular mechanisms but also minimize collateral damage,[188] offering a promising leap forward in the development of next-generation metal-based anticancer therapeutic agents.

A study by Peña *et al.* demonstrates that the synthesized Cu(II) complexes: $[CuL^{15}]_2$, $[CuL^{16}]_2$ and $[CuL^{17}]_2$, exhibit substantial selective and strong anticancer action against cancer cells (HeLa and MCF7) with IC_{50} values of around 25 μM, as compared to cisplatin, and show potential as ROS generators for targeted cancer therapy.[186] A study by Massoud *et al.* demonstrated that dinuclear Cu(II) complexes $[Cu_2(L^{18})_2](ClO_4)_2$, $[Cu_2(L^{19})_2](ClO_4)_2$, $[Cu_2(L^{20})_2]$, $[Cu_2(L^{21})_2]$, $[Cu_2(L^{22})_2(H_2O)]\cdot 2H_2O$, and $[Cu_2(L^{23})_2(H_2O)]\cdot 2H_2O$, especially $[Cu_2(L^{23})_2(H_2O)]\cdot 2H_2O$, are promising anticancer agents, outperforming cisplatin in both efficacy and breadth of activity. Their distinct mechanisms, particularly involving autophagy and cuproptosis, highlight their potential as alternatives to platinum-based drugs.[187]

6.5. Application in wastewater treatment

Wastewater polluted with over 700 000 tons of toxic, carcinogenic, and poorly degradable organic dyes each year poses serious environmental and health risks, demanding efficient treatment technologies. Among various approaches,

Fig. 15 DNA binding and cleavage mediated by ROS generated by PNCCs.

heterogeneous dark-Fenton catalysis has emerged as a superior strategy, owing to its ability to generate reactive oxygen species (ROS) for pollutant degradation without requiring light or electricity.[189] Coordination polymers, due to their structural tunability, stability, and diverse properties, have shown great potential for use as dark-Fenton catalysts. In this context, two Cu(I)-based coordination complexes, $H_2(Cu_4Br_6)[(Cu_4Br_3)(L^{28})_2(H_2O)]_2$ and $[(Cu_5Br_6)(Cu_6Br_9)[Cu_3Br(L^{28})_2]]$, were obtained through the structural transformation of $[Cu_3(TTTMB)_2(H_2O)_6Cl_6]\cdot 2H_2O$ and investigated for their dark-Fenton catalytic performance. The results revealed that both complexes delivered efficient Fenton-like degradation of methyl orange (MO) in the presence of H_2O_2 with or without photoirradiation, and they were recyclable, confirming the crucial role of Cu(I) oxidation in initiating the degradation process.[190] Additionally, a tetranuclear Cu(I)-based coordination complex, $[Cu_4(L^{29})Cl_4]$, was synthesized by the solvothermal method, exhibiting a 3D structure stabilized by hydrogen bonding and π–π interactions. It delivered efficient dark-Fenton degradation of methylene blue (MB), achieving 71.9% removal within 120 min, driven by Cu(II/I) redox cycling.[191] Furthermore, a multivalent Cu-based coordination polymer, $[Cu^{II}Cu_2^{I}(L^{31})Cl_3(SCN)]_n\cdot 2CH_3CN$, was synthesized using a polypyridyl ligand, and it demonstrated remarkable dye-degradation efficiencies of 93.5%, 80% and 80.1% for MB, rhodamine B (RhB), and MO within 120 min in dark, respectively, through the activation of H_2O_2 by Cu(I/II) redox cycling.[192] Collectively, these studies highlight the promising potential of multivalent PNCCs as stable, robust, and highly effective catalysts for wastewater purification.

Besides their role as dark-Fenton catalysts, PNCCs are also used as photo-catalysts in photo-Fenton catalysis for toxic organic dye degradation. In this regard, three Cu(II)-based coordination polymers: $\{[Cu_3(L^{30})(NO_3)_2(DMF)(H_2O)]\cdot 3(DMF)\}_n$, $[Cu_3(L^{30})(Cl)_2(DMF)_2]_n$, and $[Cu_3(L^{30})(NO_3)_4(H_2O)_4]_n$, were synthesized and tested for the photocatalytic degradation of MO and RhB under UV light. Among them, $[Cu_3(L^{30})(NO_3)_4(H_2O)_4]_n$ showed the highest degradation efficiency, achieving 73% degradation of RhB and 64% of MO within 1 h, followed by $[Cu_3(L^{30})(Cl)_2(DMF)_2]_n$ (59% for RhB and 54% for MO) and $\{[Cu_3(L^{30})(NO_3)_2(DMF)(H_2O)]\cdot 3(DMF)\}_n$ (59% for RhB and 53% for MO). The differences in the photocatalytic performances are closely associated with variations in the coordination environment of the Cu centers. In $[Cu_3(L^{30})(NO_3)_4(H_2O)_4]_n$, nitrate bridging, along with coordinated water molecules, enhances charge transfer and results in a narrower band gap (~2.39 eV), which significantly boosts photocatalytic activity. By contrast, chloride bridging in $[Cu_3(L^{30})(Cl)_2(DMF)_2]_n$ and phenoxo bridging in $\{[Cu_3(L^{30})(NO_3)_2(DMF)(H_2O)]\cdot 3(DMF)\}_n$ produce slightly larger band gaps (~2.50 eV and 2.85 eV, respectively), thereby limiting light absorption and decreasing photocatalytic efficiency. These findings clearly demonstrate that the identity of the bridging ligand and the donor environment around Cu play decisive roles in tuning the band gap and regulating photocatalytic degradation performance.[193]

6.6. Electrocatalyst for CO_2 reduction

The electrochemical reduction of CO_2 (eCO_2RR) to multi-carbon (C_2) products, such as ethylene, is highly important because it offers a sustainable route to value-added chemicals for industry while addressing climate change.[194] However, this approach faces key challenges: (i) low selectivity due to competing hydrogen evolution, (ii) complex multi-electron transfer pathways, and (ii) poor stability of molecular catalysts that frequently convert into nanoparticles during electrolysis.[195] Fortunately, PNCCs provide a promising solution to address these issues, as the proximity of multiple Cu centers facilitates C–C coupling between CO_2 reduction intermediates, a critical step toward C_2 product formation. Moreover, the utilization of robust ligands, such as phenanthroline, stabilizes the Cu-centers, prevents catalyst degradation, and improves electronic properties. Recent studies have demonstrated the significantly improved faradaic efficiencies (FE) of binuclear Cu-phenanthroline systems for C_2H_4. In this context, a conductive binuclear Cu(I)-based complex, $[Cu_2(ophen)_2]$, with a short Cu···Cu distance (2.62 Å) was synthesized for the electrochemical reduction of CO_2 to C_2H_4. The close Cu···Cu contact enables CO bridging and efficient C–C coupling, resulting in a faradaic efficiency of 55%, a current density of 580 mA cm^{-2}, and high stability over 50 h. This study shows that short Cu···Cu distances are essential for enhancing activity and selectivity in CO_2 conversion to C_2H_4.[196]

In addition, a binuclear hydroxo-bridged phenanthroline Cu(II)-based complex, $[Cu_2(phen)_2(OH)_2(H_2O)_2][Cu_2(phen)_2(OH)_2Cl_2]Cl_2\cdot 6H_2O$, with a short Cu···Cu distance was prepared as an efficient molecular catalyst for the electrochemical reduction of CO_2 to C_2 products. This catalyst attains a high FE of 62% for C_2 compounds with minimal H_2 evolution (8%) and upholds structural integrity over 15 h of continuous process.[93] However, $[Cu_2(phen)_2(OH)_2(H_2O)_2][Cu_2(phen)_2(OH)_2Cl_2]Cl_2\cdot 6H_2O$ slowly leaches into the electrolyte during CO_2 reduction, which makes them unstable for long-term and practical operation. Ligand design, another key factor for enhancing PNCCs in terms of CO_2 reduction, was employed to overcome the stability issue of $[Cu_2(phen)_2(OH)_2(H_2O)_2][Cu_2(phen)_2(OH)_2Cl_2]Cl_2\cdot 6H_2O$. The incorporation of methoxy groups into the 1,10-phenanthroline ligand critically redesigned the coordination architecture of Cu complexes, transmuting the unstable binuclear $[Cu_2(phen)_2(OH)_2(H_2O)_2][Cu_2(phen)_2(OH)_2Cl_2]Cl_2\cdot 6H_2O$ into an oligonuclear, cascade-like structure, $[Cu_8(4,7\text{-MeO-phen})_8(\mu_2\text{-}OH)_4(\mu_3\text{-}OH)_4Cl_2]$, in which 4,7-dimethoxy-1,10-phenanthroline is connected by μ_2-and μ_3-hydroxo linkages. The electron-donating -OMe substituents increased the electron density on the Cu centers, improving the framework stability and suppressing Cu leaching (from 2.5 mg mL^{-1} to 0.03 mg mL^{-1}) into the electrolyte. This ligand-induced stabilization not only enhanced water insolubility and prohibited structural collapse but also strengthened Cu–ligand interactions, preserving Cu(II) integrity under high current densities. Consequently, $[Cu_8(4,7\text{-MeO-phen})_8(\mu_2\text{-}OH)_4(\mu_3\text{-}OH)_4Cl_2]$ achieved a high faradaic efficiency (>70%) for C_2 products at 200 mA cm^{-2}, with long-term operational

stability.[197] Thus, the strategic methoxy amendment reveals how fine-tuning the ligand's electronic and steric properties can concurrently enhance the robustness and catalytic performance of molecular Cu electrocatalysts for CO_2 reduction.

Besides these two key factors, the performance and selectivity of PNCCs in eCO_2RR are also governed by the nature of the solvent and the electronic state of the Cu centers. The oxidation and electronic states of the Cu centers regulate the strength of the CO_2 and *CO intermediate binding. Mixed-valence Cu(I)/Cu(II) or transient Cu(I) species increase electron delocalization, thus enabling multi-electron transfer and C–C coupling pathways.[198] Moreover, the ligand-controlled regulation of the Cu(II)/Cu(I) redox potentials stabilizes the reactive Cu(I) sites and lowers the overpotentials, thereby improving stability and faradaic efficiency.[199] Meanwhile, the solvent directly affects the CO_2 solubility, proton availability, and stabilization of charged intermediates. Protic solvents or water-rich environments promote proton-coupled electron transfer and favor products like CO and formate ($HCO\bar{O}$). In contrast, aprotic media, such as acetonitrile, overwhelm the proton supply and alter the selectivity toward C–C coupled products.[200] Collectively, the coordination strength and solvent polarity affect the redox potential range and structure of the active Cu centers. Therefore, optimal eCO_2RR performance of PNCCs arises by harmonizing the Cu electronic configuration and solvent environment with the Cu···Cu distances and ligand design.

6.7. As a photosensitizer

6.7.1. Photosensitizer for photocatalytic CO_2 reduction. Artificial photosynthesis is a promising strategy for converting solar energy into chemical fuels, with CO_2 reduction being one of the most significant reactions for sustainable energy production and reducing global warming.[201] A photocatalytic system for CO_2 reduction includes a photosensitizer, a catalyst, and an electron donor. Traditionally, photosensitizers based on Ru, Re, Ir, and Os are highly efficient but expensive and scarce.[202,203] Organic dyes have been researched thoroughly, but they face challenges such as photobleaching and poor performance in terms of CO_2 conversion.[204,205] Recently, Cu(I)-based complexes have emerged as crucial materials, because Cu is earth-abundant, and their heteroleptic di-imine–bis-phosphine complexes display strong oxidation power and suitable reduction potentials. As a photosensitizer, binuclear Cu(I)-based complexes with a tetradentate phenanthroline–phosphine ligand, $[Cu_2(P_2dmp)_2](PF_6)_2$, exhibit high stability, extended excited-state lifetime, and strong redox ability. With a Fe(II)-based catalyst, $[Cu_2(P_2dmp)_2](PF_6)_2$ achieved a turnover number of 273 and a quantum yield of 6.7%.[206] In addition, the binuclear Cu(I)-based complex, $[Cu_2(P_2bph)_2](PF_6)_2$, was demonstrated to be a highly efficient and durable photosensitizer for CO_2 reduction. In combination with Mn-based catalysts, it delivered excellent performance: a quantum yield of 57%, a turnover number greater than 1300, and 95% selectivity.[207] The aforementioned two Cu(I)-based di-imine–bis-phosphine complexes offer robust redox abilities; however, their limited ligand stability causes rapid detachment in coordinating solvents, limiting their effectiveness as photosensitizers. This issue was resolved by modifying the di-phosphine–phenanthroline ligands with a CF_3 substituent. These structural changes significantly extended the visible-light absorption and increased the absorption intensity and stability. This modified ligand was employed for the preparation of $[Cu_2(L^{33})_2](PF_6)_2$. The $[Cu_2(L^{33})_2](PF_6)_2$ material, as a photosensitizer along with an Fe-based catalyst, achieved the highest quantum yield and remained intact in solution after irradiation for 48 h.[12] These results demonstrate the effectiveness of ligand modification in optimizing Cu(I)-based photosensitizers for photocatalytic CO_2 reduction systems.

6.7.2. Photosensitizer for photocatalytic H_2 production. Cu-based PNCCs have also proven to be efficient photosensitizers for photocatalytic hydrogen production, offering a sustainable alternative to precious-metal systems. A notable example is the polyoxometalate-based hybrid PNCC, $[Cu_5(2\text{-ptz})_6(H_2O)_4(GeW_{16}O_{40})]\cdot 4H_2O$, which achieved a hydrogen evolution rate of 3813 μmol g^{-1} h^{-1} under visible light without the use of noble-metal cocatalysts, the highest reported among traditional polyoxometalate-based materials.[208] The improved activity is ascribed to the formation of heteropoly blue species that extend absorption into the visible region, efficient electron–hole separation facilitated by Cu layers, and improved dispersion of polyoxometalate units.[208] These findings demonstrate the strong potential of Cu complexes as photosensitizers for cost-effective and stable H_2 production systems. However, this remains a relatively less explored area, highlighting the need for further research to fully realize the potential of PNCCs as photosensitizers for H_2 generation.

6.8. Electrocatalysts for H_2 production

Owing to its high energy density and environmentally friendly nature, hydrogen is considered a vital clean fuel.[209] Water-splitting technology provides a sustainable route for its production, including two critical half-reactions: the oxygen evolution reaction (OER) and the hydrogen evolution reaction (HER).[210] Platinum- and other noble metal-based catalysts remain the standard for these processes; however, their scarcity and high cost drive researchers to develop efficient alternatives based on earth-abundant metals.[211,212] Cu is particularly attractive because of its versatile redox chemistry, tunable coordination environments, and recognized catalytic performance in reactions such as CO_2 reduction,[213] nitrogen reduction,[214] and water oxidation.[215,216] While nanostructured Cu-based materials have shown strong HER activity across different pH ranges,[11] molecular Cu complexes, especially polynuclear species, have received far less consideration. Their limited study arises largely from stability issues under reducing conditions, where complexes frequently decompose into heterogeneous Cu species.[217]

Recent literature has demonstrated that well-designed PNCCs can overcome these challenges. By bringing multiple Cu centers into proximity, they mimic hydrogenase enzymes, allowing cooperative proton binding and efficient electron transfer. A binuclear Cu-complex, $[Cu_2(\mu\text{-}OH)(\mu\text{-}NO_3)(L^{31})_2]$, with a Schiff base ligand derived from salicylaldehyde and histidine, was developed as an efficient HER electrocatalyst, exhibiting exceptional activity in

both aqueous and non-aqueous media. It displays low overpotentials (~150–270 mV), high turnover frequency (~13 200 s^{-1}), and long-term stability during controlled potential electrolysis, highlighting its promise as a cost-effective, earth-abundant catalyst for hydrogen production.[218] Despite these advances, research on PNCCs for hydrogen evolution remains sparse. This underexplored area offers substantial potential, and further studies on their rational design, stability, and integration into photocatalytic and electrocatalytic systems are strongly recommended.

7. Future recommendations

To date, significant progress has been made on (PNCCs); however, further studies are still required to enhance their scalability, structural integrity, stability, and functionality. Future studies on PNCCs should emphasize the design of innovative multifunctional ligands with tunable coordination sites, pre-organized templates, and environmentally benevolent synthetic approaches, such as green, biomimetic, and mechanochemical strategies, to improve structural diversity and sustainability. The existing methods employed for the synthesis of polynuclear copper complexes (PNCCs) often require long reaction times to achieve stable products. Therefore, further efforts are needed to improve current synthetic strategies or to develop new approaches capable of producing PNCCs more efficiently within shorter timeframes. Apart from synthetic strategies, integration of *in situ* spectroscopic techniques with computational tools, including DFT, molecular dynamics, and emerging machine learning models, will be essential for gaining deeper insights into electronic structures and for establishing clear structure–property correlations, particularly in relation to nuclearity, bridging motifs, and cooperative effects. On the application front, PNCCs are promising materials for use as anticancer agents, antimicrobial entities, and photoluminescent materials for OLEDs. However, they have been investigated less extensively as catalysts for CO_2 reduction, water oxidation and H_2 production. At the same time, challenges such as scalability, long-term stability, recyclability, and toxicity must be systematically investigated to permit their real-world utilization. Overall, the convergence of synthetic creativity, advanced characterization, and computational modeling is expected to guide the rational development of next-generation polynuclear copper complexes with widespread impact across chemistry, materials science, and biology.

8. Conclusions

PNCCs are an interesting and versatile class of coordination compounds, exhibiting widespread structural diversity originating from the nature of the ligands, solvent, Cu-to-ligand ratios, pH of the reaction media, and counterions. In this review, we have summarized their synthetic approaches, including solvothermal, direct or self-assembly, coordination-driven self-assembly, solvothermal methods, template-based, and supramolecular approaches. We also explored their characteristic features studied using various techniques, including FTIR, Raman and UV-visible spectroscopy, mass spectrometry, and single-crystal/powder XRD analyses. Additionally, we summarized their magnetic properties and diverse applications, including applications in catalysis and the selective separation of C_2H_2 from the C_2H_4/C_2H_2 mixture and as antimicrobial and antioxidant agents. We also explored their DNA-binding affinity and potential anticancer activity, alongside their roles as photoemitters and charge-transport layers in OLEDs. In addition, we discussed their potential as electrocatalysts and photosensitizers for CO_2 reduction and H_2 production, along with their roles as photo- and electro-catalysts for the degradation of toxic organic pollutants in wastewater. These complexes will play an essential role as next-generation materials in both material science and biomedical technologies, with progressive innovation in their synthesis, ligand design and practical applications. Despite this significant development, several future directions remain open for further research to improve their performance and utility. For example, researchers can explore novel ligands that offer greater flexibility and control over the assembly of multinuclear copper complex structures. There is a need for more controlled and green synthetic protocols that can precisely deliver a high yield of polynuclear complexes with desired nuclearities and topologies to optimize their applications. A deep understanding of the mechanisms governing how the solvent, pH of reaction media and nature and structure of ligands influence the self-assembly and stability of polynuclear copper complexes is essential. Such insights will extend their applications to emerging areas, such as molecular electronics, environmental remediation, CO_2 conversion into valuable gases (such as methane) and targeted drug delivery.

Author contributions

This manuscript has been written with the contribution of all authors. All authors take responsibility for the entire content of this manuscript and have approved its submission.

Conflicts of interest

The authors declare no conflicts of interest.

Data availability

No primary research results, software or code have been included, and no new data were generated or analysed as part of this review.

Acknowledgements

This work is financially supported by the research office United Arab Emirates University.

References

1 Y. Yang, R. Hao, Q. Wu and P. Luo, *Inorganic Chemistry Frontiers Structural Regulation of NHC-Protected Copper (I) Clusters through Substitution for Photoluminescence Enhancement*, 2024, 4757–4769.

2 C. Santini, M. Pellei, V. Gandin, M. Porchia, F. Tisato and C. Marzano, Advances in copper complexes as anticancer agents, *Chem. Rev.*, 2014, **114**, 815–862.
3 M. Gennari, M. Lanfranchi, R. Cammi, M. A. Pellinghelli and L. Marchiò, Mononuclear and polynuclear copper(I) complexes with a new N,N′,S-donor ligand and with structural analogies to the copper thionein core, *Inorg. Chem.*, 2007, **46**, 10143–10152.
4 D. C. Onwudiwe and A. C. Ekennia, Synthesis, characterization, thermal, antimicrobial and antioxidant studies of some transition metal dithiocarbamates, *Res. Chem. Intermed.*, 2017, **43**, 1465–1485.
5 S. Das, P. Banerjee, S.-M. Peng, G.-H. Lee, J. Kim and S. Goswami, Mononuclear to Polynuclear Transition Induced by Ligand Coordination: Synthesis, X-ray Structure, and Properties of Mono-, Di-, and Polynuclear Copper(II) Complexes of Pyridyl-Containing Azo Ligands, *Inorg. Chem.*, 2006, **45**, 562–570.
6 A. Noor, A. Shahzad, E. Khan, M. N. Tahir, G. S. Khan, A. ur Rashid and M. Said, Polynuclear Cu(I) and Ag(I) Complexes of 1,3-Diisobutyl Thiourea, Synthesis, Crystal Structure and Antioxidant Potentials, *Inorganics*, 2022, **10**, 185.
7 P. Cortes, A. M. Atria, M. Contreras, M. T. Garland, O. Peña and G. Corsini, Magnetic properties and antibacterial activity of tetranuclear copper complexes bridged by oxo group, *J. Chil. Chem. Soc.*, 2006, **51**, 957–960.
8 S. Das, P. Banerjee, S.-M. Peng, G.-H. Lee, J. Kim and S. Goswami, Mononuclear to Polynuclear Transition Induced by Ligand Coordination: Synthesis, X-ray Structure, and Properties of Mono-, Di-, and Polynuclear Copper(II) Complexes of Pyridyl-Containing Azo Ligands, *Inorg. Chem.*, 2006, **45**, 562–570.
9 R. Jlassi, A. P. C. Ribeiro, M. F. C. Guedes Da Silva, K. T. Mahmudov, M. N. Kopylovich, T. B. Anisimova, H. Naïli, G. A. O. Tiago and A. J. L. Pombeiro, Polynuclear copper(II) complexes as catalysts for the peroxidative oxidation of cyclohexane in a room-temperature ionic liquid, *Eur. J. Inorg. Chem.*, 2014, **2014**, 4541–4550.
10 A. Noor, A. Shahzad, E. Khan, M. N. Tahir, G. S. Khan, A. ur Rashid and M. Said, Polynuclear Cu(I) and Ag(I) Complexes of 1,3-Diisobutyl Thiourea, Synthesis, Crystal Structure and Antioxidant Potentials, *Inorganics*, 2022, **10**, 185.
11 R. Fernández-Climent, J. Redondo, M. García-Tecedor, M. C. Spadaro, J. Li, D. Chartrand, F. Schiller, J. Pazos, M. F. Hurtado, V. de la Peña O'Shea, N. Kornienko, J. Arbiol, S. Barja, C. A. Mesa and S. Giménez, Highly Durable Nanoporous Cu2–xS Films for Efficient Hydrogen Evolution Electrocatalysis under Mild pH Conditions, *ACS Catal.*, 2023, **13**, 10457–10467.
12 H. Takeda, Y. Monma and O. Ishitani, Highly Functional Dinuclear CuI-Complex Photosensitizers for Photocatalytic CO_2 Reduction, *ACS Catal.*, 2021, **11**, 11973–11984.
13 J. Li, L. Jiang, S. Chen, A. Kirchon, B. Li, Y. Li and H. C. Zhou, Metal-Organic Framework Containing Planar Metal-Binding Sites: Efficiently and Cost-Effectively Enhancing the Kinetic Separation of C_2H_2/C_2H_4, *J. Am. Chem. Soc.*, 2019, **141**, 3807–3811.
14 J.-L. Chen, Z.-H. Guo, H.-G. Yu, L.-H. He, S.-J. Liu, H.-R. Wen and J.-Y. Wang, Luminescent dinuclear copper(I) complexes bearing 1,4-bis(diphenylphosphino)butane and functionalized 3-(2′-pyridyl)pyrazole mixed ligands, *Dalton Trans.*, 2016, **45**, 696–705.
15 A. Bhattacharjee, S. Halder, K. Ghosh, C. Rizzoli and P. Roy, Mono-, tri- and polynuclear copper(II) complexes of Schiff-base ligands: Synthesis, characterization and catalytic activity towards alcohol oxidation, *New J. Chem.*, 2017, **41**, 5696–5706.
16 R. Federation, R. Federation and I. Introduction, Copper and nickel chelate complexes with polydentate N, O-ligands : structure and magnetic properties of polynuclear complexes, *Russ. Chem. Rev.*, 2015, **84**, 310–333.
17 M. Zienkiewicz-machnik and A. Kubas, Cationic–anionic complexes of Cu(II) and Co(II) with N-scorpionate ligand – structure, Spectroscopy, and Catecholase Activity, *Dalton Trans.*, 2025, **13**, 5268–5285.
18 S. Brooker and R. W. Hogue, Spin crossover in discrete polynuclear iron(ii) complexes, *Chem Soc Rev.*, 2018, **19**, 7303–7338.
19 D. Bacciu, C. Chen, P. Surawatanawong, B. M. Foxman and O. V Ozerov, *High-Spin Manganese (II) Complexes of an Amido/Bis (Phosphine)PNP Ligand*, 2010, pp. 5328–5334.
20 S. B. Monomethylated, M. B. Meredith, J. A. Crisp, E. D. Brady, T. P. Hanusa, G. T. Yee, N. R. Brooks, B. E. Kucera and V. G. Young, *High-Spin and Spin-Crossover Behavior in Monomethylated Bis(indenyl) chromium(II) Complexes*, 2006, pp. 4945–4952.
21 A. Krężel and W. Maret, The biological inorganic chemistry of zinc ions, *Arch Biochem Biophys.*, 2016, **611**, 3–19.
22 K. Peng, B. Liang, W. Liu and Z. Mao, What blocks more anticancer platinum complexes from experiment to clinic : Major problems and potential strategies from drug design perspectives, *Coord. Chem. Rev.*, 2021, **449**, 214210.
23 E. Khan, S. Khan, Z. Gul and M. Muhammad, Medicinal Importance, Coordination Chemistry with Selected Metals (Cu, Ag, Au) and Chemosensing of Thiourea Derivatives. A Review, *Crit Rev Anal Chem.*, 2021, **51**(8), 812–834.
24 J. Hafeez, M. Bilal, N. Rasool, U. Hafeez, S. Adnan, A. Shah, S. Imran and Z. Amiruddin, Synthesis of ruthenium complexes and their catalytic applications : A review, *Arab. J. Chem.*, 2022, **15**, 104165.
25 V. N. Kokozay, O. Y. Vassilyeva, P. Weinberger, M. Wasinger and W. Linert, Direct Synthesis of Polynuclear Complexes, *Rev. Inorg. Chem.*, 2000, **20**, 255–282.
26 V. Pavlenko, V. Kokozay and O. Babich, Direct Synthesis of Tetranuclear Complexes of Copper(II) with μ4-Bridging Oxygen, *Z. Naturforsch., B:J. Chem. Sci.*, 1993, **48**, 1321–1324.
27 M. Du, X. Bu, Y. Guo and J. Ribas, Ligand Design for Alkali-Metal-Templated Self-Assembly of Unique High-Nuclearity Cu II Aggregates with Diverse Coordination Cage Units: Crystal Structures and Properties, *Chem.–Eur. J.*, 2004, **10**, 1345–1354.

28 T. F. Mastropietro and G. De Munno, Supramolecular self-assembly of cytidine monophosphate-di-copper building blocks, *J. Coord. Chem.*, 2022, **75**, 1886–1898.
29 G.-X. Wang, W.-Y. Zhao and Z. Xing, Two new olefin-Cu(I) coordination polymers based on 2,5-dimethyl piperazine: synthesis, crystal structure and photoluminescent property, *Inorg. Nano-Met. Chem.*, 2025, **55**, 559–564.
30 P. Schmeinck, D. Sretenović, J. Guhl, R. Kühnemuth, C. A. M. Seidel, C. M. Marian, M. Suta and C. Ganter, Luminescent Copper(I)-Complexes with an Anionic NHC obtained via a Coordination Polymer as Versatile Precursor, *Eur. J. Inorg. Chem.*, 2023, **26**(27), DOI: 10.1002/ejic.202300416.
31 C. Gawlig, J. Jung, D. Mollenhauer and S. Schindler, Synthesis and characterization of copper complexes with tripodal ligands bearing amino acid groups, *Z. Anorg. Allg. Chem.*, 2021, **647**, 951–959.
32 P. W. Seavill, K. B. Holt and J. D. Wilden, Electrochemical preparation and applications of copper(I) acetylides: a demonstration of how electrochemistry can be used to facilitate sustainability in homogeneous catalysis, *Green Chem.*, 2018, **20**, 5474–5478.
33 S. Kolay, S. Maity, D. Bain, S. Chakraborty and A. Patra, Self-assembly of copper nanoclusters: isomeric ligand effect on morphological evolution, *Nanoscale Adv.*, 2021, **3**, 5570–5575.
34 J. Xu, W.-D. Si, C. Zhang, W. Tian, D. Sun, L. Shi and X. Xin, Self-assembly of copper nanoclusters into highly ordered hexagonal platform microcrystals with enhanced thermally activated delayed fluorescence, *Chem. Eng. J.*, 2025, **520**, 165772.
35 M. Dolai and U. Saha, A simple Cu(II) complex of phenolic oxime: synthesis, crystal structure, supramolecular interactions, DFT calculation and catecholase activity study, *Heliyon*, 2020, **6**, e04942.
36 F.-Y. Cheng, C.-Y. Tsai, B.-H. Huang, K.-Y. Lu, C.-C. Lin and B.-T. Ko, Mono- and dinuclear copper complexes coordinated on NNO-tridentate Schiff-base derivatives for copolymerization of cyclohexene oxide and cyclic anhydrides, *Dalton Trans.*, 2019, **48**, 4667–4676.
37 S. Kang, K. Nam and S. Kim, Template Synthesis of Copper (II) Complexes of N_3 O-Donor Macrotricycles, *Bull. Korean Chem. Soc.*, 2004, **25**, 2–5.
38 J. Kumar, D. Singh, A. Jangra, H. Kumar, P. Kumar, S. Kumar, R. Khanna and R. Kumar, Synthesis, spectral, biological, and computational studies of template engineered macrocyclic metal complexes, *J. Coord. Chem.*, 2022, **75**, 2962–2977.
39 H. Goudarziafshar, S. Yousefi, Y. Abbasi Tyula, M. Dušek and V. Eigner, Template synthesis, DNA binding, antimicrobial activity, Hirshfeld surface analysis, and 1D helical supramolecular structure of a novel binuclear copper(ii) Schiff base complex, *RSC Adv.*, 2022, **12**, 13580–13592.
40 B. Vimala, S. R. Jayapradha and A. Selvan, Template Synthesis and Characterization of Transition Metal Complexes of 13, 15 and 17-Membered Tetraamide Macrocyclic Disubstituted Dimethyl Tetrasubstituted Tetraazacycloalka Tetrasubstituted Tetraene Disubstiuted Diol, *Asian J. Chem.*, 2020, **32**, 488–494.
41 Z. Zhang and M. J. Zaworotko, Template-directed synthesis of metal–organic materials, *Chem. Soc. Rev.*, 2014, **43**, 5444–5455.
42 M. Sebastian, V. Arun, P. P. Robinson, P. Leeju, G. Varsha, D. Varghese and K. K. M. Yusuff, Template synthesis and spectral characterization of some Schiff base complexes derived from quinoxaline-2-carboxaldehyde and <scp>L</scp> -histidine, *J. Coord. Chem.*, 2011, **64**, 525–533.
43 S. Mathur and S. Tabassum, Template synthesis of novel carboxamide dinuclear copper (II) complex: spectral characterization and reactivity towards calf-thymus DNA, *BioMetals*, 2008, **21**, 299–310.
44 P. Pandey, A. Verma, K. Bretosh, J. P. Sutter and S. S. Sunkari, Template directed synthesis of half condensed Schiff base complexes of Cu(II) and Co(III): Structural and magnetic studies, *Polyhedron*, 2019, **164**, 80–89.
45 M. Lorenzo Oliva-de Dios, M. G. Sánchez-Anguiano, R. M. Jiménez-Barrera, H. Reyes-Pérez, M. Loredo-Cancino, M. G. Flores-Amaro, A. Obregón-Zúñiga, R. Chan-Navarro and M. C. García-López, New hydrophilic mesoporous copper(II) coordination polymers obtained from poly(ethylene terephthalate) (PET) waste for diesel removal in water, *Sep. Purif. Technol.*, 2024, **343**, 127108.
46 S. Wang, X. Zhou, X. Ding, X. Wang, Y. Jin, Z. Zhou, X. Lu, W. Yang and H. Wang, Post-Cobaltization of Crystalline Trinuclear Copper Cluster-Based Metal–Organic Frameworks for Photocatalytic CO_2 Reduction, *ChemSusChem*, 2025, **18**(11), DOI: 10.1002/cssc.202402648.
47 M.-X. Li, H. Wang, S.-W. Liang, M. Shao, X. He, Z.-X. Wang and S.-R. Zhu, Solvothermal Synthesis and Diverse Coordinate Structures of a Series of Luminescent Copper(I) Thiocyanate Coordination Polymers Based on N-Heterocyclic Ligands, *Cryst. Growth Des.*, 2009, **9**, 4626–4633.
48 T. Ren, H. Zhu, P. Zhu and D. Jia, Syntheses, structures, photoelectricity and photocatalysis of Cu(I) iodide hybrids and thiolate derived from dithiodipyridine, *Inorg. Chim. Acta*, 2024, **571**, 122215.
49 A. Majumder, S. Sk, A. Das, G. Vijaykumar, M. K. Sahoo, J. N. Behera and M. Bera, Ancillary-Ligand-Assisted Variation in Nuclearities Leading to the Formation of Di-, Tri-, and Tetranuclear Copper(II) Complexes with Multifaceted Carboxylate Coordination Chemistry, *ACS Omega*, 2022, **7**, 39985–39997.
50 I. F. M. Costa, M. V. Kirillova, V. André, T. A. Fernandes and A. M. Kirillov, Time-Dependent Self-Assembly of Copper(II) Coordination Polymers and Tetranuclear Rings: Catalysts for Oxidative Functionalization of Saturated Hydrocarbons, *Inorg. Chem.*, 2021, **60**, 14491–14503.
51 A. N. Gusev, V. F. Shulgin and M. A. Kiskin, Self-Assembly of Polynuclear Complexes Based on Spacer- Armed Pyridylazoles, *J. Struct. Chem.*, 2019, **60**, 335–355.

52 A. Lopera, A. Gil-Martínez, J. Pitarch-Jarque, B. Verdejo, S. Blasco, M. P. Clares, H. R. Jiménez and E. García-España, Influence of the chain length and metal : ligand ratio on the self-organization processes of Cu^{2+} complexes of [1 + 1] 1*H* -pyrazole azamacrocycles, *Dalton Trans.*, 2020, **49**, 8614–8624.
53 S. S. Tandon, S. D. Bunge, N. Patel, E. C. Wang and L. K. Thompson, Self-Assembly of Antiferromagnetically-Coupled Copper(II) Supramolecular Architectures with Diverse Structural Complexities, *Molecules*, 2020, **25**, 5549.
54 A. Lopez and J. Liu, Self-Assembly of Nucleobase, Nucleoside and Nucleotide Coordination Polymers: From Synthesis to Applications, *ChemNanoMat*, 2017, **3**, 670–684.
55 H. Zhu, L. Pesce, R. Chowdhury, W. Xue, K. Wu, T. K. Ronson, R. H. Friend, G. M. Pavan and J. R. Nitschke, Stereocontrolled Self-Assembly of a Helicate-Bridged Cu I 12 L 4 Cage That Emits Circularly Polarized Light, *J. Am. Chem. Soc.*, 2024, **146**, 2379–2386.
56 Y.-Q. Xiao, P. Shang, G.-K. Yang, X.-Q. Pu, K.-W. Jiang, Z.-W. Jiang, C. Wu, L.-C. Gui, J.-P. Wang and X. Jiang, Ligand conformation directed self-assembly of heteroleptic Cu(I) complexes and luminescent sensing properties for Zn2+, *J. Solid State Chem.*, 2024, **330**, 124464.
57 M. Du, X. Bu, Y. Guo and J. Ribas, Ligand Design for Alkali-Metal-Templated Self-Assembly of Unique High-Nuclearity Cu II Aggregates with Diverse Coordination Cage Units: Crystal Structures and Properties, *Chem.–Eur. J.*, 2004, **10**, 1345–1354.
58 A. Majumder, S. Sk, A. Das, G. Vijaykumar, M. K. Sahoo, J. N. Behera and M. Bera, Ancillary-Ligand-Assisted Variation in Nuclearities Leading to the Formation of Di-, Tri-, and Tetranuclear Copper(II) Complexes with Multifaceted Carboxylate Coordination Chemistry, *ACS Omega*, 2022, **7**, 39985–39997.
59 I. F. M. Costa, M. V. Kirillova, V. André, T. A. Fernandes and A. M. Kirillov, Time-Dependent Self-Assembly of Copper(II) Coordination Polymers and Tetranuclear Rings: Catalysts for Oxidative Functionalization of Saturated Hydrocarbons, *Inorg. Chem.*, 2021, **60**, 14491–14503.
60 A. N. Gusev, V. F. Shulgin and M. A. Kiskin, Self-Assembly of Polynuclear Complexes Based on Spacer- Armed Pyridylazoles, *J. Struct. Chem.*, 2019, **60**, 335–355.
61 S. S. Tandon, S. D. Bunge, N. Patel, E. C. Wang and L. K. Thompson, Self-Assembly of Antiferromagnetically-Coupled Copper(II) Supramolecular Architectures with Diverse Structural Complexities, *Molecules*, 2020, **25**, 5549.
62 A. Lopez and J. Liu, Self-Assembly of Nucleobase, Nucleoside and Nucleotide Coordination Polymers: From Synthesis to Applications, *ChemNanoMat*, 2017, **3**, 670–684.
63 M. Fleischmann, L. Dütsch, M. Elsayed Moussa, G. Balázs, W. Kremer, C. Lescop and M. Scheer, Self-Assembly of Reactive Linear Cu 3 Building Blocks for Supramolecular Coordination Chemistry and Their Reactivity toward E n Ligand Complexes, *Inorg. Chem.*, 2016, **55**, 2840–2854.
64 R. Ishikawa, S. Ueno, H. Iguchi, B. K. Breedlove, M. Yamashita and S. Kawata, Supramolecular self-assembled coordination architecture composed of a doubly bis(2-pyridyl)pyrazolate bridged dinuclear Cu(II) complex and 7,7′,8,8′,-tetracyano- p -quinodimethanide radicals, *CrystEngComm*, 2020, **22**, 159–163.
65 B. L. Liao, S. X. Li, J. J. Guo, J. J. Jia and Y. M. Jiang, Self assembly of three new copper coordination polymers based on N-[(3-pyridine)-sulfonyl]aspartate: Synthesis and structure, *Russ. J. Coord. Chem.*, 2016, **42**, 285–291.
66 X.-Y. Li, L.-Q. Liu, M.-L. Ma, X.-L. Zhao and K. Wen, Coordination-driven self-assembly of discrete and polymeric copper(II) and dicopper(II) supramolecular structures based on oxacalix[2]benzene[2]pyrazines, *Dalton Trans.*, 2010, **39**, 8646.
67 T. F. Mastropietro and G. De Munno, Supramolecular self-assembly of cytidine monophosphate-di-copper building blocks, *J. Coord. Chem.*, 2022, **75**, 1886–1898.
68 A. Dorazco-González, S. Martinez-Vargas, S. Hernández-Ortega and J. Valdés-Martínez, Directed self-assembly of mono and dinuclear copper(ii) isophthalates into 1D polymeric structures. Design and an unusual cocrystallization, *CrystEngComm*, 2013, **15**, 5961.
69 K. Shi, L. Mathivathanan, R. Herchel, A. K. Boudalis and R. G. Raptis, Supramolecular Assemblies of Trinuclear Copper(II)-Pyrazolato Units: A Structural, Magnetic and EPR Study, *Chemistry*, 2020, **2**, 626–644.
70 E. Mijangos, J. Sánchez Costa, O. Roubeau, S. J. Teat, P. Gamez, J. Reedijk and L. Gasque, Self-Assembly of an Infinite Copper(II) Chiral Metallohelicate, *Cryst. Growth Des.*, 2008, **8**, 3187–3192.
71 M. M. Bishop, A. H. W. Lee, L. F. Lindoy, P. Turner, B. W. Skelton and A. H. White, Self-assembly of Hydrogen-bonded Supramolecular Structures Based on the Neutral Pseudo-macrocyclic Complex Bis(dimethylglyoximato)copper(II), *Supramol. Chem.*, 2005, **17**, 37–45.
72 D. Quiñone, S. Martínez, F. Bozoglián, C. Bazzicalupi, J. Torres, N. Veiga, A. Bianchi and C. Kremer, Solution Studies and Crystal Structures of Heteropolynuclear Potassium/Copper Complexes with Phytate and Aromatic Polyamines: Self-Assembly through Coordinative and Supramolecular Interactions, *Chempluschem*, 2019, **84**, 540–552.
73 T. Hirao and T. Haino, in *Supramolecular Nanotechnology*, Wiley, 2023, pp. 1085–1100.
74 A. Mohamadou, J. Moreau, L. Dupont and E. Wenger, Inorganica Chimica Acta Equilibrium and structural studies of copper(II) complexes with a tridentate ligand containing amide , pyrazyl and pyridyl nitrogen donors : Effect of anions coligands on crystal structures of copper (II) complexes, *Inorg. Chim. Acta*, 2012, **383**, 267–276.
75 D. Kim, H. Ki, D. Im, Y. Lee, S. Lee, J. Heo, S. Eom, E. H. Choi, D. Ahn and H. Ihee, Excited-State Structural Dynamics of the Cubane-Type Metal Cluster $[Cu_4I_4(py)_4]$ Explored by Time-Resolved X-Ray Liquidography, *Adv. Sci.*, 2025, **12**(14), DOI: 10.1002/advs.202414970.
76 D. Bissessar, T. Thierry, J. Egly, V. Giuso, T. Achard, P. Steffanut, M. Mauro and S. Bellemin-Laponnaz, Cubane Copper(I) Iodide Clusters with Remotely

Functionalized Phosphine Ligands: Synthesis, Structural Characterization and Optical Properties, *Symmetry*, 2023, **15**, 1210.

77 K. Abdi, H. Hadadzadeh, M. Weil and H. A. Rudbari, *Mono- and Polynuclear copper(II) Complexes Based on 2,4,6-Tris(2-Pyridyl)- 1,3,5-triazine and its Hydrolyzed Form*, Elsevier B.V., 2014, vol. 416.

78 R. Pérez-Aguirre, G. Beobide, O. Castillo, I. De Pedro, A. Luque, S. Pérez-Yáñez, J. Rodríguez Fernández and P. Román, 3D magnetically ordered open supramolecular architectures based on ferrimagnetic Cu/adenine/hydroxide heptameric wheels, *Inorg. Chem.*, 2016, **55**, 7755–7763.

79 Z.-X. Zhang, N. Tuo, H.-W. Zhang, Y.-R. Zheng, L. Wang, L.-M. Pu, W.-B. Xu, H.-T. Long and W.-K. Dong, Exploring the synthesis, structure and properties of two phenoxy-bridged polynuclear Cu(II) and Ni(II) complexes containing salamo-based bicompartmental ligand, *J. Mol. Struct.*, 2025, **1320**, 139692.

80 M. Szymańska, M. Kubicki, G. N. Roviello, G. Consiglio, M. A. Fik-Jaskółka and V. Patroniak, New Cu(I) square grid-type and Ni(II) triangle-type complexes: synthesis and characterization of effective binders of DNA and serum albumins, *Dalton Trans.*, 2022, **51**, 15648–15658.

81 M. P. Tang, L. Zhu, Y. Deng, Y. Shi and S. K. Lai, Water and Air Stable Copper(I) Complexes of Tetracationic Catenane Ligands for Oxidative C À C Cross-Coupling, *Angewandte*, 2024, 1–6.

82 C. M. Vetromile, A. Lozano, S. Feola and R. W. Larsen, Solution stability of Cu (II) metal–organic polyhedra, *Inorg. Chim. Acta*, 2011, **378**, 36–41.

83 F. Lacemon, A. Lorbach, A. Eichhorn, F. Cisnetti and A. Steffen, dicopper(I)–NHC–picolyl complexes–fast, *Chem. Commun.*, 2015, 4–7.

84 Q. Wang, R. P. Murphy, M. R. Gau, P. J. Carroll and N. C. Tomson, Controlling the Size of Molecular Copper Clusters Supported by a Multinucleating Macrocycle, *Inorg. chem.*, 2024, **63**(39), 18332–18344.

85 A. E. Behar and G. Maayan, The First Cu(I)-Peptoid Complex:Enabling Metal Ion Stability and Selectivity via Backbone Helicity, *Chem. Eur. J.*, 2023, **29**, DOI: 10.1002/chem.202301118.

86 A. S. Patil and S. S. Chavan, Inorganica Chimica Acta Synthesis , characterization and catalytic study of Schiff base copper(I) complexes for C–C and C–N coupling reactions, *Inorg. Chim. Acta*, 2025, **575**, 122420.

87 L. Boubakri, S. Yasar, V. Dorcet, T. Roisnel, C. Bruneau and I. Ozdemir, Synthesis and catalytic applications of palladium N-heterocyclic carbene complexes as efficient pre-catalysts for Suzuki–Miyaura and Sonogashira coupling reactions, *New J. Chem.*, 2017, **41**, 5105–5113.

88 S. S. Massoud, F. R. Louka, M. A. Gazzaz, M. M. Henary, R. C. Fischer and F. A. Mautner, Polynuclear copper(II) complexes bridged by polycarboxylates of aromatic and N -heterocyclic compounds, *Polyhedron*, 2016, **111**, 45–52.

89 N. Ribeiro, S. Roy, N. Butenko, I. Cavaco, T. Pinheiro, I. Alho, F. Marques, F. Avecilla, J. Costa and I. Correia, New Cu(II) complexes with pyrazolyl derived Schiff base ligands: Synthesis and biological evaluation, *J. Inorg. Biochem.*, 2017, **174**, 63–75.

90 H. Coo, S. M. Lo, S. S. Chui, L. Shek, Z. Lin, X. X. Zhang, G. Wen, I. D. Williams, C. W. Bay, H. Kong and R. V February, Solvothermal Synthesis of a Stable Coordination Polymer with Copper-I- Copper-II Dimer Units, *J. Am. Chem. Soc.*, 2000, **4**, 6810–6811.

91 B. Ay, K. Sugai, T. Ishida and dinuclear Mononuclear, Mononuclear, dinuclear, and polynuclear bis(2-pyrimidylcarbonyl)amido copper(II) complexes: Synthesis, structure, thermal and magnetic properties, *Inorg. Chim Acta*, 2025, **589**, DOI: 10.1016/j.ica.2025.122930.

92 B. Ay, R. Takano, T. Ishida and E. Yildiz, Tricopper(II) bis(2-((hydrogen phosphonato)methyl) benzylphosphonate) as a layered oxo-bridged copper(II) coordination polymer: Synthesis, structure, magnetic property, and catalytic activity, *Polyhedron*, 2022, **225**, 116038.

93 N. Liu, S. Bartling, A. Springer, C. Kubis, O. S. Bokareva, E. Salaya, J. Sun, Z. Zhang, S. Wohlrab, A. M. Abdel-Mageed, H. Liang and R. Francke, Heterogenized Molecular Electrocatalyst Based on a Hydroxo-Bridged Binuclear Copper(II) Phenanthroline Compound for Selective Reduction of CO_2 to Ethylene, *Adv. Mater.*, 2024, **36**(6), DOI: 10.1002/adma.202309526.

94 M. Ghorbanpour, B. Soltani, C. J. Ziegler and K. Jamshidi-ghaleh, Inorganica Chimica Acta Novel pyrazolate-bridged binuclear Ni(II), Cu(II) and Zn(II) complexes: Synthesis, X-ray crystal structure and nonlinear optical studies, *Inorg. Chim. Acta*, 2021, **514**, 119957.

95 Y. La, Y. Yan, L. Gan, L. Xu and W. Dong, Inorganica Chimica Acta Novel phenoxo-bridged di- and tri-nuclear Cu(II) salamo-like complexes driven by various counter-anions, *Inorg. Chim. Acta, n.d.*, **2023**, 546, DOI: 10.1016/j.ica.2022.121336.

96 R. Sugich-Miranda, R. R. Sotelo-Mundo, E. Silva-Campa, J. Hernández, G. A. Gonzalez-Aguilar and E. F. Velazquez-Contreras, Antioxidant capacity of binuclear Cu(II)-cyclophanes, insights from two synthetic bioactive molecules, *J. Biochem. Mol. Toxicol.*, 2010, **24**, 379–383.

97 G. Deacon, Relationships between the carbon-oxygen stretching frequencies of carboxylato complexes and the type of carboxylate coordination, *Coord. Chem. Rev.*, 1980, **33**, 227–250.

98 F. R. Louka, S. J. Haq, H. R. Guidry, B. R. Williams, M. M. Henary, R. C. Fischer, A. Torvisco, S. S. Massoud and F. A. Mautner, Polynuclear and coordination polymers of copper(II) complexes assembled by flexible polyamines and bridging rigid N-heterocyclic multicarboxylates, *Inorg. Chim. Acta*, 2020, **500**, 119240.

99 S. S. Massoud, F. R. Louka, M. A. Gazzaz, M. M. Henary, R. C. Fischer and F. A. Mautner, Polynuclear copper(II) complexes bridged by polycarboxylates of aromatic and N-heterocyclic compounds, *Polyhedron*, 2016, **111**, 45–52.

100 P. Soosan Thomas, S. Philip and K. Mohanan, Synthesis and Spectroscopic Characterization of Some Transition Metal Complexes of Schiff Base 3-(2-hydroxyphenylimino)

methyl-4,5,-dimethyl-1-phenylpyrazol-3-in-2-one, *Orient. J. Chem.*, 2017, **33**, 2787–2795.

101 A. Ray, D. Sadhukhan, G. M. Rosair, C. J. Gómez-garcía and S. Mitra, An unprecedented Cu(II)– Schiff base complex existing as two different trinuclear units with strong antiferromagnetic couplings, *Polyhedron*, 2009, **28**, 3542–3550.

102 M. Iqbal, S. Ali, M. N. Tahir, A. Nawaz, P. A. Anderson and W. Khan, Mono- and poly-nuclear copper(II) carboxylates with flourous ligands: Synthesis, structure and improved properties, *Inorg. Chim. Acta*, 2019, **498**, 119177.

103 J. M. Lázaro Martínez, A. K. Chattah, G. A. Monti, M. F. Leal Denis, G. Y. Buldain and V. Campo Dall' Orto, New copper(II) complexes of polyampholyte and polyelectrolyte polymers: Solid-state NMR, FTIR, XRPD and thermal analyses, *Polymer*, 2008, **49**, 5482–5489.

104 L. M. S. G. Applegarth, C. R. Corbeil, D. J. W. Mercer, C. C. Pye and P. R. Tremaine, Raman and ab Initio Investigation of Aqueous Cu(I) Chloride Complexes from 25 to 80 °C, *J. Phys. Chem. B*, 2014, **118**, 204–214.

105 P. L. Holland, C. J. Cramer, E. C. Wilkinson, S. Mahapatra, K. R. Rodgers, S. Itoh, M. Taki, S. Fukuzumi, L. Que and W. B. Tolman, Resonance Raman spectroscopy as a probe of the bis(μ-oxo)dicopper core, *J. Am. Chem. Soc.*, 2000, **122**, 792–802.

106 F. Arjmand, S. Parveen, M. Afzal and M. Shahid, Synthesis, characterization, biological studies (DNA binding, cleavage, antibacterial and topoisomerase I) and molecular docking of copper(II) benzimidazole complexes, *J. Photochem. Photobiol. B Biol.*, 2012, **114**, 15–26.

107 B. J. Hathaway and D. E. Billing, The electronic properties and stereochemistry of mono-nuclear complexes of the copper(II) ion, *Coord. Chem. Rev.*, 1970, **5**, 143–207.

108 J. V. Folgado, E. E. A. Beltrn-Porter and D. Beltrn-Porter, Synthesis and spectral studies of N-2-pyridinylcarbonyl-2-pyridinecarxoximidate copper(II) complexes, *Transit. Met. Chem.*, 1987, **12**, 306–310.

109 A. Mohamadou, J. Moreau, L. Dupont and E. Wenger, Inorganica Chimica Acta Equilibrium and structural studies of copper(II) complexes with a tridentate ligand containing amide , pyrazyl and pyridyl nitrogen donors : Effect of anions coligands on crystal structures of copper(II) complexes, *Inorg. Chim. Acta*, 2012, **383**, 267–276.

110 N. Hari, S. Mandal, A. Jana, H. A. Sparkes and S. Mohanta, Syntheses, crystal structures, magnetic properties and ESI-MS studies of a series of trinuclear CuIIMIICuII compounds (M = Cu, Ni, Co, Fe, Mn, Zn), *RSC Adv.*, 2018, **8**, 7315–7329.

111 S. Bera, S. Majumdar and S. Chattopadhyay, A comprehensive overview on the synthesis and characterization of nickel, copper and hetero-nuclear copper/lanthanoid and nickel/lanthanoid complexes with salicylaldehyde-based azine ligands, *Polyhedron*, 2022, **225**, 116068.

112 A. Ali, X-ray Diffraction Techniques for Mineral Characterization : A Review for Engineers of the Fundamentals, *Minerals*, 2022, **12**(2), 205.

113 D. Ilies, E. Pahontu, S. Shova, R. Georgescu, N. Stanica, R. Olar, A. Gulea and T. Rosu, Synthesis, characterization, crystal structure and antimicrobial activity of copper(II) complexes with a thiosemicarbazone derived from 3-formyl-6-methylchromone, *Polyhedron*, 2014, **81**, 123–131.

114 J. Cuevas, M. Á. Cabrera, C. Fernández, C. Mota-Heredia, R. Fernández, E. Torres, M. J. Turrero and A. I. Ruiz, Bentonite Powder XRD Quantitative Analysis Using Rietveld Refinement: Revisiting and Updating Bulk Semiquantitative Mineralogical Compositions, *Minerals*, 2022, **12**, 772.

115 M. Ju, J. Kim and J. Shin, <scp>EPR</scp> spectroscopy: A versatile tool for exploring transition metal complexes in organometallic and bioinorganic chemistry, *Bull. Korean Chem. Soc.*, 2024, **45**, 835–862.

116 B. Bennett and J. M. Kowalski, Chapter Thirteen - EPR Methods for Biological Cu(II): L-Band CW and NARS, *Methods Enzymol.*, 2015, 341–361.

117 P. J. Carl, S. L. Baccam and S. C. Larsen, Interpretation of the EPR Spectra of Nitrogen-Containing Compounds Adsorbed on Copper-Exchanged Zeolites, *J. Phys. Chem. B*, 2000, **104**, 8848–8854.

118 S. V. Yurtaeva, I. F. Gilmutdinov, A. A. Rodionov, R. B. Zaripov, M. P. Kutyreva, O. V. Bondar, O. V. Nedopekin, N. R. Khafizov and O. N. Kadkin, Ferromagnetically Coupled Copper(II) Clusters Incorporated in Functionalized Boltorn H30 Hyperbranched Polymer Architecture: ESR, Magnetic Susceptibility Measurements, and Quantum-Chemical Calculations, *ACS Omega*, 2019, **4**, 16450–16461.

119 M. Wakizaka and M. Yamashita, Quantum magnetism of spin qubits in S = 1/2 Cu(II) systems in discrete complexes, chains, and metal-organic frameworks, *Chem. Phys. Rev*, 2025, **6**(1), DOI: 10.1063/5.0226942.

120 V. V. Minin, E. A. Ugolkova, N. N. Efimov, N. V. Gogoleva and V. V. Avdeeva, Comparative analysis of EPR parameters in X-, Q-, W-bands for exchange-coupled copper(II) dimers, *Inorg. Chem. Commun.*, 2023, **158**, 111646.

121 O. Schiemann and T. F. Prisner, Long-range distance determinations in biomacromolecules by EPR spectroscopy, *Q. Rev. Biophys.*, 2007, **40**, 1–53.

122 A. Bhattacharyya, A. Bauzá, S. Sproules, L. S. Natrajan, A. Frontera and S. Chattopadhyay, A polynuclear and two dinuclear copper (II) Schiff base complexes: Synthesis, characterization, self-assembly, magnetic property and DFT study, *Polyhedron*, 2017, **137**, 332–346.

123 M. Sutradhar, E. C. B. A. Alegria and T. R. Barman, 1D Copper (II) -Aroylhydrazone Coordination Polymers : Magnetic Properties and Microwave Assisted Oxidation of a Secondary, *Alcohol*, 2020, **8**, 1–10.

124 M. Aamir Iqbal, N. Ashraf, W. Shahid, D. Afzal, F. Idrees and R. Ahmad, in *Density Functional Theory - Recent Advances, New Perspectives and Applications*, IntechOpen, 2022.

125 R. Acevedo-Chávez, M. E. Costas and R. Escudero, Allopurinol– and Hypoxanthine–Copper(II) Compounds.

Spectral and Magnetic Studies of Novel Dinuclear Coordination Compounds with Bridging Hypoxanthine, *Inorg. Chem.*, 1996, **35**, 7430–7439.

126 C. Aronica, E. Jeanneau, H. El Moll, D. Luneau, B. Gillon, A. Goujon, A. Cousson, M. A. Carvajal and V. Robert, Ferromagnetic interaction in an asymmetric end-to-end Azido Double-bridged copper(II) dinuclear complex: A combined structure, magnetic, polarized neutron diffraction and theoretical study, *Chem. - Eur. J.*, 2007, **13**, 3666–3674.

127 L. L. Wang, Y. M. Sun, Z. N. Qi and C. B. Liu, Magnetic interactions in two heterobridged dinuclear copper(II) complexes: Orbital complementarity or countercomplementarity?, *J. Phys. Chem. A*, 2008, **112**, 8418–8422.

128 I. Valencia, Y. Ávila-Torres, N. Barba-Behrens and I. L. Garzón, Structural, vibrational, and electronic properties of an uncoordinated pseudoephedrine derivative and its mononuclear and trinuclear copper(II)-coordinated compounds: A combined theoretical and experimental study, *J. Mol. Struct.*, 2014, **1076**, 387–395.

129 Y. Liu, S. Chatterjee, G. E. Cutsail, S. Peredkov, S. K. Gupta, S. Dechert, S. DeBeer and F. Meyer, Cu4S Cluster in "0-Hole" and "1-Hole" States: Geometric and Electronic Structure Variations for the Active CuZ* Site of N2O Reductase, *J. Am. Chem. Soc.*, 2023, **145**, 18477–18486.

130 R. A. El-Kasaby, E. S. Al-Farraj, A. Abdou and A. M. Abu-Dief, Synthenovelsis, spectral analysis, physicochemical investigation and biomedical potential of some Cu(II), Ru(III) and VO(II) complexes with anthraquinone-based Schiff base supported by DFT and molecular docking insights, *J. Mol. Struct.*, 2025, **1345**, 143010.

131 J. G. Woollard-Shore, J. P. Holland, M. W. Jones and J. R. Dilworth, Nitritereduction by copper complexes, *Dalton Trans.*, 2010, **39**, 1576–1585.

132 R. Chandra Maji, S. Mishra, A. Bhandari, R. Singh, M. M. Olmstead and A. K. Patra, A Copper(II) Nitrite That Exhibits Change of Nitrite Binding Mode and Formation of Copper(II) Nitrosyl Prior to Nitric Oxide Evolution, *Inorg. Chem.*, 2018, **57**, 1550–1561.

133 A. Mondal, K. P. Reddy, J. A. Bertke and S. Kundu, Phenol Reduces Nitrite to NO at Copper(II): Role of a Proton-Responsive Outer Coordination Sphere in Phenol Oxidation, *J. Am. Chem. Soc.*, 2020, **142**, 1726–1730.

134 S. Gupta, S. Arora, A. Mondal, S. C. E. Stieber, P. Gupta and S. Kundu, A Copper(II)-Nitrite Complex Hydrogen-Bonded to a Protonated Amine in the Second-Coordination-Sphere, *Eur. J. Inorg. Chem.*, 2018, **57**, 1550–1561.

135 B. S. Anju, N. R. Nair and S. Kundu, Nitrite and Nitric Oxide Interconversion at Mononuclear Copper(II): Insight into the Role of the Red Copper Site in Denitrification, *Angew. Chem., Int. Ed.*, 2023, **62**(48), DOI: 10.1002/anie.202311523.

136 Y. Kametani and Y. Shiota, Mechanistic studies of NOx reduction reactions involving copper complexes: encouragement of DFT calculations, *Dalton Trans.*, 2024, **53**, 19081–19087.

137 P. Seppälä, R. Sillanpää and A. Lehtonen, Structural diversity of copper (II) amino alcoholate complexes, *Coord. Chem. Rev.*, 2017, **347**, 98–114.

138 C. E. Housecroft and A. G. SHARPE, Inorganic Chemistry, *Pearson*, 2018.

139 M. Knorr, F. Guyon, A. Khatyr, C. Strohmann, M. Allain, S. M. Aly, A. Lapprand, D. Fortin and P. D. Harvey, Construction of (CuX)2n cluster-containing (X = Br, I; n = 1, 2) coordination polymers assembled by dithioethers ArS(CH2)(m)SAr (Ar = Ph, p-Tol; m = 3, 5): effect of the spacer length, aryl group, and metal-to-ligand ratio on the dimensionality, cluster nuclearity, and the luminescence properties of the metal-organic frameworks, *Inorg.chem.*, 2012, **51**, 9917–9934.

140 M. S. H. Faizi, M. Ahmad, A. Ali and V. A. Potaskalov, Crystal structure of 5-[(4-carboxybenzyl)oxy]isophthalic acid, *Acta Crystallogr., Sect. E:Crystallogr. Commun.*, 2016, **72**, 1219–1222.

141 Q. Yue and E.-Q. Gao, Azide and carboxylate as simultaneous coupler for magnetic coordination polymers, *Coord. Chem. Rev.*, 2019, **382**, 1–31.

142 S. Zhang, W. Shi and P. Cheng, The coordination chemistry of N-heterocyclic carboxylic acid: A comparison of the coordination polymers constructed by 4,5-imidazoledicarboxylic acid and 1H-1,2,3-triazole-4,5-dicarboxylic acid, *Coord. Chem. Rev.*, 2017, **352**, 108–150.

143 L.-X. You, S.-J. Wang, G. Xiong, F. Ding, K. W. Meert, D. Poelman, P. F. Smet, B.-Y. Ren, Y.-W. Tian and Y.-G. Sun, Synthesis, structure and properties of 2D lanthanide coordination polymers based on N-heterocyclic arylpolycarboxylate ligands, *Dalton Trans.*, 2014, **43**, 17385–17394.

144 F. R. Louka, S. J. Haq, H. R. Guidry, B. R. Williams, M. M. Henary, R. C. Fischer, A. Torvisco, S. S. Massoud and F. A. Mautner, Polynuclear and coordination polymers of copper(II) complexes assembled by flexible polyamines and bridging rigid N-heterocyclic multicarboxylates, *Inorg. Chim. Acta*, 2020, **500**, 119240.

145 A. W. Addison, T. N. Rao, J. Reedijk, J. van Rijn and G. C. Verschoor, Synthesis, structure, and spectroscopic properties of copper(II) compounds containing nitrogen–sulphur donor ligands; the crystal and molecular structure of aqua[1,7-bis(N-methylbenzimidazol-2′-yl)-2,6-dithiaheptane]copper(II) pe, *J. Chem. Soc.*, 1984, 1349–1356.

146 Y. Zhang, Y. Huang, Y. Ding, Y. Zheng and W. Dong, Synthesis , crystal structure , properties , and theoretical studies of novel tetra-nuclear copper (II) salamo-like complex containing four- and five-coordinated geometries, *J. Mol. Struct.*, 2023, **1291**, 136051.

147 L. Yang, D. R. Powell and R. P. Houser, Structural variation in copper(I) complexes with pyridylmethylamide ligands: structural analysis with a new four-coordinate geometry index, τ_4, *Dalton Trans.*, 2007, 955–964.

148 K. Robinson, G. V. Gibbs and P. H. Ribbe, Quadratic Elongation: A Quantitative Measure of Distortion in Coordination Polyhedra, *Science*, 1971, **172**, 567–570.

149 A. Noor, A. Shahzad, E. Khan, M. N. Tahir, G. S. Khan, A. Rashid and M. Said, Polynuclear Cu(I) and Ag(I) Complexes of 1,3-Diisobutyl Thiourea, Synthesis, Crystal Structure and Antioxidant Potentials, *Inorganics*, 2022, **10**, 185.

150 J. T. Tan, W. J. Zhao, S. P. Chen, X. Li, Y. L. Lu, X. Feng and X. W. Yang, Synthesis, structure, and luminescent properties of two novel polynuclear complexes of 1,3-di(pyridin-2-yl)propane-1,3-dione, *Chem. Pap.*, 2012, **66**, 47–53.

151 P. Bombicz, I. Mutikainen, M. Krunks, T. Leskelä, J. Madarász and L. Niinistö, Synthesis, vibrational spectra and X-ray structures of copper(I) thiourea complexes, *Inorg. Chim. Acta*, 2004, **357**, 513–525.

152 G. Battaini, A. Granata, E. Monzani, M. Gullotti and L. Casella, Biomimetic Oxidations by Dinuclear and Trinuclear Copper Complexes, *Adv. Inorg. Chem.*, 2006, **58**, 185–233.

153 S. Ahmad, M. Altaf, H. Stoeckli-Evans, T. Rüffer, H. Lang, M. Mufakkar and A. Waheed, Crystal structures of trinuclear chlorido (N,N'-diethylthiourea)copper(I) and a second polymorph of iodidotris(N,N'-diethylthiourea) copper(I), *J. Chem. Crystallogr.*, 2010, **40**, 639–645.

154 A. Majumder, S. Sk, A. Das, G. Vijaykumar, M. K. Sahoo, J. N. Behera and M. Bera, Ancillary-Ligand-Assisted Variation in Nuclearities Leading to the Formation of Di-, Tri-, and Tetranuclear Copper(II) Complexes with Multifaceted Carboxylate Coordination Chemistry, *ACS Omega*, 2022, **7**, 39985–39997.

155 E. S. Bazhina, A. A. Bovkunova, M. A. Shmelev, K. A. Babeshkin, N. N. Efimov, I. L. Eremenko and M. A. Kiskin, Solvent-dependent formation of 1D coordination polymers based on polynuclear copper (II)-carboxylate fragments and 4- (pyridine-3-yl), *Polyhedron*, 2022, **228**, 116174.

156 K. Singh, J. R. Long, P. Stavropoulos and R. V June, Polynuclear Complexes of Copper (I) and the 2- (3(5)-Pyrazolyl)-6-methylpyridine Ligand : Structures and Reactivity toward, *Small Mol.*, 1998, **3**, 1073–1079.

157 C. Bizzarri, E. Spuling, D. M. Knoll, D. Volz and S. Bräse, Sustainable metal complexes for organic light-emitting diodes (OLEDs), *Coord. Chem. Rev.*, 2018, **373**, 49–82.

158 R. Hamze, J. L. Peltier, D. Sylvinson, M. Jung, J. Cardenas, R. Haiges, M. Soleilhavoup, R. Jazzar, P. I. Djurovich, G. Bertrand and M. E. Thompson, Eliminating nonradiative decay in Cu(I) emitters: >99% quantum efficiency and microsecond lifetime, *Science*, 2019, **363**, 601–606.

159 J. Schaab, P. Djurovich and M. Thompson, *Two Coordinate, Monovalent Copper Complexes as Chromophores and Luminophores*, 2023, DOI: 10.26434/chemrxiv-2023-6rvrn.

160 N. Kandasamy, N. Keerthi and J. Jeyasekaran, Mixed Ligand Copper(I) Complexes as Emitters Enable Higher OLED Device Performance for Energy-Harvesting Applications, *ACS Appl. Electron. Mater.*, 2023, **5**, 4805–4815.

161 Y. Tan, A. Ying, J. Xie, G. Xie and S. Gong, Luminescent carbene–copper(I)–amide polymers for efficient host-free solution-processed OLEDs, *Chem. Sci.*, 2024, **15**, 11382–11390.

162 S. Stal, B. Huitorel, T. Coustham, N. Stephant, F. Massuyeau, T. Gacoin, L. Bouteiller and S. Perruchas, Photoactive CuI-Cross-Linked Polyurethane Materials, *ACS Appl. Mater. Interfaces*, 2022, **14**, 47931–47940.

163 X. W. Chen, H. L. Yuan, L. H. He, J. L. Chen, S. J. Liu, H. R. Wen, G. Zhou, J. Y. Wang and W. Y. Wong, A Sublimable Dinuclear Cuprous Complex Showing Selective Luminescence Vapochromism in the Crystalline State, *Inorg. Chem.*, 2019, **58**, 14478–14489.

164 Q. Xiao, J. Zheng, M. Li, S. Zhan, J. Wang and D. Li, Mechanically Triggered Fluorescence/Phosphorescence Switching in the Excimers of Planar Trinuclear Copper(I) Pyrazolate Complexes, *Inorg. Chem.*, 2014, **53**, 11604–11615.

165 F. G. Kerry, *Industrial Gas Handbook*, CRC Press, 2007.

166 P. J. Bereciartua, Á. Cantín, A. Corma, J. L. Jordá, M. Palomino, F. Rey, S. Valencia, E. W. Corcoran, P. Kortunov, P. I. Ravikovitch, A. Burton, C. Yoon, Y. Wang, C. Paur, J. Guzman, A. R. Bishop and G. L. Casty, Control of zeolite framework flexibility and pore topology for separation of ethane and ethylene, *Science*, 2017, **358**, 1068–1071.

167 S. M. S. Islam, R. Yasmeen, G. Verma, S. M. Tekarli, V. N. Nesterov, S. Ma and M. A. Omary, A Copper-Based Metal–Organic Framework for Selective Separation of C2 Hydrocarbons from Methane at Ambient Conditions: Experiment and Simulation, *Inorg. Chem.*, 2024, **63**, 8664–8673.

168 N. Das, A. Maibam, H. Yun, B. Boro, C. S. Hong, R. Babarao and J. Mondal, Revving Up a Designed Copper Catecholate Porous Organic Polymer for Its Potent Ethylene Adsorption than Ethane, *Inorg. Chem.*, 2024, **63**, 19759–19768.

169 X. Wang, M. Zhu, S. Li, G. Xu, Z. Zhang and F. Yang, Novel mono- , bi- , tri- and tetra-nuclear copper complexes that inhibit tumor growth through apoptosis and anti-angiogenesis, *J. Inorg. Biochem.*, 2024, **250**, 112403.

170 M. Dolaz, M. Tu and M. Di, *Synthesis, Characterization and Stability Constants of Polynuclear Metal Complexes*, 2004, 528–536.

171 M. A. El, F. M. Elzawawi, A. A. A. Aziz, K. M. Nassir, S. M. Abu and E. Wafa, New Schiff base ligand and its novel Cr(III), Mn(II), Co(II), Ni(II), Cu(II), Zn(II) complexes : spectral investigation , biological applications , and semiconducting properties, *Sci. Rep.*, 2022, 1–21.

172 M. Shebl, Synthesis, spectral studies, and antimicrobial activity of binary and ternary Cu(II), Ni(II), and Fe(III) complexes of new hexadentate Schiff bases derived from 4,6-diacetylresorcinol and amino acids, *J. Coord. Chem.*, 2019, **62**, 3217–3231.

173 O. Krasnovskaya, A. Naumov, D. Guk, P. Gorelkin, A. Erofeev, E. Beloglazkina and A. Majouga, Copper Coordination Compounds as Biologically Active Agents, *Int. J. Mol. Sci.*, 2020, **21**, 3965.

174 Y. Zhang, Z. Ma, P. Qiao, C. Gao, J. Tian, J. Zhao, W. Du, J. Xu and S. Yan, Design and biological evaluations of mono- and di-nuclear copper (II) complexes: Nuclease

activity, cytotoxicity and apoptosis, *Polyhedron*, 2021, **193**, 114880.

175 P. Arthi, A. Haleel, P. Srinivasan, D. Prabhu, C. Arulvasu and A. Kalilur Rahiman, Antibacterial, DNA interaction and cytotoxic activities of pendant-armed polyamine macrocyclic dinuclear nickel(II) and copper(II) complexes, *Spectrochim. Acta, Part A*, 2014, **129**, 400–414.

176 R. Olar, M. Badea, M. Bacalum, M. Răileanu, L. L. Ruță, I. C. Farcașanu, A. M. Rostas, I. D. Vlaicu, M. Popa and M. C. Chifiriuc, Antiproliferative and antibacterial properties of biocompatible copper(II) complexes bearing chelating N,N-heterocycle ligands and potential mechanisms of action, *BioMetals*, 2021, **34**, 1155–1172.

177 C. White, J. Lee, T. Kambe, K. Fritsche and M. J. Petris, A Role for the ATP7A Copper-transporting ATPase in Macrophage Bactericidal Activity, *J. Biol. Chem.*, 2009, **284**, 33949–33956.

178 Y. A. Gur'eva, O. A. Zalevskaya, O. G. Shevchenko, P. A. Slepukhin, V. A. Makarov and A. V. Kuchin, Copper(II) complexes with terpene derivatives of ethylenediamine: synthesis, and antibacterial, antifungal and antioxidant activity, *RSC Adv.*, 2022, **12**, 8841–8851.

179 M. Iqbal, S. Ali, M. Nawaz and N. Ali, Dihydroxo-bridged dimeric Cu(II) system containing sandwiched non-coordinating phenylacetate anion: Crystal structure , spectroscopic , anti-bacterial , anti-fungal and DNA-binding studies of [(phen)(H_2O)Cu(OH)$_2$Cu(H_2O)(phen)] 2L. 6, *J. Mol. Struct.*, 2017, **1143**, 23–30.

180 J. Y. Caro-Ramirez, J. E. Parente, G. M. Gaddi, N. Martini, C. A. Franca, N. M. Urquiza, L. Lezama, O. E. Piro, G. A. Echeverría, P. A. M. Williams and E. G. Ferrer, The biocatalytic activity of the "lantern-like" binuclear copper complex with trisulfide bridges mimicking SOD metallo-proteins, *Polyhedron*, 2022, **221**, 115879.

181 L. Rana, Dheeraj and K. Mahiya, Synthesis and evaluation of copper(II) complexes for peroxidase-mimicking activity, *J. Mol. Struct.*, 2025, **1319**, 139609.

182 A. Cendron, M. Chianese, K. Zarzycki, P. Ruzza, C. Honisch, J. Brasuń and M. Carraro, Chelating Properties of N6O-Donors Toward Cu(II) Ions: Speciation in Aqueous Environments and Catalytic Activity of the Dinuclear Complexes, *Molecules*, 2024, **29**, 5708.

183 A. Squarcina, A. Santoro, N. Hickey, R. De Zorzi, M. Carraro, S. Geremia, M. Bortolus, M. Di Valentin and M. Bonchio, Neutralization of Reactive Oxygen Species at Dinuclear Cu(II)-Cores: Tuning the Antioxidant Manifold in Water by Ligand Design, *ACS Catal.*, 2020, **10**, 7295–7306.

184 K. Abdi, H. Hadadzadeh, M. Weil and H. A. Rudbari, Mono- and polynuclear copper(II) complexes based on 2,4,6-tris(2-pyridyl)-1,3,5-triazine and its hydrolyzed form, *Inorg. Chim Acta,.*, 2014, **416**, 109–121.

185 M. Iqbal, S. Ali, M. Nawaz and N. Ali, Dihydroxo-bridged dimeric Cu(II) system containing sandwiched non-coordinating phenylacetate anion: Crystal structure , spectroscopic , anti-bacterial , anti-fungal and DNA-binding studies of [(phen)(H_2O)Cu(OH)$_2$Cu(H_2O)(phen)] 2L. 6, *J. Mol. Struct.*, 2017, **1143**, 23–30.

186 Q. Peña, G. Sciortino, J. D. Maréchal, S. Bertaina, A. J. Simaan, J. Lorenzo, M. Capdevila, P. Bayón, O. Iranzo and Ò. Palacios, Copper(II) N, N, O-Chelating Complexes as Potential Anticancer Agents, *Inorg. Chem.*, 2021, **60**, 2939–2952.

187 S. S. Massoud, F. R. Louka, N. M. H. Salem, R. C. Fischer, A. Torvisco, F. A. Mautner, J. Vančo, J. Belza, Z. Dvořák and Z. Trávníček, Dinuclear doubly bridged phenoxido copper(II) complexes as efficient anticancer agents, *Eur. J. Med. Chem.*, 2023, **246**, 114992.

188 P. Ji, P. Wang, H. Chen, Y. Xu, J. Ge, Z. Tian and Z. Yan, Potential of Copper and Copper Compounds for Anticancer Applications, *Pharmaceuticals*, 2023, **16**, 234.

189 W. L. de Oliveira, E. F. de Oliveira, T. dos S. da Cruz, W. V. F. do C. Batista, C. Moraes, F. V. Pereira, M. R. Forim, G. A. Atta Diab, I. F. Teixeira, M. C. Pereira and J. P. de Mesquita, Preparation and Characterization of a Coordination Polymer Based on Iron (III)-Cyamelurate as a Superior Catalyst for Heterogeneous Fenton-Like Processes, *Langmuir*, 2023, **39**, 5002–5011.

190 Z.-Y. Zhang, G.-D. Zhang, X.-X. Sheng, Q.-W. Ding, Y.-Z. Bai, Y. Su, H.-K. Liu and Z. Su, Efficient MO Dye Degradation Catalyst of Cu(I)-Based Coordination Complex from Dissolution–Recrystallization Structural Transformation, *Cryst. Growth Des.*, 2021, **21**, 333–343.

191 L. Li, Y. Zhao, J.-J. Wang, H. Chen, H. Li, J. Wang, Y. Wang, Y. Bai and D. Dang, The [CuI_4Cl_4] cluster of a coordination complex based on polypyridyl ligand for heterogeneous Fenton-like MB degradation without illumination and electrocatalytic reduction of H_2O_2 and K_2Cr_2O7, *Dye. Pigment.*, 2022, **207**, 110763.

192 L. Li, X.-S. Wang, J.-J. Wang, B. Qin, C. Shi, B. Du, J. Yang, Y. Bai and D.-B. Dang, A Multivalent Copper Polypyridyl Coordination Polymer for Heterogeneous Dark-Fenton Degradation of Organic Dyes, *Cryst. Growth Des.*, 2025, **25**, 5371–5379.

193 N. Hussain and V. K. Bhardwaj, The influence of different coordination environments on one-dimensional Cu(II) coordination polymers for the photo-degradation of organic dyes, *Dalton Trans.*, 2016, **45**, 7697–7707.

194 M. G. Kibria, J. P. Edwards, C. M. Gabardo, C. Dinh, A. Seifitokaldani, D. Sinton and E. H. Sargent, Electrochemical CO_2 Reduction into Chemical Feedstocks: From Mechanistic Electrocatalysis Models to System Design, *Adv. Mater.*, 2019, **31**(31), DOI: 10.1002/adma.201807166.

195 D. Gao, R. M. Arán-Ais, H. S. Jeon and B. Roldan Cuenya, Rational catalyst and electrolyte design for CO_2 electroreduction towards multicarbon products, *Nat. Catal.*, 2019, **2**, 198–210.

196 J.-M. Heng, H.-L. Zhu, Z.-H. Zhao, D.-S. Huang, J.-Y. Li, P.-Q. Liao and X.-M. Chen, A Conductive Dinuclear Cuprous Complex Mimicking the Active Edge Site of the Copper(100)/(111) Plane for Selective Electroreduction of CO_2 to C_2H_4 at Industrial Current Density, *Research*, 2022, **2022**, 0008.

197 N. Liu, T. M. Pham, Y. Han, L. Yang, O. S. Bokareva, S. Bartling, A. Springer, A. Spannenberg, C. Kubis, J. Weiss, D. E. Doronkin, W. Ju and R. Francke, Heterogenized Copper (II) Phenanthroline Catalysts for Electroreduction of CO_2 to C_2 Compounds: Substitution on the Ligand Causes Structural Changes to the Molecular Framework and Stability Enhancement, *Adv Mater.*, 2025, **13702**, 1–12.

198 J. Lu, J. Liu, L. Zhang, L. Dong, S. Li and Y. Lan, *Crystalline Mixed-Valence Copper Supramolecular Isomers for Electroreduction of CO_2 to Hydrocarbons*, 2021, 23477–23484.

199 L. Wang, Mixed-valence Cu-based metal-organic framework for selective CO2 electroreduction to C1 liquid fuels with high energy conversion efficiency, *Nano Res.*, 2025, **18**, 1–8.

200 C. Deacon-price, A. H. M. Silva, C. S. Santana, M. T. M. Koper and A. C. Garcia, Solvent Effect on Electrochemical CO_2 Reduction Reaction on Nanostructured Copper Electrodes, *J. Phys. Chem. C*, 2023, **127**(29), 14518–14527.

201 H. Takeda, C. Cometto, O. Ishitani and M. Robert, Electrons, Photons, Protons and Earth-Abundant Metal Complexes for Molecular Catalysis of CO_2 Reduction, *ACS Catal.*, 2017, **7**, 70–88.

202 Y. Kuramochi, O. Ishitani and H. Ishida, Reaction mechanisms of catalytic photochemical CO_2 reduction using Re(I) and Ru(II) complexes, *Coord. Chem. Rev.*, 2018, **373**, 333–356.

203 Y. Yamazaki, H. Takeda and O. Ishitani, Photocatalytic reduction of CO2 using metal complexes, *J. Photochem. Photobiol. C Photochem. Rev.*, 2015, **25**, 106–137.

204 J. Bonin, M. Robert and M. Routier, Selective and Efficient Photocatalytic CO_2 Reduction to CO Using Visible Light and an Iron-Based Homogeneous Catalyst, *J. Am. Chem. Soc.*, 2014, **136**, 16768–16771.

205 Z. Guo, S. Cheng, C. Cometto, E. Anxolabéhère-Mallart, S.-M. Ng, C.-C. Ko, G. Liu, L. Chen, M. Robert and T.-C. Lau, Highly Efficient and Selective Photocatalytic CO_2 Reduction by Iron and Cobalt Quaterpyridine Complexes, *J. Am. Chem. Soc.*, 2016, **138**, 9413–9416.

206 H. Takeda, K. Ohashi, A. Sekine and O. Ishitani, Photocatalytic CO_2 Reduction Using Cu(I) Photosensitizers with a Fe(II) Catalyst, *J. Am. Chem. Soc.*, 2016, **138**, 4354–4357.

207 H. Takeda, H. Kamiyama, K. Okamoto, M. Irimajiri, T. Mizutani, K. Koike, A. Sekine and O. Ishitani, Highly Efficient and Robust Photocatalytic Systems for CO_2 Reduction Consisting of a Cu(I) Photosensitizer and Mn(I) Catalysts, *J. Am. Chem. Soc.*, 2018, **140**, 17241–17254.

208 Q. Shen, C. J. Gómez-García, W. Sun, X. Lai, H. Pang and H. Ma, Improving the photocatalytic H_2 evolution activity of Keggin polyoxometalates anchoring copper-azole complexes, *Green Chem.*, 2021, **23**, 3104–3114.

209 T. F. Qahtan, I. O. Alade, M. S. Rahaman and T. A. Saleh, Mapping the research landscape of hydrogen production through electrocatalysis: A decade of progress and key trends, *Renew. Sustain. Energy Rev.*, 2023, **184**, 113490.

210 S. O. Jeje, T. Marazani, J. O. Obiko and M. B. Shongwe, Advancing the hydrogen production economy: A comprehensive review of technologies, sustainability, and future prospects, *Int. J. Hydrogen Energy*, 2024, **78**, 642–661.

211 J. Chen, C. Chen, M. Qin, B. Li, B. Lin, Q. Mao, H. Yang, B. Liu and Y. Wang, Reversible hydrogen spillover in Ru-WO3-x enhances hydrogen evolution activity in neutral pH water splitting, *Nat. Commun.*, 2022, **13**, 5382.

212 X. Wang, X. Li, D. Kong, L. Zhao, Y. Cui, Y. Wang, T. Cai, Q. Xue, Z. Yan and W. Xing, Platinum-free electrocatalysts for hydrogen oxidation reaction in alkaline media, *Nano Energy*, 2022, **104**, 107877.

213 L. Xie, Y. Jiang, W. Zhu, S. Ding, Y. Zhou and J.-J. Zhu, Cu-based catalyst designs in CO_2 electroreduction: precise modulation of reaction intermediates for high-value chemical generation, *Chem. Sci.*, 2023, **14**, 13629–13660.

214 Y.-X. Lin, S.-N. Zhang, Z.-H. Xue, J.-J. Zhang, H. Su, T.-J. Zhao, G.-Y. Zhai, X.-H. Li, M. Antonietti and J.-S. Chen, Boosting selective nitrogen reduction to ammonia on electron-deficient copper nanoparticles, *Nat. Commun.*, 2019, **10**, 4380.

215 S. M. Barnett, K. I. Goldberg and J. M. Mayer, A soluble copper–bipyridine water-oxidation electrocatalyst, *Nat. Chem.*, 2012, **4**, 498–502.

216 T. Zhang, C. Wang, S. Liu, J.-L. Wang and W. Lin, A Biomimetic Copper Water Oxidation Catalyst with Low Overpotential, *J. Am. Chem. Soc.*, 2014, **136**, 273–281.

217 H. A. Younus, N. Ahmad, M. Al-Abri, R. Al-Hajri and S. Zhang, Molecular Nature of Electrodeposits in Electrochemical Water Oxidation, *Adv. Energy Mater.*, 2023, **13**(25), DOI: 10.1002/aenm.202300896.

218 H. Emam, R. Al Hajri, N. Ahmad, F. M. Elantabli, M. El-Rabiei, A. Hassan, M. Al Abri and H. A. Younus, Bio-Inspired histidine-based copper complex: An efficient and robust electrocatalyst for electrochemical hydrogen evolution, *Int. J. Hydrogen Energy*, 2025, **137**, 976–986.